MEMORANDUM FOR: Leon B. Engle, Project Manager
                   Project Directorate II-2
                   Division of Reactor Projects - I/II

FROM: C. Y. Cheng, Chief
                   Materials Engineering Branch
                   Division of Engineering and Systems Technology

SUBJECT: NORTH ANNA UNITS 1 and 2 - CLOSEOUT OF BULLETIN 88-02
                   ISSUES (TACs 67315 AND 67316)

The Materials Engineering Branch, Division of Engineering and Systems Technology, has completed its review of actions taken by Virginia Electric Power Company (the licensee) to resolve the issues in NRC Bulletin 88-02, "Rapidly Propagating Fatigue Cracks in Steam Generator Tubes". The licensee's actions are documented in its letter dated March 24, 1988.

Our Safety Evaluation is enclosed. We find that the actions taken by the licensee fully resolve the issues identified in the bulletin and are acceptable. This finding is subject to adoption of additional administrative controls by the licensee as described in the conclusions of the enclosed SER.

With this memorandum, our action relative to TAC Nos. 67315 and 67316 is complete.

/S/

C. Y. Cheng, Chief
Materials Engineering Branch
Division of Engineering and Systems
Technology

cc: F. Miraglia
     L. Shao
     J. Richardson
     C. Berlinger
     D. Neighbors
     S. Varga
     G. Lainas
     H. Berkow

DISTRIBUTION:
Central Files
EMTB RF
EMTB PF
CYCheng
KRWichman
EMurphy

CONTACT: E. Murphy, EMTB/DEST
          X20945

*See Previous Concurrence

*DEST:EMTB	*DEST:EMTB	DEST:EMTB
EMurphy:tys	KRWichman	CYCheng
11/ /88	11/ /88	11/16/88

D/58

8811210236

MEMORANDUM FOR: Leon B. Engle, Project Manager
                   Project Directorate II-2
                   Division of Reactor Projects - II/III

FROM: C. Y. Cheng, Chief
                   Materials Engineering Branch
                   Division of Engineering and Systems Technology

SUBJECT: NORTH ANNA UNITS 1 and 2 - CLOSEOUT OF BULLETIN 88-02
                   ISSUES (TACs 67315 AND 67316)

The Materials Engineering Branch, Division of Engineering and Systems Technology,
has completed its review of actions taken by Virginia Electric Power Company
(the licensee) to resolve the issues in NRC Bulletin 88-02, "Rapidly Propagating
Fatigue Cracks in Steam Generator Tubes". The licensee's actions are documented
in its letter dated March 24, 1988.

Our Safety Evaluation is enclosed. We find that the actions taken by the
licensee fully resolve the issues identified in the bulletin and are acceptable.
This finding is subject to adoption of additional administrative controls by the
licensee as described in the conclusions of the enclosed SER.

With this memorandum, our action relative to TAC Nos. 67315 and 67316 is
complete.

                                        C. Y. Cheng, Chief
                                        Materials Engineering Branch
                                        Division of Engineering and Systems
                                          Technology

cc: F. Miraglia
     L. Shao
     J. Richardson
     C. Berlinger
     D. Neighbors
     S. Varga
     G. Lainas   DISTRIBUTION:
     H. Berkow   Central Files
                                                  EMTB RF
                                                  EMTB PF
                                                  CYCheng
CONTACT: E. Murphy, EMTB/DEST   KRWichman
          X20945   EMurphy

DEST:EMTB   DEST:EMTB   DEST:EMTB
EMurphy:tys   KRWichman   CYCheng
11/ /88   11/15/88   11/ /88

SAFETY EVALUATION REPORT

VIRGINIA ELECTRIC AND POWER COMPANY
NORTH ANNA UNITS 1 AND 2

CLOSEOUT OF BULLETIN 88-02 ISSUES

MATERIALS ENGINEERING BRANCH
DIVISION OF ENGINEERING AND SYSTEMS TECHNOLOGY

1.   INTRODUCTION

By letter dated March 24, 1988 (Reference 1), Virginia Electric and Power Company
(the licensee) submitted its response to NRC Bulletin 88-02, "Rapidly Propagating
Fatigue Cracks in Steam Generator Tubes". Bulletin 88-02 requested that
licensees for plants with Westinghouse steam generators employing carbon steel
support plates take certain actions (specified in the bulletin) to minimize the
potential for a steam generator tube rupture event caused by a rapidly propagat-
ing fatigue crack such as occurred at North Anna Unit 1 on July 15, 1987.

2.   DISCUSSION

2.1 North Anna Unit 1

Actions taken by the licensee and their Westinghouse consultant to investigate
and correct the conditions which led to the July 15, 1987 SGTR event were
provided in (1) the licensee's report, "North Anna Unit 1 July 15, 1987, Steam
Generator Tube Rupture Report," September 15, 1987, Revision 1 (Reference 2),
and (2) Westinghouse reports WCAP-11601 (proprietary version) and WCAP-11602
(non-proprietary version) (Reference 3).

The failure mechanism was established by Westinghouse as fatigue due to excessive
flow induced vibration associated with a fluid-elastic instability. To prevent
future fatigue crack initiation, the licensee installed a downcomer flow resis-
tance plate in each steam generator to reduce the steam generator crossflow
velocities and, thus, the stability ratios for all tubes. In addition, extensive
preventive plugging was performed on tubes with potentially high stability ratios
which were unsupported by anti-vibration bars (AVBs). This preventive plugging
program included all unsupported tubes beyond row 8 and unsupported row 8 tubes
which appeared to be subject to localized flow peaking effects. These corrective
actions were estimated by Westinghouse to reduce the maximum stability ratio for
unsupported tubes remaining in service by at least 22% compared to the stability
ratio for the tube which ruptured. This reduction in stability ratio satisfies
the 10% criterion developed by Westinghouse to ensure that alternating stress
levels are sufficiently small to preclude fatigue crack initiation for the re-
maining lifetime of the plant.

In addition to the above corrective actions, the licensee committed to and
implemented an enhanced primary-to-secondary leak rate monitoring program which
provides added assurance that the plant will be shutdown in a timely fashion
before a leaking through wall crack can propagate to failure. In addition, the
licensee submitted a license amendment request by letter dated December 4, 1987
to incorporate this enhanced monitoring program as part of the Technical
Specifications.

By letter dated December 11, 1987 (Reference 4), the staff issued its Safety Evaluation authorizing North Anna Unit 1 to return to 100% of licensed power. The staff concluded in the Safety Evaluation that the licensee had implemented acceptable diagnostic and corrective actions to prevent a similar fatigue failure in the future. The licensee's actions and the staff's December 11, 1987. Safety Evaluation pre-dated issuance of Bulletin 88-02 on February 5, 1988.

Although the December 11, 1987 Safety Evaluation endorsed the licensee's enhanced leak rate monitoring program, it did not address the licensee's proposal to include this enhanced program as part of the Technical Specifications. The staff expects to complete action on the requested change to the Technical Specifications within the next few weeks.

As part of its March 24, 1988 response to Bulletin 88-02, the licensee enclosed Revision 2 of its "Steam Generator Tube Rupture Report" (Reference 5). The licensee concludes that the actions documented in the Revision 2 report (Reference 5) and WCAP-11601 (Reference 3) resolve the issues identified in Bulletin 88-02.

2.2 Evaluation

The staff has reviewed the above-mentioned Revision 2 report (Reference 5) and finds that the updated information contained in this report does not affect the essential facts upon which the staff relied in its December 11, 1987 Safety Evaluation authorizing North Anna Unit 1 to return to 100% of licensed power operation.

A discussed earlier, the staff's conclusions in its December 11, 1987 SER were based in part on information contained in Westinghouse reports WCAP-11601 and WCAP-11602 (Reference 3). Information contained in more recent Westinghouse reports issued on behalf of other plants (e.g., Reference 6) indicate that local flow peaking effects associated with certain "as built" AVB insertion depth configurations play a more important role in causing high stability ratios than was recognized in Reference 3. The staff's generic evaluation of the more recent Westinghouse studies of local flow peaking effects is documented in Reference 7.

However, the staff's review of Reference 3 indicates that regions of the most significant flow peaking effects were included in the licensee's preventive plugging program at North Anna Unit 1. Therefore, the staff finds that direct consideration of the higher flow peaking effects now being estimated by Westinghouse would further increase the estimated stability ratio reductions which have been achieved at North Anna Unit 1 through preventive plugging. Thus, the more recent information which has become available concerning flow peaking effects does not impact the staff's conclusions in the December 11, 1987 Safety Evaluation.

3. NORTH ANNA UNIT 2

3.1 Discussion

The program implemented at North Anna Unit 2 to minimize the likelyhood of rapidly propagating fatigue cracks is described in Westinghouse report SG-88-03-016 (Reference 8) which was enclosed with the licensee's March 24,

1988 submittal. This program is very similar to that implemented at Unit 1. This included installation of downcomer flow resistance plates and preventive plugging of all tubes beyond row 8 which are not effectively supported by AVBs. These actions are estimated to reduce the stability ratios for the most limiting tubes remaining in service (i.e., tubes in row 8) by 24% compared to the tube which ruptured at North Anna Unit 1. This reduction satisfies the 10% reduction criteria developed by Westinghouse for North Anna Unit 1 and which was reviewed by the staff in its December 11, 1987 Safety Evaluation. The estimated reduction assumes flow peaking factors for tubes remaining in service equal to the 1.47 value exhibited by the tube which ruptured at North Anna Unit 1. Westinghouse states that row 8 tubes remaining in service have negligible potential for flow peaking and thus can be expected to exhibit stability ratios significantly smaller than 76% of that associated with the tube rupture at Unit 1.

The licensee's program for Unit 2 also included implementation of the enhanced primary-to-secondary leak rate monitoring program implemented at North Anna Unit 1. The licensee's request, dated December 4, 1987, to incorporate this enhanced monitoring program as part of the Technical Specifications applies to Unit 2 as well as Unit 1.

3.2 Evaluation

The licensee's program for Unit 2 is essentially the same as that implemented for North Anna Unit 1 which was reviewed and approved in the staff's Safety Evaluation dated December 11, 1987. The staff's review of the Westinghouse report for Unit 2, however, indicates that several tubes in row 8 may in fact exhibit a degree of flow peaking, contrary to the finding reached by Westinghouse. Although Westinghouse did not specifically address the flow peaking factors for these tubes, it is the staff's judgement, based on its review of flow peaking factor test data published in more recent Westinghouse reports (e.g., Reference 6), that the flow peaking factors for these row 8 tubes would be well within the 1.64 upper bound obtained from Westinghouse test data for the most limiting AVB configurations observed at any PWR to date. Making the extremely conservative assumption that certain row 8 tubes exhibit a flow peaking factor of 1.64, the staff estimates that the maximum stability ratios for row 8 tubes would still be 15% smaller than the stability ratio for the tube which ruptured at North Anna Unit 1. This still satisfies the 10% acceptance criteria developed by Westinghouse. Thus, the staff finds that the licensee's program for North Anna Unit 2 is acceptable.

4. CONCLUSIONS

Corrective actions at North Anna Units 1 and 2 in the form of installation of downcomer flow resistance plates and preventive plugging effectively minimize the likelyhood of rapidly propagating fatigue cracks of the type which led to the SGTR event in July 1987. The enhanced primary-to-secondary leak rate monitoring program implemented at both units provides added assurance that rapidly increasing leaks will be detected ensuring timely plant shutdown before rupture occurs. The staff concludes that the licensee has satisfactorily resolved the issues identified in Bulletin 88-02. Consistent with conclusions reached by the staff for other plants (see Reference 7), these findings are subject to the development of administrative controls by the licensee to ensure

- 4 -

that updated stability ratio and fatigue usage calculations are performed in the event of any significant changes to the steam generator operating parameters (e.g., steam flow and pressure, circulation ratio) relative to the reference parameters assumed in References 3 and 8 for units 1 and 2, respectively.

REFERENCES

1. Licensee's letter dated March 24, 1988, "North Anna Power Station Units 1 and 2, Response to Bulletin 88-02." NRC Accession No. 8803300328.

2. Licensee's letter dated September 15, 1987, enclosing licensee's report "North Anna Unit 1 July 15, 1987, Steam Generator Tube Rupture Report," Revision 1. NRC Accession No. 8709160239.

3. Westinghouse report WCAP-11601 (Proprietary Version) and WCAP-11602 (Non-Proprietary Version), "North Anna Unit 1 Steam Generator Tube Rupture and Remedial Actions Technical Evaluation," September 1987. NRC Accession Nos. 8710050087 and 8710050084.

4. NRC letter dated December 11, 1987 to Mr. W. L. Stewart, Virginia Electric and Power Company, enclosing proprietary and non-proprietary versions of staff's Safety Evaluation authorizing 100% power operation of North Anna Unit 1 following steam generator tube rupture event on July 15, 1987.

5. Licensee's report, "North Anna Unit 1 July 15, 1987, Steam Generator Tube Rupture Report," Revision 2. (This report is docketed as part of Reference 1 above.)

6. Westinghouse Report WCAP-11799 (Proprietary Version) and WCAP 11800 (Non-Proprietary Version), "Beaver Valley Units 1 and 2 - Evaluation for Tube Vibration Induced Fatigue," April 1988. NRC Accession No. 8805160073.

7. NRC staff memorandum dated August 19, 1988, C. Cheng to D. Neighbors, "Evaluation of Westinghouse Methodology to Address Item C.2 of NRC Bulletin 88-02".

8. Westinghouse report STD-7.2.2.1-8079, SG-88-03-016, "North Anna 2 Steam Generator Tube Fatigue Evaluation and Remedial Actions Report," dated March 16, 1988. NRC Accession No. 8803300330.
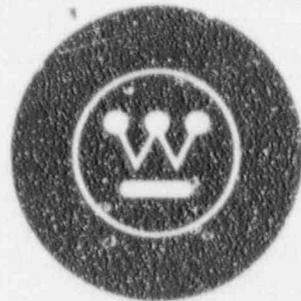
WCAP-12266

NORTH ANNA UNIT 2
EVALUATION FOR TUBE VIBRATION INDUCED FATIGUE

Westinghouse Energy Systems
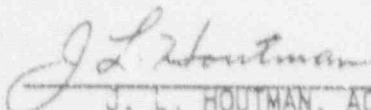
WCAP-12266

V.7

NORTH ANNA UNIT 2
EVALUATION FOR TUBE VIBRATION INDUCED FATIGUE

D/59

MAY 1989

AUTHORS: H. J. CONNORS M. H. HU
    T. M. FRICK   A. Y. LEE
    J. M. HALL   R. M. WILSON
    G. W. HOPKINS R. M. WEPFER
    J. L. HOUTMAN

APPROVED: _J. L. Houtman_____
    J. L. HOUTMAN, ACTING MANAGER
    STEAM GENERATOR ENGINEERING

9224M:1E-050189-1

ABSTRACT

On July 15, 1987, a steam generator tube rupture event occurred at North Anna
Unit 1. The cause of the tube rupture has been determined to be high cycle
fatigue. The source of the loads associated with the fatigue mechanism is a
combination of a mean stress level in the tube with a superimposed alternating
stress. The mean stress is the result of manufacturing induced residual
stress, applied stress and stress due to denting of the tube at the top tube
support plate, while the alternating stress is due to out-of-plane deflection
of the tube U-bend attributed to flow induced vibration. For tubes without
AVB support, local flow peaking effects at unsupported tubes are a significant
contribution to tube vibration amplitudes.

Subsequent to the tube rupture, a tube fatigue analysis was performed for the
North Anna 2 plant, and several modifications were implemented. Downcomer
flow resistance plates were installed in all steam generators, resulting in a
nominal [

                    $]^{a,c}$

Testing since this October, 1987, evaluation has determined that single-sided
support of the tubes is sufficient to limit fluidelastic excitation of the
tubes. Non-uniform AVB insertion configurations have been tested to define
AVB positions which, dependent upon local flow conditions, produce excessive
tube vibration. This analysis provides the justification for the removal of a
majority of the sentinel plugs installed in North Anna #2. The justification
is developed from a detailed AVB insertion mapping, updated thermal/hydraulic
analysis, and vibration analysis. The fatigue analysis considered the effects
of prior operating history on tube fatigue and of a postulated T_{hot} reduction.
The report concludes that two previously-installed sentinel plugs may be
required to remain in place, depending upon future operating conditions and
desired service period, and the remaining 116 sentinel plugs may be removed.

SUMMARY OF ABBREVIATIONS

ASME	-	American Society of Mechanical Engineers
ATHOS	-	Analysis of the Thermal Hydraulics of Steam Generators
AVB	-	Anti-Vibration Bar
AVT	-	All Volatile Treatment
ECT	-	Eody Current Test
EPRI	-	Electric Power Research Institute
FFT	-	Fast Fourier Transform
FLOVIB	-	Flow Induced Vibrations
MEVF	-	Modal Effective Void Fraction
OD	-	Outside Diameter
RMS	-	Root Mean Square
SR	-	Stability Ratio
TSP	-	Tube Support Plate

°F	-	degrees Fahrenheit
hr	-	hour
ksi	-	measure of stress - 1000 pounds per square inch
lb	-	pound
mils	-	0.001 inch
MW	-	mega watt
psi	-	measure of stress - pounds per square inch
psia	-	measure of pressure - absolute

TABLE OF CONTENTS

TABLE OF CONTENTS (CONTINUED)

LIST OF FIGURES

LIST OF FIGURES (Continued)

LIST OF TABLES

1.0 INTRODUCTION

This report documents the re-evaluation of steam generator tubing at North Anna Unit 2 for susceptibility to fatigue-induced cracking of the type experienced at North Anna Unit 1 in July, 1987. Its purpose is to identify susceptible tubes and thereby justify de-plugging tubes that were plugged in 1987 with sentinel plugs. The evaluation includes three-dimensional flow analysis of the tube bundle, air-tests performed to support the vibration analytical procedure, field measurements to establish AVB locations, structural and vibration analysis of selected tubes, and fatigue usage calculations to predict cumulative usage for critical tubes. The evaluation utilizes operating conditions specific to North Anna Unit 2 in order to account for plant specific features of the tube loading and response.

Section 2 of the report provides a summary of the North Anna Unit 2 evaluation results and overall conclusions. Section 3 provides background for the tube rupture event which occurred at North Anna Unit 1 including results of the examination of the ruptured tube and a discussion of the rupture mechanism. The criteria for predicting the fatigue usage for tubes having an environment conducive to this type of rupture are discussed in Section 4. Section 5 provides a summary of test data which supports the analytical vibration evaluation of the candidate tubes. A summary of field measurements used to determine AVB locations and to identify unsupported tubes is provided in Section 6. Section 7 provides the results of a thermal hydraulic analysis to establish flow field characteristics at the top support plate which are subsequently used to assist in identifying tubes which may be dynamically unstable. Section 8 presents an update of the methodology originally used to evaluate the tube rupture at North Anna Unit 1. The final section, Section 9, presents results of the structural and vibration assessment. This section describes stability ratio and tube stress distributions, and accumulated fatigue usage, for the North Anna Unit 2 steam generator small radius U-tubes.

2.0 SUMMARY AND CONCLUSIONS

The North Anna Unit 2 steam generators have been evaluated for the susceptibility of unsupported U-bend tubing with denting at the top tube support plate to a fatigue rupture of the type experienced at Row 9 Column 51 (R9C51) of Steam Generator C at North Anna Unit 1. The evaluation uses Eddy Current Test (ECT) data interpreted by Westinghouse.

2.1 Background

The initiation of the circumferential crack in the tube at the top of the top tube support plate at North Anna 1 has been attributed to limited displacement, fluid elastic instability. This condition is believed to have prevailed in the R9C51 tube since the tube experienced denting at the support plate. A combination of conditions were present that led to the rupture. The tube was not supported by an anti-vibration bar (AVB), had a higher flow field due to local flow peaking as a result of non-uniform insertion depths of AVBs, had reduced damping due to denting at the top support plate, and had reduced fatigue properties due to the environment of the all volatile treatment (AVT) chemistry of the secondary water and the additional mean stress from the denting.

2.2 Evaluation Criteria

The criteria established to provide a fatigue usage less than 1.0 for a finite period of time (i.e., 40 years) is a 10% reduction in stability ratio that provides at least a 58% reduction in stress amplitude (to < 4.0 ksi) for a Row 9 tube in the North Anna 1 steam generators (SGs). This reduction is required to produce a fatigue usage of < 0.021 per year for a Row 9 tube in North Anna and therefore greater than 40 year fatigue life objective. This same fatigue criteria is applied as the principal criteria in the fatigue evaluation reported herein.

The fluidelastic stability ratio is the ratio of the effective velocity divided by the critical velocity. A value greater than unity (1.0) indicates instability. The stress ratio is the expected stress amplitude in a North Anna tube divided by the stress amplitude for the North Anna 1, R9C51 tube.

Displacements are computed for the unsupported U-bend tubes in Rows 11 and inward, (descending row number) using relative stability ratios to R9C51 of North Anna 1 and an appropriate power law relationship based on instability displacement versus flow velocity. Different U-bend radius tubes will have different stiffness and frequency and, therefore, different stress and fatigue usage per year than the Row 9 North Anna tube. These effects are accounted for in a stress ratio technique. The stress ratio is formulated so that a stress ratio of 1.0 or less produces acceptable stress amplitudes and fatigue usage for the North Anna tubing for the reference fuel cycle analyzed. Therefore, a stress ratio less than 1.0 provides the next level of acceptance criteria for unsupported tubes for which the relative stability ratio, including flow peaking, exceed 0.9.

The stability ratios for North Anna 2 tubing, the corresponding stress amplitude, and the resulting cumulative fatigue usage must be evaluated relative to the ruptured tube at Row 9 Column 51, North Anna 1, Steam Generator C, for two reasons. The local effect on the flow field due to various AVB insertion depths is not within the capability of available analysis techniques and is determined by test as a ratio between two AVB configurations. In addition, an analysis and examination of the ruptured tube at North Anna 1 provided a range of initiating stress amplitudes, but could only bound the possible stability ratios that correspond to these stress amplitudes. Therefore, to minimize the influence of uncertainties, the evaluation of North Anna 2 tubing has been based on relative stability ratios, relative flow peaking factors, and stress ratios.

The criteria for establishing that a tube has support from an AVB and therefore eliminate it from further considerations is that it must have at least one sided AVB support present at the tube centerline. The criteria is based on test results which show that one sided AVB support is sufficient to

limit the vibration amplitude for fluidelastic excitation. AVB support is established by analysis of eddy current (EC) measurements and is a key factor in the determining the local flow peaking factors. The local flow peaking produces increased local velocities which cause an increase in stability ratio. A small percentage change in the stability ratio causes a significant change in stress amplitude. The relative flow peaking factors for North Anna tubing without direct AVB support have been determined by test. These flow peaking factors normalized to the North Anna R9C51 peaking, are applied to relative stability ratios determined by 3-D tube bundle flow analysis, to obtain the combined relative stability ratio used in the stress ratio determination.

2.3 Denting Evaluation

The Eddy Current (EC) tapes were evaluated to determine the condition of the tube/tube support interface of unsupported tubes immediately below the apexes of the AVBs. Analysis of the August-September 1987 North Anna 2 eddy current inspection data indicated that most of the tubes had crevice corrosion product buildups at the top tube support plate, but were not dented with deformation. Of the 118 tubes recommended for preventive plugging, 104 tubes were evaluated as having top tube support plate corrosion, 2 showed denting with deformation, 6 showed no detectable denting (or crevice corrosion product), and 6 were unreadable. Per the NRC Bulletin 88-02 definition, all but the 6 tubes showing no detectable denting are required to be considered as dented in the analysis. For conservatism in the evaluation, all of the tubes evaluated are postulated as being dented. The effect of denting on the fatigue usage of the tube has been conservatively maximized by assuming the maximum effect of mean stress in the tube fatigue usage evaluation and by incorporating reduced damping in the tube vibration evaluation.

2.4 AVB Insertion Depths

The North Anna Unit 2 SGs have two sets of Alloy 600 AVBs. The lower AVBs have a rectangular cross-section and extend into the tube bundle approximately as far as Row 11. They provide a nominal total clearance between a tube

without ovality and the surrounding AVBs of [   ]^{a,c} inch. Including
average tube ovality for a Row 11 tube, the nominal total tube to AVB
clearance is about [   ]^{a,c} inches.

The upper AVBs also have a rectangular cross section and extend into the tube
bundle approximately as far as Row 13, providing a nominal tube-to-AVB
clearance comparable to the inner AVBs. Since the purpose of this analysis is
to evaluate the potentially unsupported tubes at or near the point of maximum
AVB insertion, only the dimensions and EC data pertaining to the lower AVBs
are required.

The eddy current data for North Anna 2 were reviewed to identify the number of
tube/AVB intersections and the location of these intersections relative to the
apex of a given tube. This information was used in calculations to determine
the deepest penetration of a given AVB into the tube bundle. For the North
Anna 2 steam generators, the AVB support can normally be verified if EC data
shows both legs of the lower AVB, one on each side (hot leg - cold leg) of the
U-bend. This is the preferred method of establishing AVB support.

If only the apex of a North Anna 2 AVB assembly is near or touching the apex
of a tube U-bend, only one AVB signal may be seen. In this case, adequate
tube support cannot be assumed without supplemental input. Support can be
determined if projection calculations based on the AVB intercepts of higher
row number tubes in the same and adjacent columns verify insertion depth to a
point below the tube centerline. Maps of the AVB insertion depths for North
Anna 2 are shown in Figures 6-2 through 6-4. These AVB maps list the results
of the projection calculations from the smallest row tube for which suitable
data exist to make a projection.

2.5 Flow Peaking Factors

AVB position evaluations were used in evaluating the local flow peaking
factors. Local flow peaking produces increased local velocities which cause
an increase in stability ratio. A small percentage change in the stability
ratio can cause a significant change in stress amplitude. The test-based flow

peaking factors are normalized to the North Anna R9C51 peaking, and are applied to relative stability ratios determined by 3-D tube bundle flow analysis to obtain the combined relative stability ratio used in the stress ratio determination.

2.6 Tube Vibration Evaluation

The calculation of relative stability ratios for North Anna 2 makes use of detailed tube bundle flow field information computed by the ATHOS steam generator thermal/hydraulic analysis code. Code output includes three-dimensional distributions of secondary side velocity, density, and void fraction, along with primary fluid and tube wall temperatures.

Relative stability ratios of pre-DFRP, post-DFRP and post-T_{hot} reduction North Anna Unit 2 (Row 8 through Row 12) tubing (relative to Premod R9C51 of North Anna 1) are plotted in Figures 9-1, 9-2 and 9-3, respectively. These relative stability ratios include relative flow peaking factors. Stress ratios of pre-DFRP, post-DFRP, and post-T_{hot} reduction for North Anna Unit 1 are plotted in Figures 9-4, 9-5, and 9-6, and are calculated based on clamped tube conditions with denting at the tube support plate. For all three steam generators, the stress ratios for all remaining tubes in Rows 8 through 11 are less than or equal to 1.0, even when the tubes are assumed to be unsupported.

One-dimensional performance and relative stability ratio analyses of operating data for North Anna #2 have been completed for each fuel cycle since the plant became operational in 1980. These data include operation prior to the installation of downcomer flow resistance plates (and prior to the tube rupture event in Unit #1), recent operation in Cycle 6 following the installation of the plates, and projected operation with reduced primary water temperature and steam pressure. The latter conditions were based on a December 1988 test with the turbine valves wide open to obtain the lowest possible steam pressure which can be obtained while still maintaining full power. Reduced steam pressures are of interest because they result in higher, potentially more limiting stability ratios.

Comparisons of 1-D relative stability ratios calculated for each of these conditions are made with the ratios determined for the corresponding conditions in Unit #1. In all cases, the stability ratios for the Unit #2 conditions are within 1% of the ratios calculated for the corresponding conditions in Unit #1. Based on this close agreement, the results of the existing 3-D ATHOS flow field/stabilty ratio evalution for Unit #1 are applied to Unit #2, with only small adjustment factors from the 1-D stability ratio evaluations.

Lists identifying the support conditions determined in the analysis, for use with the AVB insertion maps, are provided in Tables 6-1 and 6-2. Relative stability ratios and stress ratios of North Anna #2 Row 8 through 12 tubes versus R9C51 of North Anna #1 are listed by steam generator in Tables 9-1 and 9-2. Both the relative stability ratios and the stress ratios include relative flow peaking factors. The stress ratios are calculated assuming that the tubes were dented immediately after initial startup.

Table 9-3 contains a summary of fatigue usage factors for tubes that have stress ratios near or greater than 1.00 (calculated using the more limiting Premod conditions and assuming the tubes became dented since the first cycle). As can be observed in the table, all tubes currently have fatigue usage factors less than 1.00. Future usage factors have been determined for operation under current operating conditions and for conditions where T_{hot} reduction is implemented. Results are presented for both 40 years of total operation and for 10 more years of operation. These results indicate that, for a total of 40 years of operation, two tubes are at potential risk if T_{hot} reduction is implemented. These two tubes (SG:A R9C60 and SG:B R9C35) currently have usage factors equal to 0.49 but will have projected fatigue usage factors greater than 1.00 after 40 years of total operation. Usage factors calculated after 10 more years of operation (with T_{hot}' implemented) have been determined to be 0.84.

2.7 Overall Conclusion

The results of the fatigue evaluation indicate that currently no tubes in the North Anna Unit 2 steam generators require preventative action to preclude a

North Anna Unit 1 R9C51 type tube rupture and that any tubes currently plugged with sentinel plugs, to detect such a rupture, can be returned to service. However, two tubes previously identified, SG:A R9C60 and SG:B R9C35, will require preventive action in the future, to preclude such a rupture, after at least 10 more years of service. Note that in the event of a future uprating or increase in general plugging level the potential for tube fatigue would need to be re-evaluated.

3.0 BACKGROUND

On July 15, 1987, a steam generator tube rupture occurred at the North Anna
Unit 1. The ruptured tube was determined to be Row 9 Column 51 in steam
generator "C". The location of the opening was found to be at the top tube
support plate on the cold leg side of the tube and was circumferential in
orientation with a 360 degree extent.

3.1 North Anna Unit 1 Tube Rupture Event

The cause of the tube rupture has been determined to be high cycle fatigue.
The source of the loads associated with the fatigue mechanism has been
determined to be a combination of a mean stress level in the tube and a
superimposed alternating stress. The mean stress has been determined to have
been increased to a maximum level as the result of denting of the tube at the
top tube support plate and the alternating stress has been determined to be
due to out-of-plane deflection of the tube U-bend above the top tube support
caused by flow induced vibration. These loads are consistent with a lower
bound fatigue curve for the tube material in an AVT water chemistry
environment. The vibration mechanism has been determined to be fluid elastic,
based on the magnitude of the alternating stress.

A significant contributor to the occurrence of excessive vibration is the
reduction in damping at the tube-to-tube support plate interface caused by the
denting. Also, the absence of antivibration bar (AVB) support has been
concluded to be required for requisite vibration to occur. The presence of an
AVB support restricts tube motion and thus precludes the deflection amplitude
required for fatigue. Inspection data shows that an AVB is not present for
the Row 9 Column 51 tube but that the actual AVB installation depth exceeded
the minimum requirements in all cases with data for AVBs at many other Row 9
tubes. Also contributing significantly to the level of vibration, and thus
loading, is the local flow field associated with the detailed geometry of the
steam generator, i.e., AVB insertion depths. In addition, the fatigue
properties of the tube reflect the lower range of properties expected for an

AVT environment. In summary, the prerequisite conditions derived from the evaluations were concluded to be:

Fatigue Requirements	Prerequisite Conditions
Alternating stress	Tube vibration
	- Dented support
	- Flow excitation
	- Absence of AVB
Mean stress	Denting in addition to applied stress
Material fatigue properties	AVT environment
	- Lower range of properties

3.2 Tube Examination Results

Fatigue was found to have initiated on the cold leg outside surface of Tube R9C51 immediately above the top tube support plate. No indications of significant accompanying intergranular corrosion was observed on the fracture face or on the immediately adjacent OD surfaces. Multiple fatigue initiation sites were found with major sites located at 110°, 120°, 135° and 150°, Figure 3-1. The plane of the U-bend is located at 45° with the orientation system used, or approximately 90° from the geometric center of the initiation zone at Section D-D. High cycle fatigue striation spacings approached 1 micro-inch near the origin sites, Figure 3-2. The early crack front is believed to have broken through-wall from approximately 100° to 140°. From this point on, crack growth is believed (as determined by striation spacing, striation direction, and later observations of parabolic dimples followed by equiaxed dimples) to have accelerated and to have changed direction with the resulting crack front running perpendicular to , circumferential direction.

3.3 Mechanism Assessment

To address a fatigue mechanism and to identify the cause of the loading, any loading condition that would cause cyclic stress or steady mean stress had to be considered. The analysis of Normal, Upset and Test conditions indicated a relatively low total number of cycles involved and a corresponding low fatigue usage, even when accounting for the dented tube condition at the plate. This analysis also showed an axial tensile stress contribution at the tube OD a short distance above the plate from operating pressure and temperature, thus providing a contribution to mean stress. Combining these effects with denting deflection on the tube demonstrated a high mean stress at the failure location. Vibration analysis for the tube developed the characteristics of first mode, cantilever response of the dented tube to flow induced vibration for the uncracked tube and for the tube with an increasing crack angle, beginning at 90° to the plane of the tube and progressing around on both sides to complete separation of the tube.

Crack propagation analysis matched cyclic deformation with the stress intensities and striation spacings indicated by the fracture inspection and analysis. Leakage data and crack opening analysis provided the relationship between leak rate and circumferential crack length. Leakage versus time was then predicted from the crack growth analysis and the leakage analysis with initial stress amplitudes of 5, 7, and 9 ksi   The comparison to the best estimate of plant leakage (performed after the event) showed good agreement, Figure 3-3.

Based on these results, it followed that the predominant loading mechanism responsible is a flow-induced, tube vibration loading mechanism. It was shown that of the two possible flow-induced vibration mechanisms, turbulence and fluidelastic instability, that fluidelastic instability was the most probable cause. Due to the range of expected initiation stress amplitudes (4 to 10 ksi), the fluidelastic instability would be limited in displacement to a range of approximately [   ]^{a,c}. This is less than the distance between tubes at the apex, [   ]^{d,c}. It was further

confirmed that displacement prior to the rupture was limited since no indication of tube U-bend (apex region) damage was evident in the eddy-current signals for adjacent tubes.

Given the likelihood of limited displacement, fluidelastic instability, a means of establishing the change in displacement, and corresponding change in stress amplitude, was developed for a given reduction in stability ratio (SR). Since the rupture was a fatigue mechanism, the change in stress amplitude resulting from a reduction in stability ratio was converted to a fatigue usage benefit through the use of the fatigue curve developed. Mean stress effects were included due to the presence of denting and applied loadings. The results indicated that a 10% reduction in stability ratio is needed (considering the range of possible initiation stress amplitudes) to reduce the fatigue usage per year to less than 0.02 for a tube similar to Row 9 Column 51 at North Anna Unit 1.
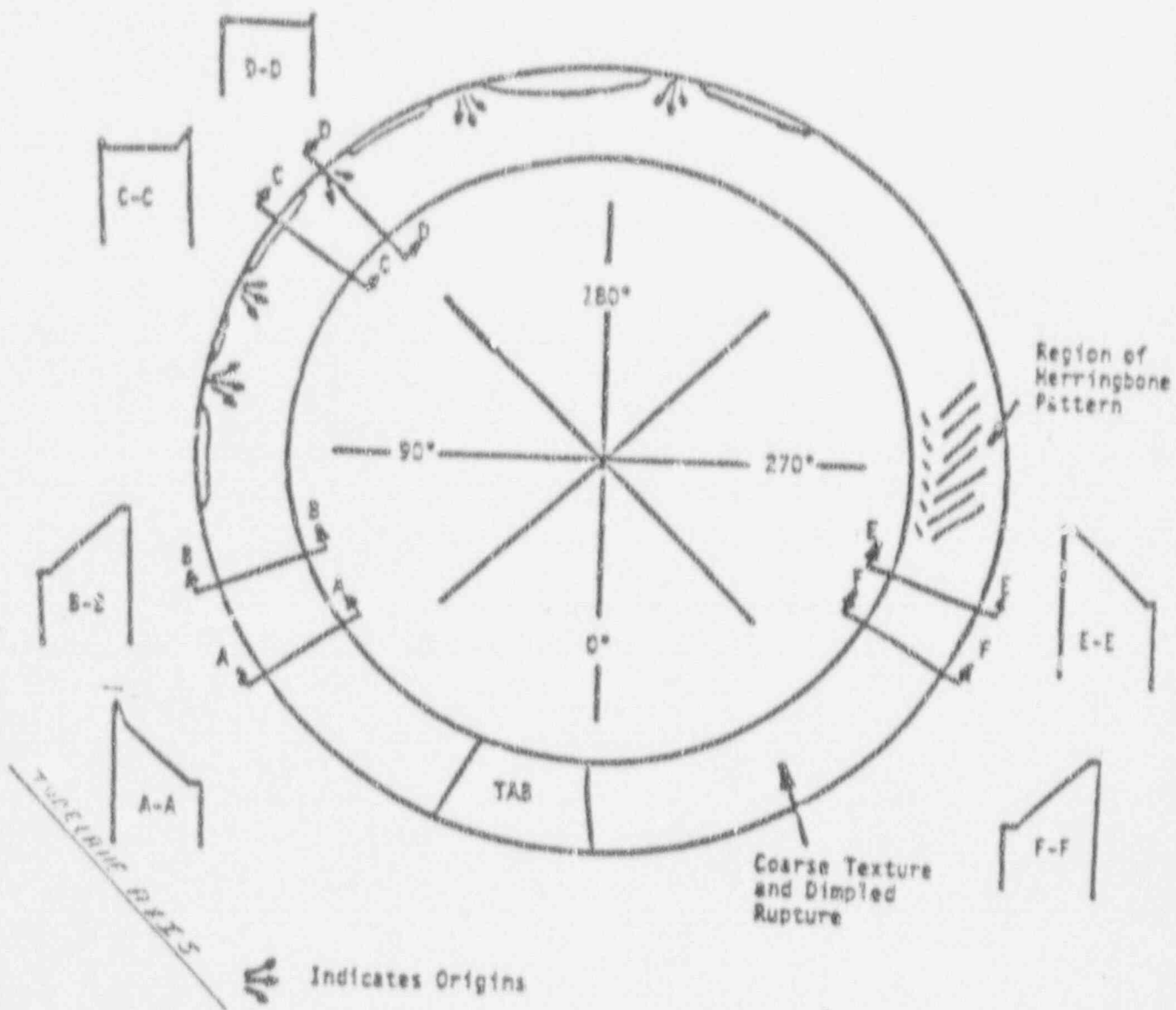
Figure 3-1 Approximate Mapping of Fracture Surface of Tube R9C51,
S/G "C" Cold Leg, North Anna Unit 1
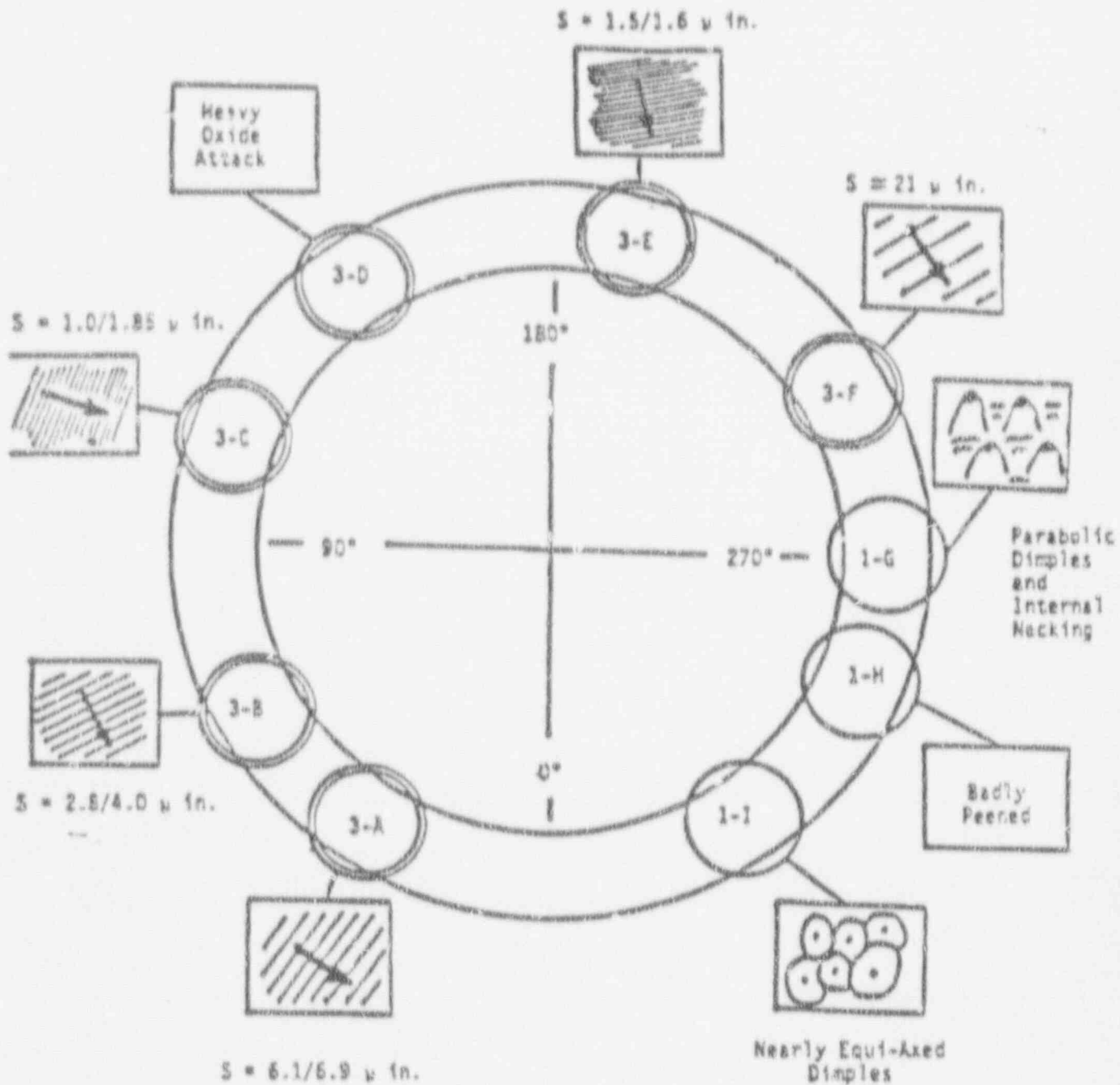
Figure 3-2 Schematic Representation of Features Observed During
TEM Fractograhic Examination of Fracture Surface of
Tube R9C51, S/G "C" Cold Leg, North Anna Unit 1

Calculated and observed leak rates versus time.
Observed values based on gaseous species condenser
air ejector

SIGMA A = 5 KSI
SIGMA A = 7 KSI
SIGMA A = 9 KSI
O   Ar-41
□   Xe-135
△   Kr-87

LEAK RATE, SFD

TIME, MINUTES
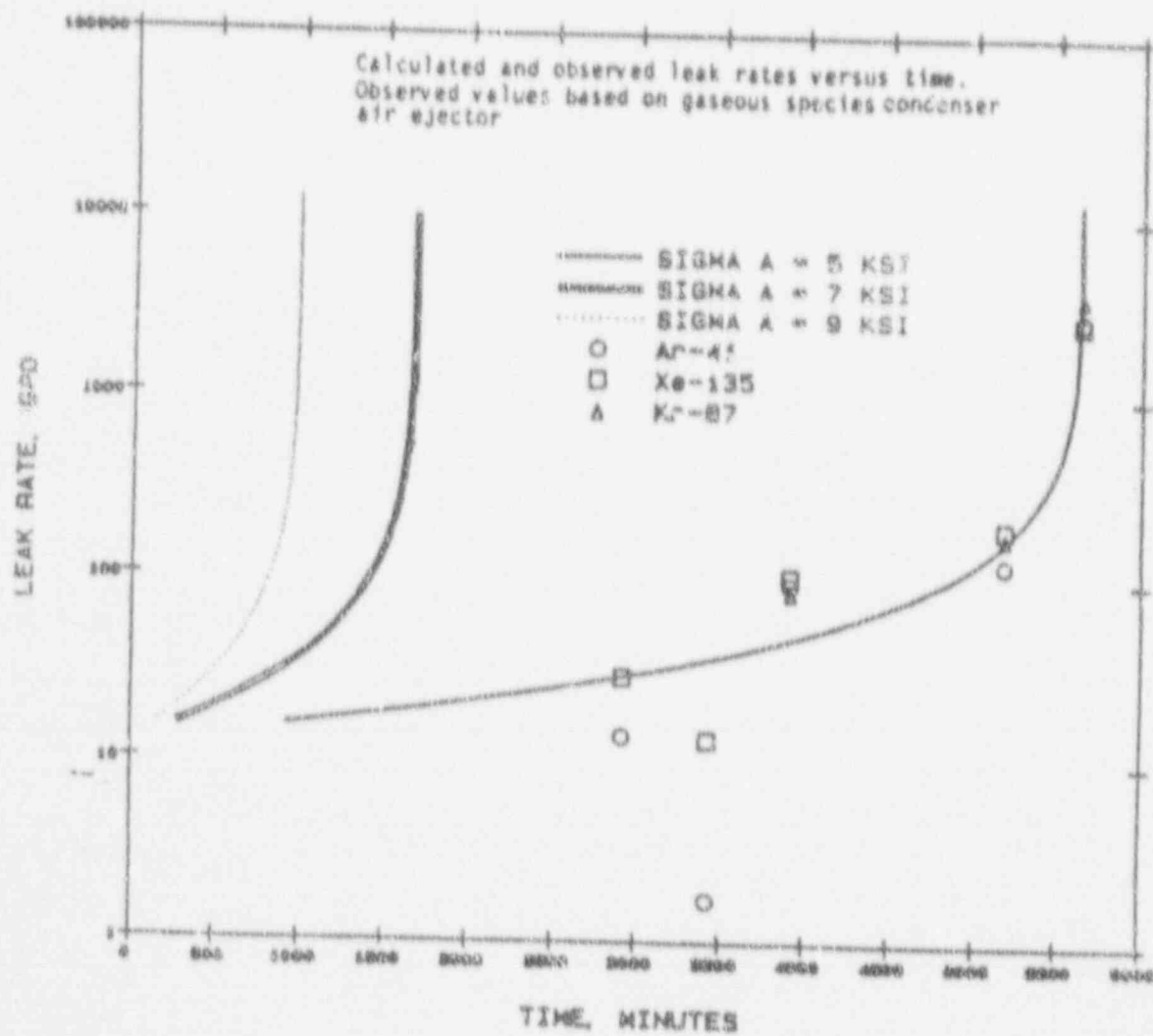
Figure 3-3 Calculated and Observed Leak Rates Versus Time

4.0 CRITERIA FOR FATIGUE ASSESSMENT

The evaluation method and acceptance criteria are based on a relative comparison with the Row 9 Column 51 tube of North Anna Unit 1 Steam Generator C. This approach is necessary because (1) methods for direct analytical prediction of actual stability ratios incorporate greater uncertainties than a relative ratio method, and (2) the stress amplitude (or displacement) associated with a specific value of stability ratio can only be estimated by the analysis of R9C51. For these reasons, the North Anna Unit 2 tubing evaluation was done on a relative basis to Row 9 Column 51 and a 10% reduction in stability ratio criteria was established to demonstrate that tubes left in service would be expected to have sufficiently low vibration stress to preclude future fatigue rupture events.

To accomplish the necessary relative assessment of North Anna Unit 2 tubing to the North Anna Unit 1 Row 9 Column 51 several criteria are utilized. First, stability ratios are calculated based on flow fields predicted by 3-D thermal hydraulic models and ratioed to the stability ratio for Row 9 Column 51. These ratios of stability ratio (called relative stability ratios) for each potentially unsupported U-bend in the North Anna Unit 2 steam generators should be equivalent to ≤ 0.9 of (the pre-modification) North Anna Unit 1 R9C51 (meeting the 10% reduction in stability ratio criteria). This provides the first level of screening of susceptible tubes incorporating all tube geometry and flow field differences in the tube dynamic evaluation. It has the inherent assumption, however, that each tube has the same local, high flow condition present at Row 9 Column 51. To account for these differences, flow peaking factors can be incorporated in the relative stability ratios and the relative stress ratios.

The next step is to obtain stress ratios, the ratio of stress in the North Anna 2 tube of interest to the stress in North Anna 1 Row 9 Column 51 and after incorporating the requirement that the relative stability ratio to Row 9 Column 51 (R9C51) for the tube of interest is equivalent to ≤ 0.9, require the stress ratio to be ≤ 1.0. The stress ratio incorporates the tube geometry differences with R9C51 in relation to the stress calculation and also

incorporates the ratio of flow peaking factor for the tube of interest to the flow peaking factor for R9C51 (flow peaking factor is defined in Section 4.2). This should provide that all tubes meeting this criteria have stress amplitudes equivalent to $\leq$ 4.0 ksi.

Finally, the cumulative fatigue usage for plant operation to date and for continued operation with the planned operating parameters is evaluated. A fatigue usage of $\leq$ 1.0 may not be satisfied by meeting the stress ratio criteria using the reference operating cycle evaluation since the reference cycle does not necessarily represent the exact duty cycle to date. Therefore, the time history of operation is evaluated on a normalized basis and used together with the stress ratio to obtain a stress amplitude history. This permits the calculation of current and future fatigue usage for comparison to 1.0.

4.1 Stability Ratio Reduction Criteria

For fluidelastic evaluation, stability ratios are determined for specific configurations of a tube. These stability ratios represent a measure of the potential for flow-induced tube vibration during service. Values greater than unity (1.0) indicate instability (see Section 5.1).

Motions developed by a tube in the fluidelastically unstable mode are quite large in comparison to the other known mechanisms. The maximum modal displacement (at the apex of the tube) is linearly related to the bending stress in the tube just above the top tube support plate. This relationship applies to any vibration in that mode. Thus, it is possible for an unstable, fixed boundary condition tube to deflect an amount in the U-bend which will produce fatigue inducing stresses.

The major features of the fluidelastic mechanism are illustrated in Figure 4-1. This figure shows the displacement response (LOG D) of a tube as a function of stability ratio (LOG SR). A straight-line plot displayed on log-log coordinates implies a relation of the form $y = A(x)^n$, where A is a constant, x is the independent variable, n is the exponent (or power to which x is raised), and y is the dependent variable. Taking logs of both sides of this equation leads to the slope-intercept form of a straight-line equation in log form, $\log y = c + n \log x$, where $c = \log A$ and represents the intercept and n is the slope. In our case the independent variable x is the stability ratio SR, and the dependent variable y is tube (fluidelastic instability induced) displacement response D, and the slope n is renamed s.

From experimental results, it is known that the turbulence response curve (on log-log coordinates) has a slope of approximately [ ]a,b,c. Test results also show that the slope for the fluidelastic response depends somewhat on the instability displacement (response amplitude). It has been shown by tests that a slope of [   ]a,b,c is a range of values corresponding to displacement amplitudes in the range of [   ]d,c, whereas below [   ]a,c are conservative values.

The reduction in response obtained from a stability ratio reduction can be expressed by the following equation:

$$\left[\right]^{a,c}$$

where D_1 and SR_1 are the known values at the point corresponding to point 1 of Figure 4-1 and D_2 and SR_2 are values corresponding to any point lower on this curve. Therefore, this equation can be used to determine the reduction in displacement response for any given reduction in stability ratio.

This equation shows that there is benefit derived from even a very small percentage change in the stability ratio. It is this reduction in displacement for a quite small reduction in stability ratio that formed the basis for demonstrating that a 10% reduction in stability ratio would be sufficient to prevent Row 9 Column 51 from rupturing by fatigue.

The fatigue curve developed for the North Anna Unit 1 tube at R9C51 is from
[

]^{a,c}. Thus,

$$
\left[\qquad\qquad\qquad \right]^{a,c}
$$

where, σ_a is the equivalent stress amplitude to σ_c that accounts
for a maximum stress of σ_y, the yield strength. The -3 sigma curve with
mean stress effects is shown in Figure 4-2 and is compared to the ASME Code
Design Fatigue Curve for Inconel 600 with the maximum effect of mean stress.
The curve utilizeo in this evaluation is clearly well below the code curve
reflecting the effect of an AVT environment on fatigue and [
                ]^{a,c} for accounting for mean stress that applies to materials
in a corrosive environment.

Two other mean stress models were investigated for the appropriateness of their
use in providing a reasonable agreement with the expected range of initiating
stress amplitudes. These were the [   ]^{a,c}
shown in Figure 4-3. With a [
        ]^{a,c}, the [

]^{a,c}.

The assessment of the benefit of a reduction in stability ratio begins with the relationship between stability ratio and deflection. For a specific tube geometry, the displacement change is directly proportional to change in stress so that stress has the same relationship with stability ratio,

$$\left[\right]^{a,c}$$

The slope in this equation can range from [   ]^{a,c} on a log scale depending on the amplitude of displacement. Knowing the stress resulting from a change in stability ratio from SR_1 to SR_2, the cycles to failure at the stress amplitude was obtained from the fatigue curve. A fatigue usage per year was then determined assuming continuous cycling at the natural frequency of the tube. The initial stress was determined to be in the range of 4.0 to 10.0 ksi by the fractography analysis.

It was further developed that the maximum initiating stress amplitude was not more than 9.5 ksi. This was based on [

]^{a,c}. The corresponding stress level is 5.6 ksi.

The maximum stress, 9.5 ksi, would be reduced to [   ]^{a,c} with a 10% reduction in stability ratio and would have a future fatigue usage of [   ]^{a,c} per year at 75% availability, Figure 4-4. The minimum stress, 5.6 ksi, would be reduced to [   ]^{a,c} ksi with a 5% reduction in stability ratio and would have future fatigue usage of [   ]^{a,c} per year, Figure 4-5. In addition, if a tube were already cracked, the crack could be as large as [   ]^{a,c} inch in length and thru-wall and would not propagate if the stress amplitudes are reduced to $\leq$ 4.0 ksi.

Subsequent to the return to power evaluation for North Anna Unit 1, the time history of operation was evaluated on a normalized basis to the last cycle, confirming the conservatism of 9.5 ksi. [

                                    ]^{a,c}, cumulative fatigue usage may then be computed to get a magnitude of alternating stress for the last cycle that results in a cumulative usage of 1.0 for the nine-year duty cycle. The result of the iterative analysis is that the probable stress associated with this fatigue curve during the last cycle of operation was approximately [   ]^{a,c} for R9C51, North Anna Unit 1, Steam Generator C, and that the major portion of the fatigue usage came in the second, third and fourth cycles. The first cycle was conservatively omitted, since denting is assumed, for purposes of this analysis, to have occurred during that first cycle. Based on this evaluation, the tube fatigue probably occurred over most of the operating history of North Anna Unit 1.

A similar calculation can be performed for the time history of operation assuming that [

   ]^{a,c}. On this basis, the effect of a 10% reduction in stability ratio is to reduce the stress amplitude to 4.0 ksi and results in a future fatigue usage of [   ]^{a,c}.

Other combinations of alternating stress and mean stress were evaluated with -3 sigma and -2 sigma fatigue curves to demonstrate the conservatism of the 10% reduction in stability ratio. Table 4-1 presents the results of the cases analyzed clearly demonstrating that the 10% reduction in stability ratio combined with a -3 sigma fatigue curve and with maximum mean stress effects is conservative. Any higher fatigue curve whether through mean stress, mean stress model, or probability, results in greater benefit for the same reduction in stability ratio. Further, for any of these higher curves, a smaller reduction in stability ratio than 10% would result in the same

in the air tests and is considered to be the best estimate of the range of the R9C51 flow peaking factor.

The range of stability ratios, 1.1 to 1.4, is based on a value of 0.63 obtained with ATHOS results without flow peaking and with nominal damping that is a function of modal effective void fraction (MEVF). MEVF is calculated using the formula:

$$a,c$$

The nominal damping reflects the nominal reduction in damping that occurs with denting at the tube support plate. Therefore, a minimum damping scenario that is independent of void fraction is not considered to be credible and is not addressed in the evaluation that follows.

4.3 Stress Ratio Considerations

In Section 4.1, a 10% reduction in stability ratio was established to reduce the stress amplitude on the Row 9 Column 51 tube of North Anna Unit 1 to a level that would not have ruptured, 4.0 ksi. To apply this same criteria to another tube in the same or another steam generator, the differences in [

$$]^{a,c}$$

$$a,c$$

The quantities with subscript NA refer to R9C51, and the quantities without subscripts refer to the tube being evaluated.

Using the displacement versus stability ratio relationship defined in Section 4.1,

a,c

By establishing their equivalent effect on the stress amplitude that produced the tube rupture at R9C51 several other effects may be accounted for. These include a lower mean stress (such as for non-dented tubes) and different frequency tubes from the [ ]^{a,c,e} hertz frequency of R9C51, North Anna 1.

In the case of lower mean stress, the stress amplitude that would have caused the failure of R9C51, North Anna 1, would have been higher. [

]^{a,c}.

A lower or higher frequency tube would not reach a usage of 1.0 in the same length of time as the R9C51 tube due to the different frequency of cycling. The usage accumulated is proportional to the frequency and, therefore, the allowable number of cycles to reach a usage of 1.0 is inversely proportional to frequency. The equivalent number of cycles to give the usage of 1.0 for a different frequency tube [is used to obtain a stress amplitude different from 9.5 ksi that gives the equivalent result. The ratio of these stresses becomes a factor times the above stress ratio expression to account for a frequency effect]^{a,c}.

Knowing the magnitude of the stress ratio allows 1) the determination of tubes that do not meet a value of $\leq$ 1, and 2) the calculation of maximum stress in the acceptable tubes,

$$\left[\right]^{a,c}$$

Having this maximum stress permits the evaluation of the maximum fatigue usage for North Anna Unit 2 tubes based on the time history expressed by normalized stability ratios for the duty cycle (see Section 7.4).

Table 4-1
Fatigue Usage per Year Resulting
From Stability Ratio Reduction

SR, % REDUCTION	STRESS BASIS[1]	FATIGUE CURVE[2]	MEAN STRESS MODEL	USAGE PER YEAR
5.	9 yrs to fail [ ]a,c			⌐a,c
5.	9 yrs to fail [ ]a,c			
5.	9 yrs to fail [ ]a,c			
10.	max. stress amplitude[4] [ ]a,c			
10.	max. stress amplitude[4] [ ]a,c			
10.	max. stress amplitude[4] [ ]a,c			
10.	max. stress amplitude[4] [ ]a,c			
10.	max. stress based on duty cycle[5] [ ]a,c			

---

(1) This gives the basis for selection of the initiating stress amplitude and its value in ksi.

(2) S_m is the maximum stress applied with $S_m = S_{mean} + S_a$.

(3) [   ]a,c.

(4) Cycles to failure implied by this combination of stress and fatigue properties is notably less than implied by the operating history. Consequently this combination is a conservative, bounding estimate.

(5) Cycles to failure implied by the operating history requires [   ]a,c fatigue curve at the maximum stress of [   ]a,c.

a,b,c

Figure 4-1 Vibration Displacement vs. Stability Ratio

B,C

Figure 4-3 Fatigue Curve for Inconel 600 in AVT Water
Comparison of Mean Stress Correction Models

B,C

Figure 4-4   Modified Fatigue with 10% Reduction in Stability
Ratio for Maximum Stress Condition

a,c
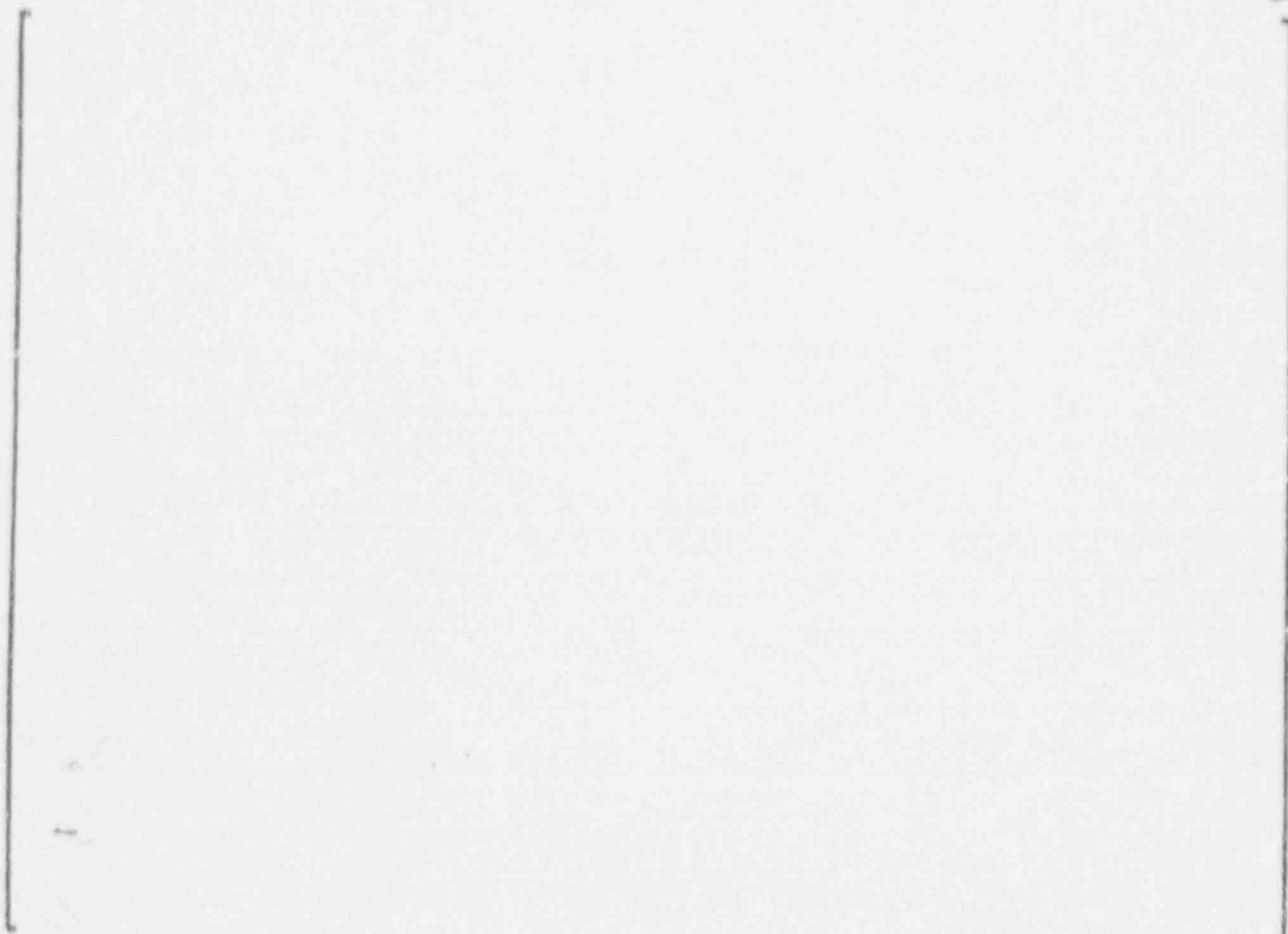
Figure 4-5 Modified Fatigue with 5% Reduction in Stability
Ratio for Minimum Stress Condition

5.0 SUPPORTING TEST DATA

This section provides a mathematical description of the fluidelastic
mechanism, which was determined to be the most likely causative mechanism for
the North Anna tube rupture, as discussed in Section 3.3, to highlight the
physical conditions and corresponding parameters directly related to the event
and associated preventative measures. The basis for establishing the
appropriate values and implications associated with these parameters are
provided. Where appropriate, test results are presented.

5.1 Stability Ratio Parameters

Fluidelastic stability ratios are obtained by evaluations for specific
configurations, in terms of active tube supports, of a specific tube. These
stability ratios represent a measure of the potential for tube vibration due
to instability during service. Fluidelastic stability evaluations are
performed with a computer program which provides for the generation of a
finite element model of the tube and tube support system. The finite element
model provides the vehicle to define the mass and stiffness matrices for the
tube and its support system. This information is used to determine the modal
frequencies (eigenvalues) and mode shapes (eigenvectors) for the linearly
supported tube being considered.

The methodology is comprised of the evaluation of the following equations:

Fluidelastic stability ratio = SR = U_{en}/U_c for mode n,

where U_c (critical velocity) and U_{en} (effective velocity) are determined
by:

$$U_c = \beta \, f_n \, D \, [(m_o \, \delta_n) \, / \, (\rho_o \, D^2)]^{1/2} \tag{1}$$

and;

$$U_{en}^2 = \frac{\sum_{j=1}^{N} (\rho_j/\rho_o) \, U_j^2 \, \phi_{jn}^2 \, z_j}{\sum_{j=1}^{N} (m_j/m_o) \, \phi_{jn}^2 \, z_j} \tag{2}$$

where,

D =   tube outside diameter, inches

U_{en} =   effective velocity for mode n, inches/sec

N =   number of nodal points of the finite element model
          =   number of degrees of freedom in the out-of-plane direction

m_j, U_j, ρ_j =   mass per unit length, crossflow velocity and fluid
               density at node j, respectively

ρ_o, m_o =   reference density and a reference mass per unit
               length, respectively (any representative values)

δ_n =   logarithmic decrement (damping)

ϕ_{jn} =   normalized displacement at node j in the nth mode of vibration

z_j =   average of distances between node j to j-1, and j to j+1

β =   an experimentally correlated stability constant

Substitution of Equations [1] and [2] into the expression which defines stability ratio, and cancellation of like terms, leads to an expression in fundamental terms (without the arbitrary reference mass and density parameters). From this resulting expression, it is seen that the stability ratio is directly related to the flow field in terms of the secondary fluid velocity times square-root-density distribution (over the tube mode shape), and inversely related to the square root of the mass distribution, square root of modal damping, tube modal frequency, and the stability constant (beta).

The uncertainty in each of these parameters is addressed in a conceptual manner in Figure 5-1. The remainder of this section (Section 5.0) provides a discussion, and, where appropriate, the experimental bases to quantitatively establish the uncertainty associated with each of these parameters. In

addition, Section 5.3 provides the experimental basis to demonstrate that tubes
with [

]^{a,c}. This

implies that those tubes [   ]^{a,c} would not have to be
modified because their instability response amplitude (and stress) would be
small. The very high degree of sensitivity of tube response (displacements and
stresses) to changes in the velocity times square-root-density distribution is
addressed in Section 4.0. This is important in determining the degree of
change that can be attained through modifications.

Frequency

It has been demonstrated by investigators that analytically determined
frequencies are quite close to their physical counterparts obtained from
measurements on real structures. Thus, the uncertainty in frequencies has been
shown to be quite small. This is particularly appropriate in the case of
dented (fixed boundary condition) tubes. Therefore, uncertainty levels
introduced by the frequency parameter are expected to be insignificant (see
also "Average Flow Field" subsection below).

Instability Constant (Beta)

The beta (stability constant) values used for stability ratio and critical
velocity evaluations (see above equations) are based on an extensive data base
comprised of both Westinghouse and other experimental results. In addition,
previous field experiences are considered. Values have been measured for full
length U-bend tubes in prototypical steam/water environments. In addition,
measurements in U-bend air models have been made with both no AVB and variable
AVB supports (Figure 5-3).

To help establish the uncertainties associated with ATHOS flow velocity and
density distribution predictions on stability analyses, the Model Boiler (MB-3)
tests performed at Mitsubishi Heavy Industries (MHI) in Japan were modeled
using ATHOS. A beta value consistent with the ATHOS predicted flow conditions
and the MB-3 measured critical velocity was determined. These analyses
supported a beta value of [   ]^{a,b,c}.

A summary of the test bases and qualifications of the beta values used for these assessments is provided by Figure 5-2. The lowest measured beta for tubes without AVBs was a value of [   ]^{a,b,c}. This value is used for the beta parameter in all stability ratio evaluations addressed in this Report (see also "Average Flow Field" subsection below).

Mass Distribution

The mass distribution parameter is based on known information on the tube and primary and secondary fluid physical properties. The total mass per unit length is comprised of that due to the tube, the internal (primary) fluid, and the external (secondary) fluid (hydrodynamic mass). Data in Reference 5-2 suggests that at operating void fractions [

]^{a,c}.

Tube Damping

Test data are available to define tube damping for clamped (fixed) tube supports, appropriate to dented tube conditions, in steam/water flow conditions. Prototypic U-bend testing has been performed under conditions leading to pinned supports. The data of Axisa in Figure 5-4 provides the principal data for clamped tube conditions in steam/water. This data was obtained for cross flow over straight tubes. Uncertainties are not defined for the data from these tests. Detailed tube damping data used in support of the stability ratio evaluations addressed in this report are provided in Section 5.2, below.

Flow Field - Velocity Times Square-Root-Density Distribution

Average and U-bend-local flow field uncertainties are addressed independently in the following.

Average Flow Field

Uncertainties in the average flow field parameters, obtained from ATHOS analyses, coupled with stability constant and frequency, are essentially the same for units with dented or non-dented top support plates. If the errors associated with these uncertainties were large, similar instabilities would be expected in the non-dented units with resulting wear at either the top support plate or inner row AVBs. Significant tube wear has not been observed in inner row tubes in operating steam generators without denting. Thus, an uncertainty estimate of about [   ]^{a,c} for the combined effects of average flow field, stability constant and frequency appears to be reasonable. To further minimize the impact of these uncertainties, the North Anna Unit 1 tubes are evaluated on a relative basis, so that constant error factors are essentially eliminated. Thus, the uncertainties associated with the average velocity times square-root-density (combined) parameter are not expected to be significant.

U-Bend Local Flow Field

Non-uniform AVB insertion depths have been shown to have effects on stability ratios. Flow peaking, brought about by the "channeling" effects of non-uniform AVBs, leads to a local perturbation in the velocity times square-root-density parameter at the apex of the tube where it will have the largest effect (because the apex is where the largest vibration displacements occur). Detailed local flow field data used in support of the stability ratio evaluations addressed in this report are provided in Section 5.2, below.

Overall Uncertainties Assessment

Based on the above discussions, and the data provided in the following sections, it is concluded that local flow peaking is likely to have contributed significantly to the instability and associated increased vibration amplitude for the failed North Anna tube. Ratios of stresses and stability ratios relative to the North Anna tube, R9C51, are utilized in this report to minimize uncertainties in the evaluations associated with instability constants, local flow field effects and tube damping.

5.2 Tube Damping Data

The damping ratio depends on several aspects of the physical system. Two primary determinants of damping are the support conditions and the flow field. It has been shown that tube support conditions (pinned vs clamped) affect the damping ratio significantly. Further, it is affected by the flow conditions, i.e., single-phase or two-phase flow. These effects are discussed below in more detail.

Reference (5-1) indicates that the damping ratio in two phase flow is a sum of contributions from structural, viscous, flow-dependent, and two-phase damping. The structural damping will be equal to the measured damping in air. However, in two-phase flow, the damping ratio increases significantly and is dependent on the void fraction or quality. It can be shown that the damping contribution from viscous effects are very small.

Damping ratios for tubes in air and in air-water flows have been measured and reported by various authors. However, the results from air-water flow are poor representations of the actual conditions in a steam generator (steam-water flow at high pressure). Therefore, where available, results from prototypic steam-water flow conditions should be used. Fortunately, within the past few years test data on tube vibration under steam-water flow has been developed for both pinned and clamped tube support conditions.

Two sources of data are particularly noteworthy and are used here. The first is a large body of recent, as yet unpublished data from high pressure steam-water tests conducted by Mitsubishi Heavy Industries (MHI). These data were gathered under pinned tube support conditions. The second is comprised of the results from tests sponsored by the Electric Power Research Institute (EPRI) and reported in References (5-2) and (5-3).

The damping ratio results from the above tests are plotted in Figure 5-4 as a function of void fraction. It is important to note that the void fraction is determined on the basis of [   ]a,c

(Reference (5-4)). The upper curve in the figure is for pinned support conditions. This curve represents a fit to a large number of data points not shown in the figure. The points on the curve are only plotting aids, rather than specific test results.

The lower curve pertains to the clamped support condition, obtained from Reference (5-3). Void fraction has been recalculated on the basis of slip flow. It may be noted that there is a significant difference in the damping ratios under the pinned and the clamped support conditions. Damping is much larger for pinned supports at all void fractions. Denting of the tubes at the top support plate effectively clamps the tubes at that location. Therefore, the clamped tube support curve is used in the current evaluation to include the effect of denting at the top tube support plate.

The Reference 5-3 data as reported show a damping value of .5% at 100% void fraction. The 100% void fraction condition has no two phase damping and is considered to be affected principally by mechanical or structural damping. Westinghouse tests of clamped tube vibration in air has shown that the mechanical damping is only [   ]a,c rather than the .5% reported in Reference (5-3). Therefore the lower curve in Figure 5-4 is the Reference (5-3) data with all damping values reduced by [   ]a,c.

5.3 Tube Vibration Amplitudes With Single-Sided AVB Support

A series of wind tunnel tests were conducted to investigate the effects of tube/AVB eccentricity on the vibration amplitudes caused by fluidelastic vibration.

[

]a,c. Prior test results obtained during the past year using this apparatus have demonstrated that the fluidelastic vibration characteristics observed in the tests performed with the cantilever tube apparatus are in good agreement with corresponding characteristics observed in wind tunnel and steam flow tests using U-bend tube arrays. A summary of these prior results is given in Table 5-1.

An overall view of the apparatus is shown in Figure 5-5. Figure 5-6 is a top view of the apparatus. [

]a,c

As shown in Figure 5-7, the tube vibration amplitude below a critical velocity is caused by [

]a,c.

Figure 5-7 shows the manner in which the zero-to-peak vibration amplitude, expressed as a ratio normalized to [   ]a,c, varies when one gap remains at [   ]a,c. For increasing velocities, up to that corresponding to a stability ratio of [

]a,c. Figure 5-8 shows typical vibration amplitude and tube/AVB impact force signals corresponding to those obtained from the tests which provided the results shown in Figure 5-7. As expected, impacting is only observed in the [   ]a,c.

It is concluded from the above test results that, [

]a,c.

5.4 Tests to Determine the Effects on Fluidelastic Instability of
     Columnwise Variations in AVB Insertion Depths

This section summarizes a series of wind tunnel tests that were conducted to investigate the effects of variations in AVB configurations on the initiation of fluidelastic vibration. Each configuration is defined as a specific set of insertion depths for the individual AVBs in the vicinity of an unsupported U-bend tube.

The tests were conducted in the wind tunnel using a modified version of the cantilever tube apparatus described in Section 5.3. Figure 5-9 shows the conceptual design of the apparatus. The straight cantilever tube,

[

]^{a,c}.

[

]^{a,c}. Figure 5-11 shows the
AVBs, when the side panel of the test section is removed. Also shown is the
top flow screen which is [

]^{a,c}. The AVB
configurations tested are shown in Figure 5-12. Configuration 1a corresponds
to tube R9C51, the failed tube at North Anna. Configuration 2a corresponds to
one of the cases in which the AVBs are inserted to a uniform depth and no local
velocity peaking effects are expected.

As shown in Figure 5-9, [

                        ]^{a,c}.

All the tubes except the instrumented tubed (corresponding to Row 10) are
[   ]^{a,c}. As discussed in Section 5.3, prior
testing indicates that this situation provides a valid model. The instrumented
tube [   ]^{a,c} as shown in Figure 5.10.
Its [   ]^{a,c} direction vibrational motion is measured using a non-contacting
transducer.

[

]^{a,c}. The instrumented tube corresponds to a Row 10 tube as shown in
Figure 5-9. However, depending on the particular AVB configuration, it can
reasonably represent a tube in Rows 8 through 11. The AVB profile in the
straight tube model is the average of Rows 8 and 11. The difference in profile
is quite small for these bounding rows.

[   ]^{a,c} using a
hot-film anemometer located as shown in Figure 5-9.

Figure 5-13 shows the rms vibration amplitude, as determined from PSD (power
spectral density) measurements made using an FFT spectrum analyzer, versus flow
velocity for Configuration 1a (which corresponds to tube R9C51 in North Anna).
Data for three repeat tests are shown and the critical velocity is identified.
The typical rapid increase in vibration amplitude when the critical velocity
for fluidelastic vibration is exceeded is evident.

The main conclusions from the tests are:

1. Tube vibration below the critical velocity is relatively small, typical of turbulence-induced vibration, and increases rapidly when the critical velocity for the initiation of fluidelastic vibration is exceeded.

2. Configuration 1b (a preliminary version of R9C51 in North Anna) has the lowest critical velocity of all the configurations tested.

3. Configuration 1b is repeatable and the configuration was rerun periodically to verify the consistency of the test apparatus.

The initial test results obtained in support of the North Anna Unit 1 evaluation are summarized in Table 5-2. The test data is presented as a velocity peaking ratio; a ratio of critical velocity for North Anna tube R9C51 configuration 1a, to that for each North Anna Unit 1 AVB configuration evaluated.

5.5 References

a,c

Table 5-1
Wind Tunnel Tests on Cantilever Tube Model

OBJECTIVE: Investigate the effects of tube/AVB fitup on flow-induced tube vibration.

APPARATUS: Array of cantilevered tubes with end supports [

]a,c.

MEASUREMENTS: Tube vibration amplitude and tube/AVB impact forces or preload forces.

RESULTS:

a,b,c

Table 5-2

Fluidelastic Instability Velocity Peaking Ratios for
Columnwise Variation in AVB Insertion Depths
(North Anna 2)

Type of Insertion Configuration	Peaking Ratio U_{1a}/U_n
	a,c

Note: U_n is instability velocity at inlet for type n of AVB insertion configuration.

a,c

Figure 5-1 Fluidelastic Instability Uncertainty Assessment

U-Bend Test Data

1) MB-3 Tests

β values of [   ]a,b,c

2) MB-2 Tests

β of [   ]a,b,c

3) Air Model Tests

β of [   ]a,b,c without AVBs

Tendency for β to increase in range of [   ]a,b,c

with inactive AVBs (gaps at AVBs)

Tendency for β to decrease toward a lower bound of

[   ]a,b,c with active AVBs

Verification of Instability Conditions

1) Flow conditions at critical velocity from MB-3

2) Measured damping for the specific tube

3) Calculated velocities from ATHOS 3D analysis

4) β determined from calculated critical values

Good agreement with reported β values

5) — ATHOS velocity data with β of [   ]a,b,c and known damping

should not significantly underestimate instability for regions of

uniform U-bend flow

Figure 5-2 Instability Constant - β

a,b,c
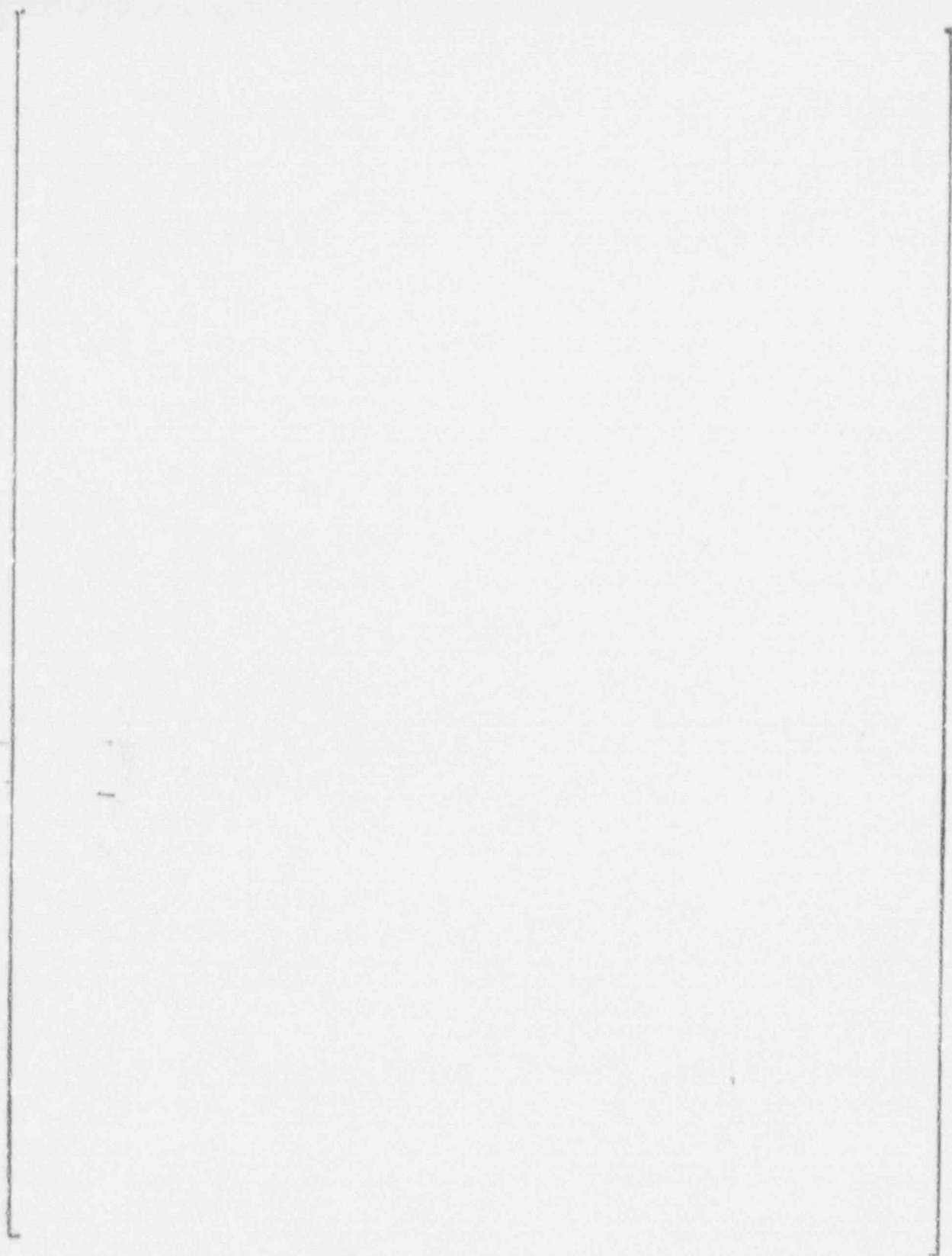
Figure 5-3 Instability Constants, β, Obtained for Curved Tubes from
Wind Tunnel Tests on the 0.214 Scale U-Bend Model

a,b,c
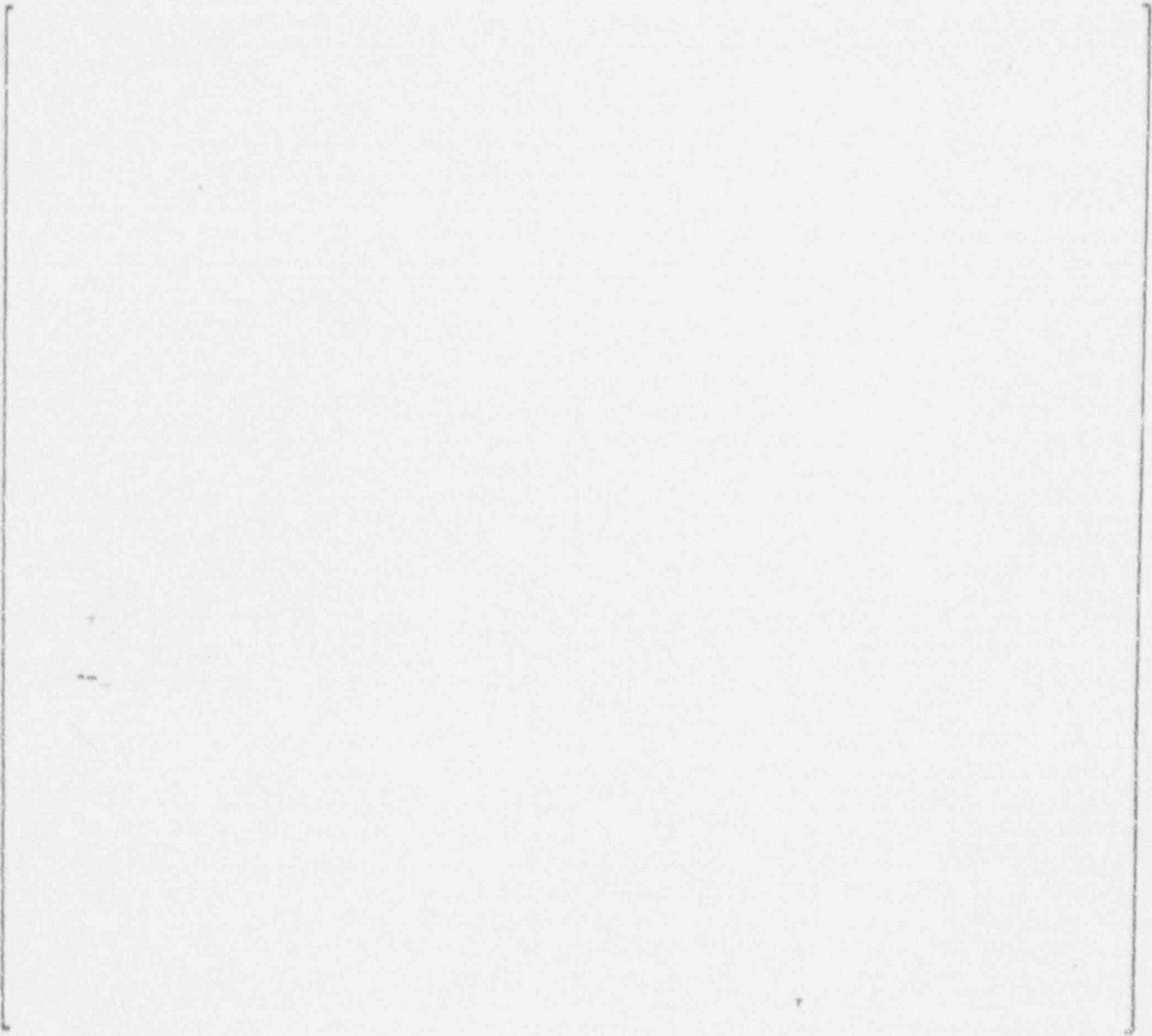
Figure 5-4 Damping vs. Slip Void Fraction

a,b,c
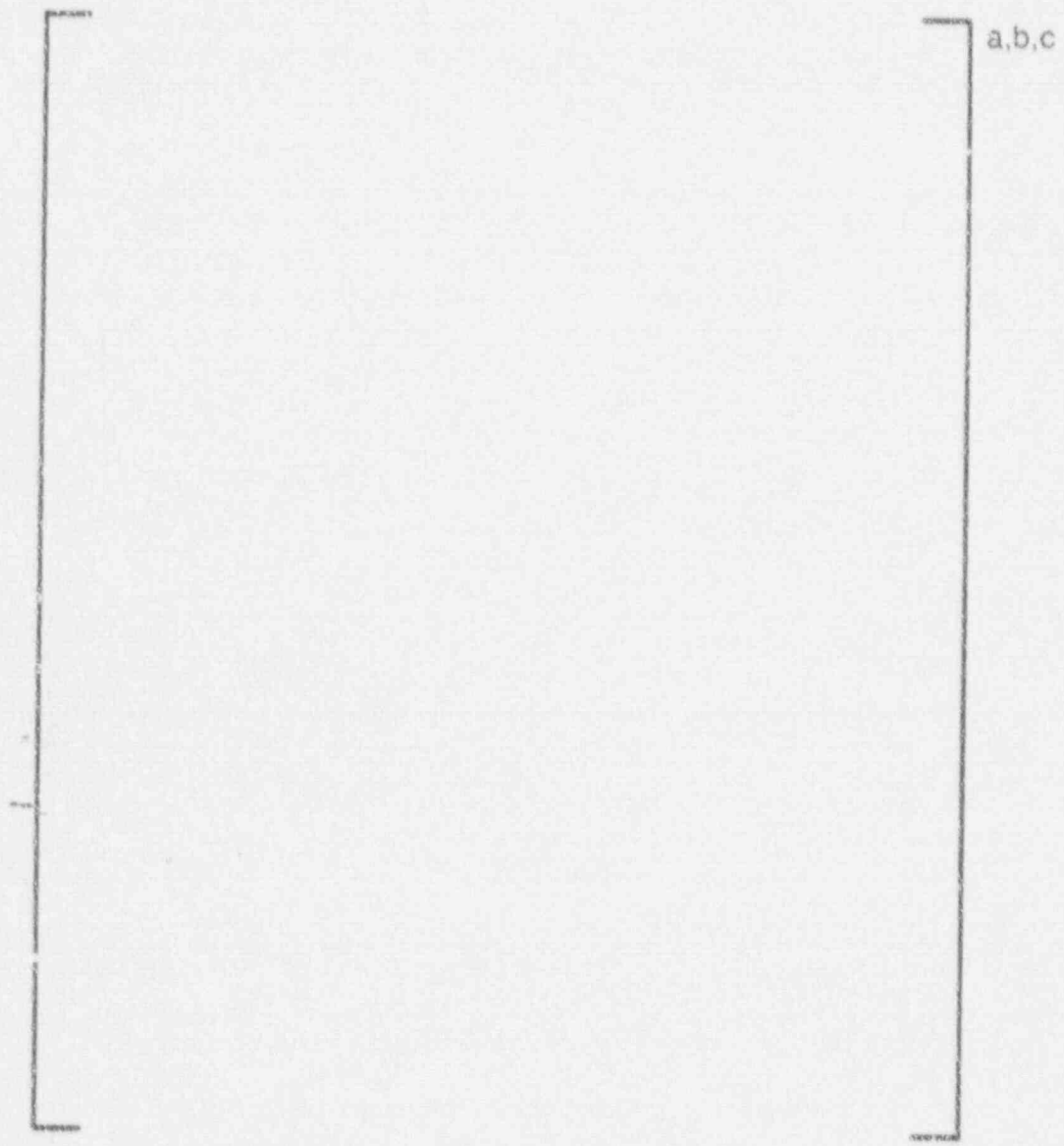
Figure 5-5 Overall View of Cantilever Tube Wind Tunnel Model

a,b,c

Figure 5-6 Top View of the Cantilever Tube Wind Tunnel Model

a,b,c

Figure 5-7 Fluidelastic Vibration Amplitude with Non-Uniform Gaps

a,b,c

Figure 5-8 Typical Vibration Amplitude and Tube/AVB Impact Force
Signals for Fluidelastic Vibration with Unequal
Tube/AVB Gaps

a,b,c

Figure 5-9 Conceptual Design of the Apparatus for Determining the
Effects of Fluidelastic Instability of Columnwise
Variations in AVB Insertion Depths

a,b,c
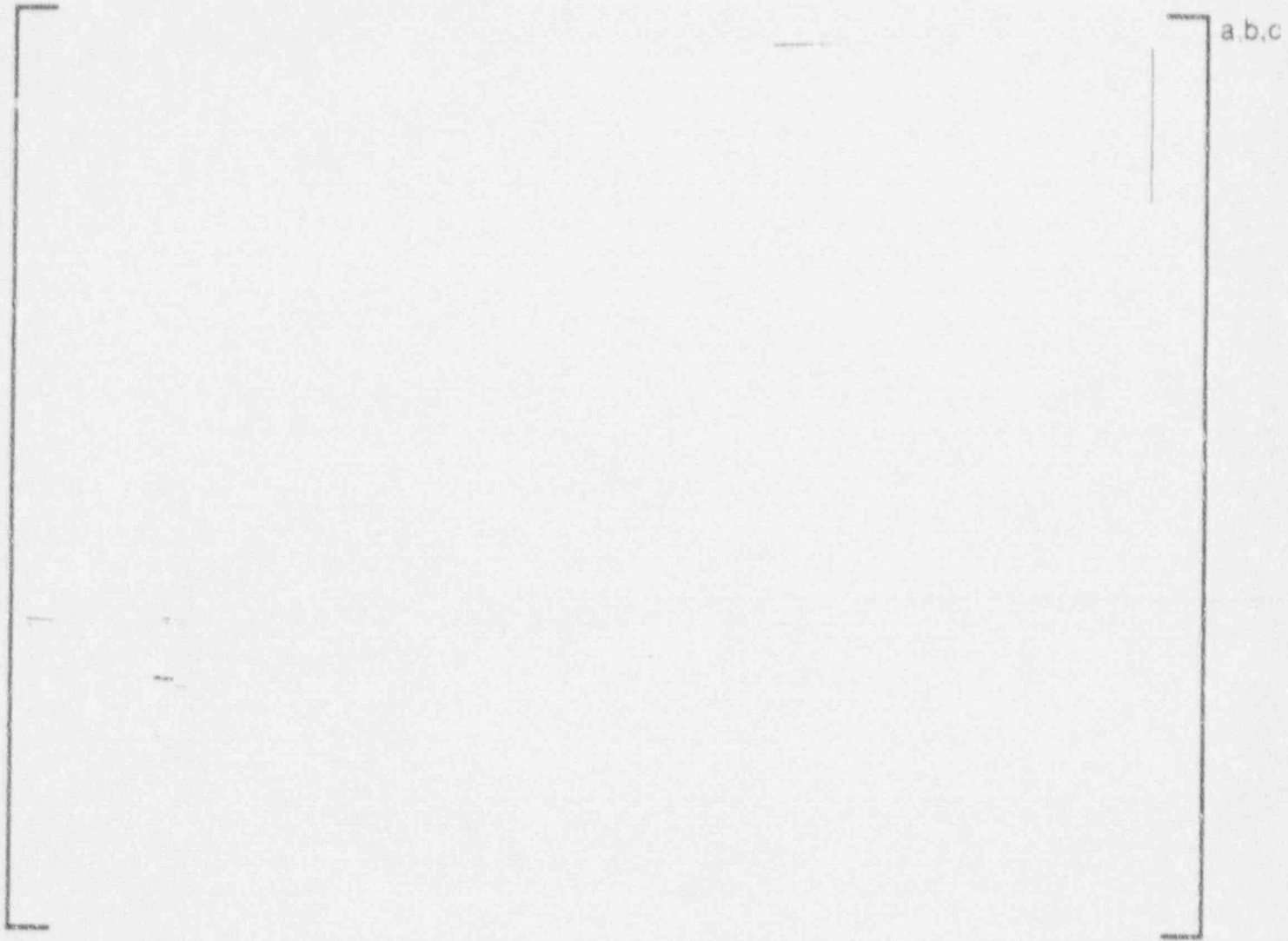
Figure 5-10 Overall View of Wind Tunnel Test Apparatus

a,b,c

Figure 5-11 Side View of Wind Tunnel Apparatus with Cover Plates
Removed to Show Simulated AVBs for Field Modified Units
and Top Flow Screen

TYPE OF AVB INSERTION		TYPE OF AVB INSERTION		TYPE OF AVB INSERTION	
1a	a,c	2a	a,c	5a	a,c
1b		4a		5b	
1e		4b		5c	
1o		4f		6a	
1w		4r		8c	
1z		4s		8b	

Figure 5-12 AVB Configurations Tested - North Anna Unit 2

a,b,c

Figure 5-13 Typical Variation of RMS Vibration Amplitude with Flow
Velocity for Configuration 1a in Figure 5-12

6.0 EDDY CURRENT DATA AND AVB POSITIONS

6.1 AVB Assembly Design

[

]^{a,c,e} Upper AVBs which are inserted beyond the design depth occasionally show on the EC traces for the Row 12 tubes. Since the purpose of this analysis is to evaluate potentially unsupported tubes at or near the point of maximum AVB insertion, only the dimensions and EC data pertaining to the lower AVBs is used.

6.2 Eddy Current Data for AVB Positions

The AVB insertion depths were determined on the basis of the interpretation of the eddy current data. To locate the AVBs, the eddy current data traces from the August-September 1987 inspection were searched for the characteristic peaks seen in the signals which indicate the intersection of an AVB (or a tube support plate) with the tube. A typical signal is shown in Figure 6-1. About 1,176 tubes from among the three steam generators were examined for these signals. The U-bend signals for North Anna #2 were relatively free of signal disturbances usually attributed to copper deposited on the outsides of the tubes.

6.3 AVB Projection and Mapping

Since ambiguity can occur in the interpretation of the ECT data due to the inability of ECT to differentiate on which side of a tube a "visible" AVB is located, other information was used to assist in establishing the location of

the AVBs. [

$$]^{a,c}$$

The projection technique is useful in determining the AVB positions where
suspected noisy or spurious ECT signals prevent direct observation of the
AVBs, and where data are unavailable due to plugged tubes. [

$$]^{a,c}$$

For single AVB contacts, [

$$]^{a,c}$$ Table 6-1 lists the "1-AVB" signals at locations near the
projected apex of the AVB which have been evaluated as being supported.

The AVB position maps are shown in Figures 6-4 to 6-6. [

$$]^{a,c}$$ Table 6-2 lists tubes in Rows 7 through 10 which are
evaluated in the analysis as being unsupported.

The observation that [

]ᵃ,ᶜ

b.4 Tube Denting at the Top Tube Support Plate

As previously noted, tube denting was determined to be a prerequisite for the
North Anna #1-type tube fatigue mechanism, and therefore of interest in the
North Anna #2 tube evaluation. Tube support plate crevice corrosion products
and tube dent sizes as small as 1-2 mils (0.001" to 0.002") are detectable by
eddy current testing. Although the difference between tube denting and the
presence of crevice corrosion products may be significant in terms of the tube
fatigue mechanism, it is conservative to consider a tube to be dented if
either tube denting with deformation or top tube support plate crevice
corrosion products were detected. All North Anna #2 tubes were assumed to be
dented with deformation, which produces the maximum effect of mean stresses
for fatigue evaluations due to yielding of the tube at the top tube support
plate.

Eddy current evaluations of North Anna #2 crevices from the August-September,
1987, inspection indicated that most of the tubes had crevice corrosion
product buildups at the top tube support plate, but were not dented with
deformation. Of the 118 tubes which were sentinel plugged, 104 tubes were
evaluated as having "corrosion with magnetite" at the top tube support plate
intersection, 2 showed "denting with deformation", 6 showed "no detectable
denting" (or crevice corrosion product), and 6 were "unreadable". The
"corrosion with magnetite", "denting with deformation", and "unreadable"
conditions are considered as meeting the NRC Bulletin 88-02 definition of
"denting". As noted above, all tubes were considered dented in this analysis.

6.5 AVB Map Interpretations by Generator

A description of the AVB position mapping in each of the North Anna #2 steam
generators is provided below.

SG-A

The AVB map is given in Figure 6-2. All Row 10, Row 11 and Row 12 tubes are
supported. Twenty-five (25) Row 9 tubes, sixty-eight (68) Row 8 tubes, and
ninety (90) Row 7 tubes are unsupported. Sentinel plugs were installed in
forty-five (45) tubes in this steam generator.

R9C60 was [

                                                    ]^{a,c} and was

evaluated as potentially susceptible to fatigue, but only when Thot reduction
is implemented. This tube was previously sentinel plugged, based upon the
October 1987 evaluation.

Of the remaining tubes, R9C35 is the highest loaded tube in this steam
generator. A conservative flow peaking factor of [

                                   ]^{a,c} The AVB map for SG-A (Figure 6-2)
has been corrected from the letter report (Westinghouse transmittal #
VRA-89-533, R. N. Easterling to W. R. Cartwright) to show R9C35 as acceptable
for sentinel plug removal. In addition the map was corrected to indicate
tubes R9C77 and R9C78 as sentinel plugged; these were previously indicated as
having been inspected, but not plugged.

SG-B

The AVB map is shown in Figure 6-3. All Row 10, Row 11 and Row 12 tubes are
supported. Seventeen (17) Row 9 tubes, forty-nine (49) Row 8 tubes, and

eighty-four (84) Row 7 tubes are unsupported. Sentinel plugs were installed in twenty-nine (29) tubes in this steam generator.

R9C35 was evaluated as [

]^{a,c} This tube was previously sentinel plugged, based upon the October 1987 evaluation.

Of the remaining tubes, R8C60 is the highest loaded tube in this steam generator. A conservative flow peaking factor of [
]^{a,c}

SG-C

The AVB map is shown in Figure 6-4. All Row 11 and Row 12 tubes are supported. Five Row 10 tubes, twenty-seven (27) Row 9 tubes, fifty (50) Row 8 tubes, and ninety (90) Row 7 tubes are unsupported. Sentinel plugs were installed in forty-four (44) tubes in this steam generator.

R10C60 was evaluated as unsupported, although [

]^{a,c}

The AVB positions [

]^{a,c}

R9C60 and R9C35 are the highest loaded tubes in this steam generator. [
]^{a,c}

TABLE 6-1

North Anna #2
1 AVB Signals Determined to be Supported

North Anna #2 Steam Generator A

Row 12	None
Row 11	None
Row 10	None
Row 9	Columns 10, 12-16, 61, 85
Row 8	Columns 31, 73, 74
Row 7	None

North Anna #2 Steam Generator B

Row 12	None
Row 11	None
Row 10	None
Row 9	Columns 15, 53, 60
Row 8	Columns 17, 61
Row 7	None

North Anna #2 Steam Generator C

Row 12	None
Row 11	None
Row 10	Columns 41-43, 46, 48, 51, 54, 55
Row 9	None
Row 8	Columns 37, 58, 59
Row 7	None

TABLE 6-2

North Anna #2
Unsupported Tube Summary

North Anna #2 Steam Generator A

Row 12	No unsupported tubes
Row 11	No unsupported tubes
Row 10	No unsupported tubes
Row 9	Columns 11, 35, 40-55, 60, 79-84
Row 8	Columns 2-16, 25, 32-35, 38-57, 60-54, 67-72, 77-93
Row 7	Columns 2-18, 21-93

North Anna #2 Steam Generator b

Row 12	No unsupported tubes
Row 11	No unsupported tubes
Row 10	No unsupported tubes
Row 9	Columns 34, 35, 40-52, 92, 93
Row 8	Columns 9-16, 23-28, 31-35, 38-56, 60, 79-85, 91-93
Row 7	Columns 2-57, 60-64, 67-72, 77-93

North Anna #2 Steam Generator C

Row 12	No unsupported tubes
Row 11	No unsupported tubes
Row 10	Columns 44, 45, 49, 50, 60
Row 9	Columns 35, 40-56, 60, 61, 79-85
Row 8	Columns 10-16, 32-35, 38-57, 60-64, 68-70, 77-87
Row 7	Columns 2-18, 21-93
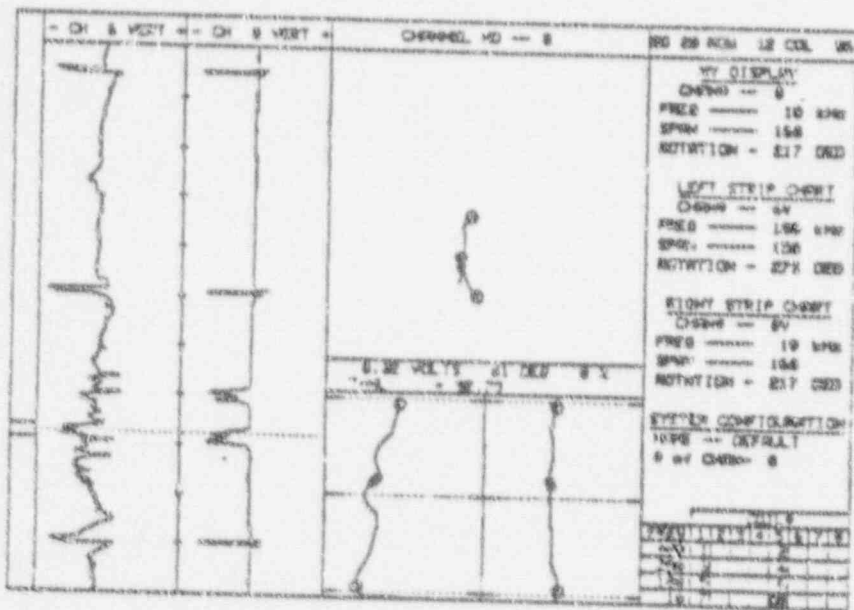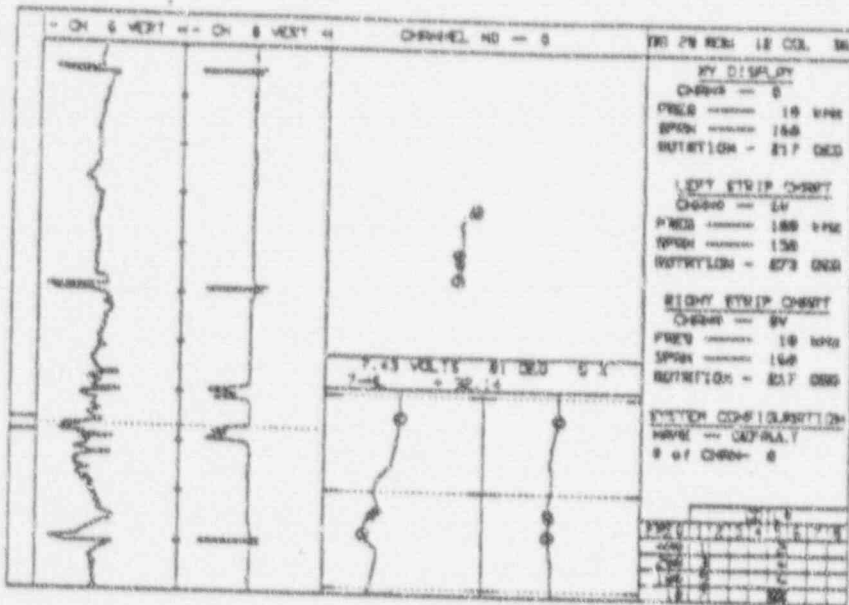
Figure 5-1 AVB Insertion Depth Confirmation

Row 11

Row 10

Row 9

Row 8
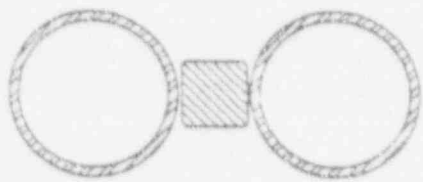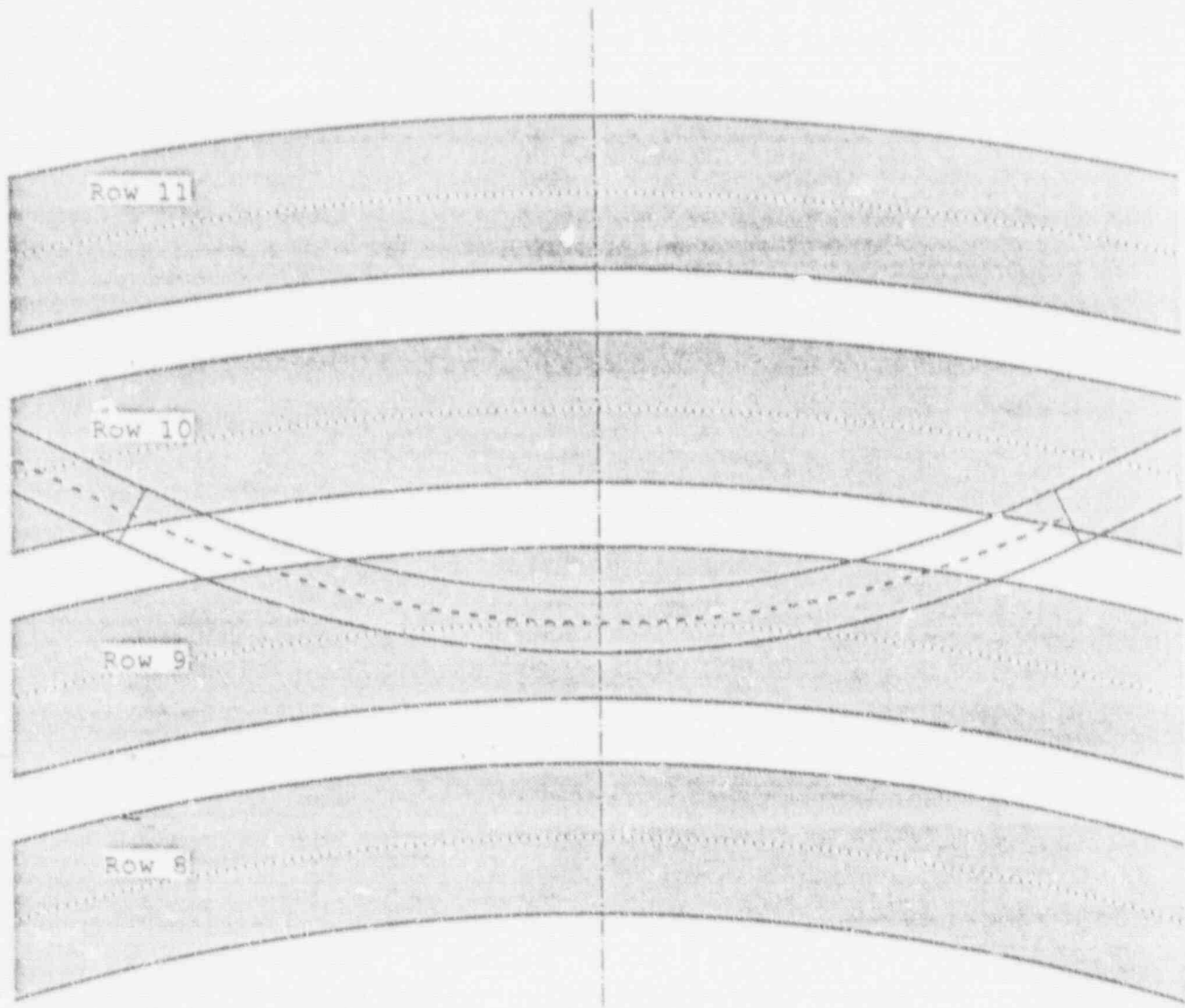
NTS

Figure 6-2   AVB Projection Depth = 9.00

Row 11

Row 10

Row 9

Row 8
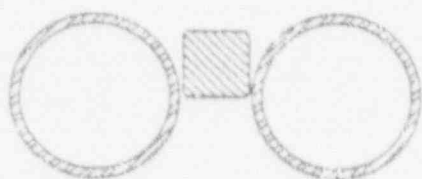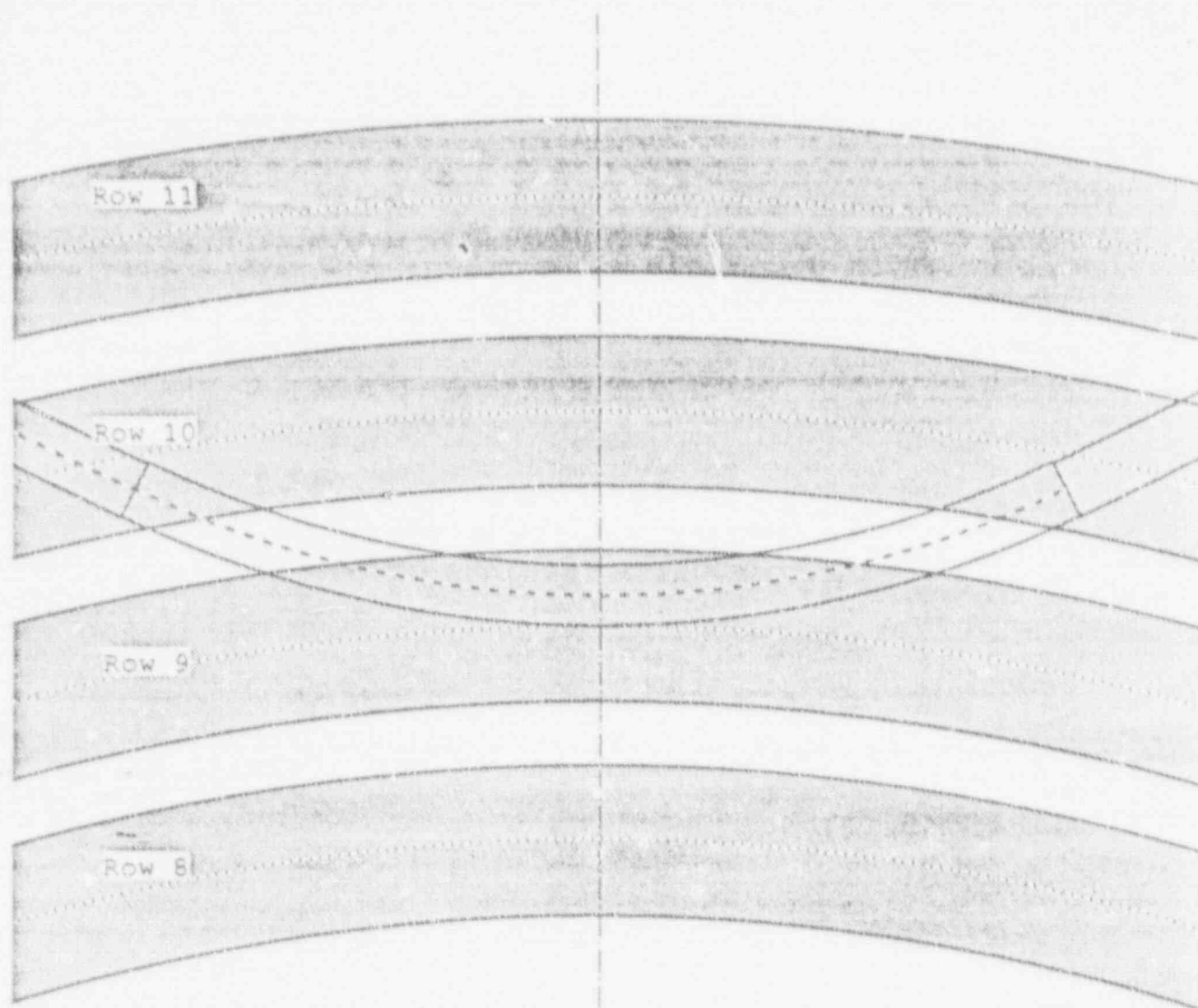
NTS

Figure 6-3 AVB Projection Depth = 9.15

Figure 6-4   North Anna #2 SG-A AVB Positions
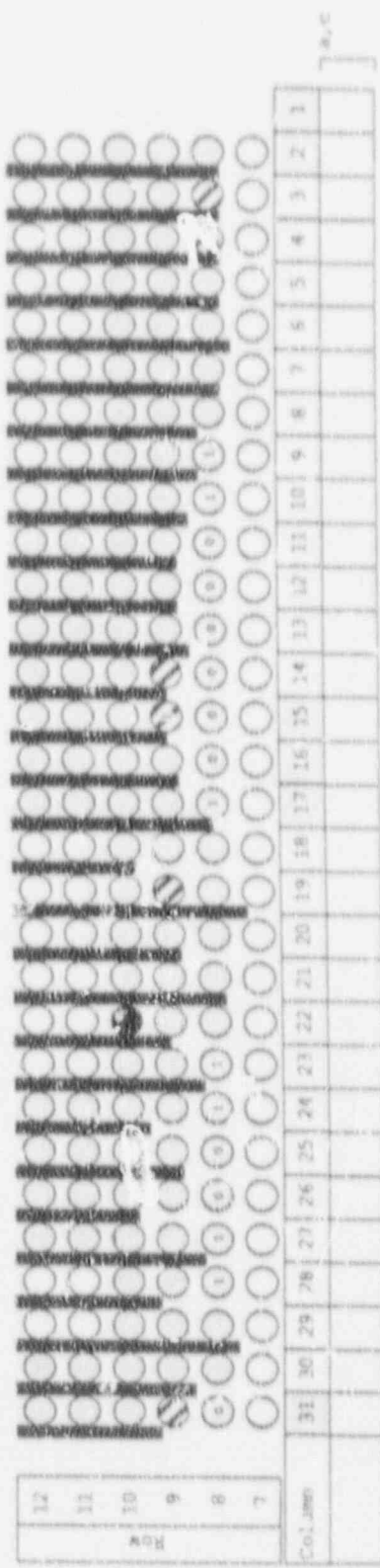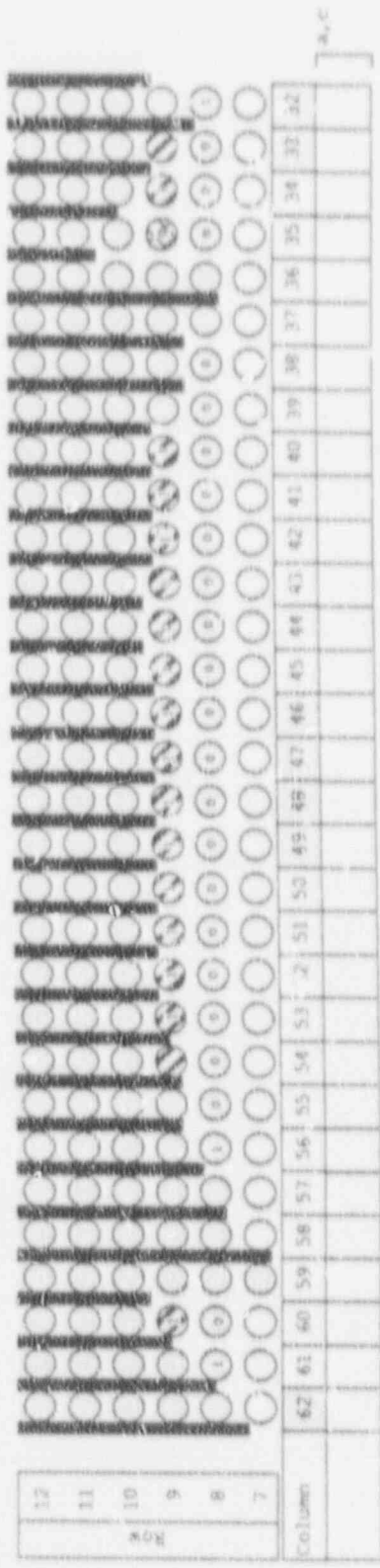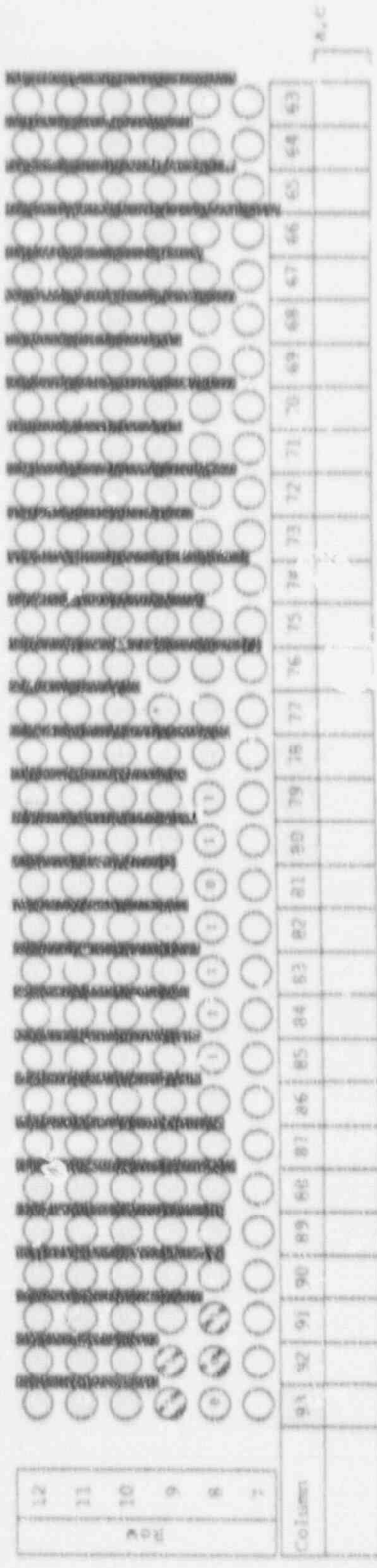
Figure 6-5   North Anna #2 SG-B AVB Positions
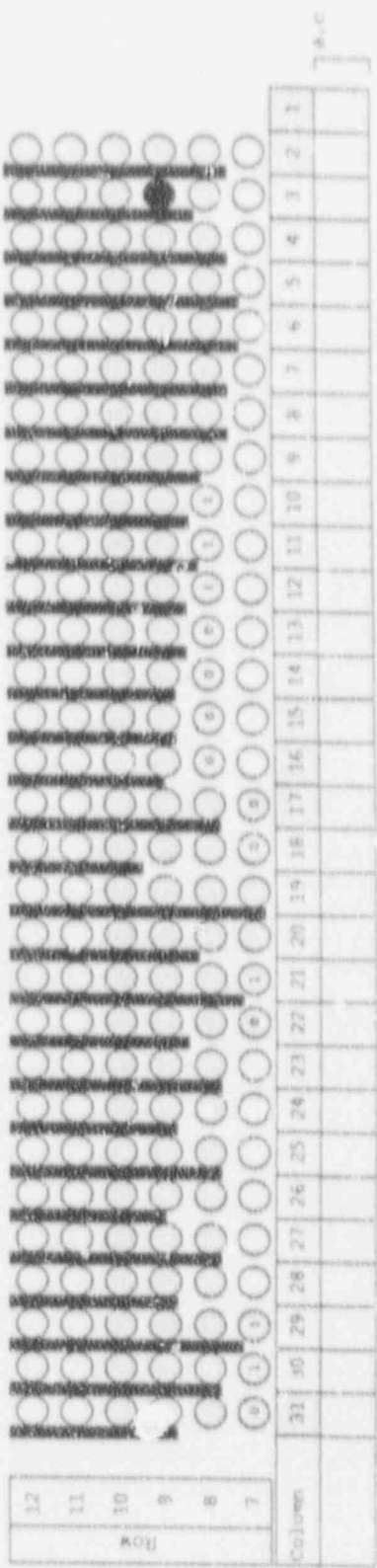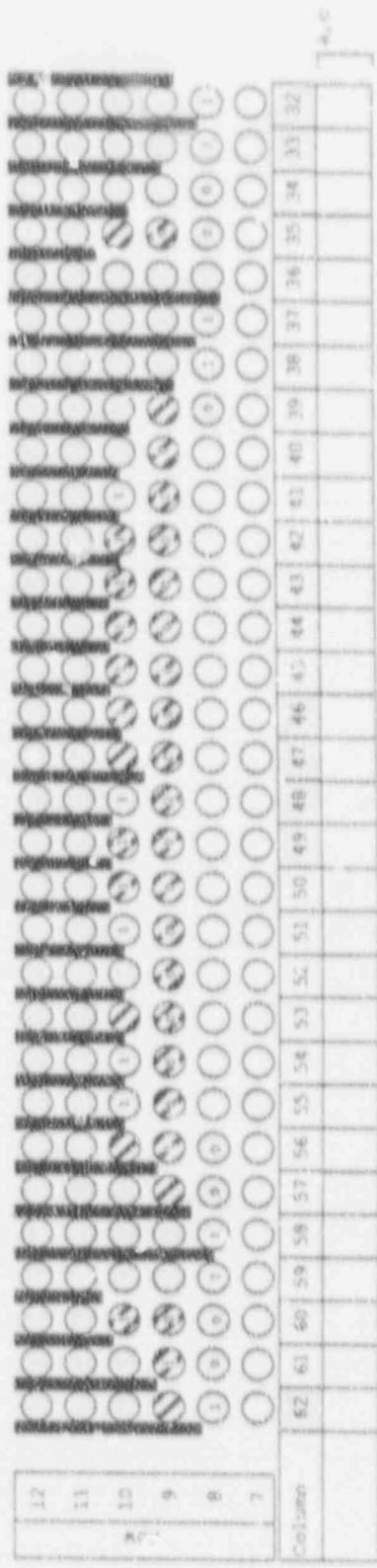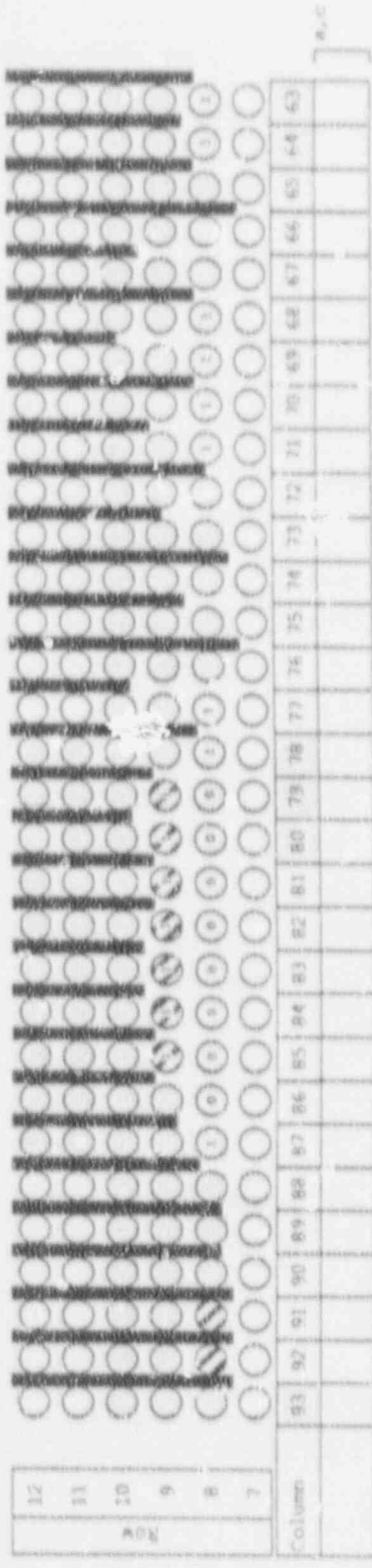
Figure 6-6   North Anna #2 SG-C AVB Positions

7.0 THERMAL AND HYDRAULIC ANALYSIS

This section presents the results of a thermal and hydraulic analysis of the flow field on the secondary side of the steam generator using the 3-D ATHOS computer code, Reference (7-1). The major results of the analysis are the water/steam velocity components, density, void fraction, and the primary and secondary fluid and tube wall temperatures. The distributions of the tube gap velocity and density along a given tube were obtained by reducing the ATHOS results. In the following subsection, operating condition data for North Anna 2 are presented. Data for three conditions are included: (1) operation in Cycle 5B prior to the installation of downcomer resistance plates, (2) recent operation in Cycle 6 with the new downcomer resistance plates installed, and (3) operation with reduced primary fluid temperatures. A description of an ATHOS model and some sample results previously completed for North Anna Unit 1 operation with downcomer resistance plates installed are included in the next two sections. The final section describes an analysis of the operating history data for North Anna 2. This analysis defines a parameter termed the normalized stability ratio which provides a relative indication of the effect of past operation on the plant's fluidelastic stability ratio.

7.1 North Anna 2 Steam Generator Operating Conditions

Recent steam generator operating condition data for North Anna Unit 2 were provided by Virginia Power and are summarized below. The data are representative of operation in Cycle 6 with the new downcomer resistance plates installed in all three generators.

Recent Full Load Operating Parameters for North Anna 2 (SG A)
    a. Steam pressure – 894 psia
    b. Steam Flowrate – 4.25×10^6 lbm/hr
    c. Feedwater Temperature – 434.8°F
    d. Primary Inlet and Outlet Temperatures – T_{in} = 617.9°F, T_{out} = 552.5°F
    e. Thermal Load – 975.1 $MW_{thermal}$ (100.7% of full power)

With the above data, calculations were completed using the Westinghouse SG performance computer code, GENF, to verify the plant data and to establish a complete list of operating conditions required for the ATHOS analysis. The GENF code determines the primary side temperatures and steam flow rate required to obtain the specified steam pressure at the given power rating. Besides confirming these parameters, the code calculates the circulation ratio which is of primary importance to the stability ratio analysis since it, together with the steam flow, establishes the total bundle flow rate and average loading on the tubes. It also provides an overall indication of the voids within the tube bundle since the bundle exit quality is inversely proportional to the circulation ratio (X_{exit} = 1/circ ratio).

The calculated circulation ratio along with the other thermal/hydraulic conditions for Unit 2/Cycle 6 are listed in Table 7-1. Note that the circulation ratio includes the effect of downcomer resistance plates which were installed in Unit 2 prior to the November 1987 restart (following the tube rupture event in Unit 1). For comparison, Table 7-1 also includes parameters for operation in Cycle 5B prior to the installation of the plates. The added flow resistance associated with the plate has led to a significant reduction in the circulation ratio compared to prior operation [
]^{a,c}. The resulting decrease in bundle flow and loading of the tubes in the U-bend has greatly reduced the potential for fluidelastic vibration instability.

Table 7-1 also includes a set of operating conditions having reduced primary fluid temperatures which the utility is considering for future operation. These conditions were also supplied by Virginia Power and are based on an actual test with the turbine valve wide open at full power. The measured steam pressure from this test (823 psia), therefore, represents the lowest pressure which can exist, without making turbine modifications, while still maintaining full power. Performance calculations were also completed for this set of conditions. Note that the reduced temperature condition has essentially the same steam flow rate, circulation ratio, and bundle flow rate as exist for the recent operating condition. The steam pressure reduction from 894 to 823 psia, however, is significant since it will result in higher

fluidelastic stability ratios as a result of both higher U-bend tube gap velocities and decreased damping.

Also included in Table 7-1 are the corresponding operating conditions for Unit 1, i.e., prior to the tube rupture event, post-rupture operation with downcomer resistance plates installed, and proposed operation with reduced primary fluid temperature. A comparison of the corresponding Unit 1 and 2 conditions indicates that only small differences exist in some of the parameters. The effect of differences in operating conditions on stability ratios can be determined with a one-dimensional (1D) relative stability ratio calculation method. Adjustment factors determined from the 1D method also provide a means of generating simulated 3D stability ratios for an alternate set of operating conditions without having to complete a specific, detailed 3D flow field calculation.

The 1D relative stability ratios for all three operating conditio s in both units are also listed in Table 7-1. A detailed description of the 1D relative stability ratio is provided in a later sub-section, as it applies to the analysis of historical operating data. However, for the present discussion it is sufficient to state that the 1D relative stability ratio is primarily dependent upon three operating parameters: power level/steam flow, steam pressure, and the circulation ratio. (Primary side temperatures have only a very minor influence on stability ratios). As mentioned previously, the steam flow rate and circulation ratio influence the total bundle flow rate and tube-to-tube gap velocity in the U-bend. The steam pressure also influences the gap velocity via the void fraction and density, however, its major impact is on the tube damping. High U-bend flow along with low steam pressure results in a higher loading on the tubes with reduced damping. Both of these factors lead to higher, more limiting stability ratios.

As indicated by the comparison in Table 7-1, the relative stability ratios calculated for each condition in Unit 2 are within 1% of the ratios calculated for the corresponding conditions in Unit 1. In particular, for pre-modification operation, the Unit 2 value is only 1.009 x the reference Pre-Mod Unit 1 value. The slightly higher value is the result of decreased

damping associated with a lower steam pressure (870 vs 890 psia). For recent operation, the ratios are 0.897 and 0.890, respectively, for Units 1 and 2. Ratios calculated for proposed operations with reduced primary temperature are higher compared to current operation. Again, however, the ratios for Units 1 and 2 are nearly the same, 0.950 and 0.944, respectively.

The fact that the operating conditions and 1D relative stability ratios for Units 1 and 2 are so close is important, in that it permits the application of existing 3D stability ratios derived from ATHOS flow field calculations for Unit 1, along with small stability ratio adjustment factors derived from the 1D method. In particular, a reference set of Pre-Mod 3D stability ratios is generated for Unit 2 by applying the 1.009 adjustment factor to the existing 3D stability ratios for Pre-Mod Unit 1. Simulated 3D stability ratios for other Unit 2 conditions can then be generated by applying the appropriate adjustment factors to this reference of 3D ratios for Unit 2: a) for recent operation in Cycle 6, the adjusting factor is 0.890/1.009 = 0.882 and b) for reduced temperature operation is 0.944/1.009 = 0.936.

The similarity of operating conditions and 1D relative stability ratios for Units 1 and 2 also means that the ATHOS 3D flow field simulation described in the next two sections based on Unit 1 recent operation is also applicable to current operation in Unit 2.

Justification for use of a simplified, one-dimensional, relative stability ratio adjustment factor is provided by making comparisons with the results obtained from more detailed three-dimensional flow field/tube vibration calculations. The attached Figure 7-1 presents the comparison of the results of the two calculation methods for ten other 51, 44, and 27 Series generators which have been evaluated, to date. The three-dimensional results are based on use of bundle flow fields predicted with the ATHOS3 computer code (Reference 7-1). Both cylindrical and Cartesian models have been used in the ATHOS3 simulations. Note that the results plotted in Figure 7-1 do not include the effects of anti-vibration bars.

The comparisons indicate that the 1D method provides a good or modestly conservative prediction of the 3D relative stability ratios for these similar

generator models. Note, in particular, that the 1D method essentially bounds the maximum 3D ratios observed for each tube row. This is so for the smaller radius tubes which, based on past experience, are typically the tube rows of interest in the tube vibration/fatigue evaluations. The variation in ratios for the plants within each steam generator model reflects differences in the basic thermal/hydraulic operating conditions (Wsteam, Psteam, and circ ratio). Further, this plant-to-plant variation is maintained for each of the tube rows which are plotted. The fact that the plant-to-plant variation in the 1D ratios follows the 3D trends, indicates that the operating condition contribution to the relative stability ratio can be adequately accounted for by the 1D approach.

Overall, the comparison demonstrates that the 1D calculation method can provide meaningful relative stability ratios in support of tube fluidelastic vibration/fatigue assessments. In particular, the one-dimensional technique can be used to adjust tube-specific stability ratios determined from detailed three-dimensional calculations for the effects of differences in thermal/hydraulic operating conditions. This 1D-to-3D adjustment is justifiable as long as its applied within a group of steam generators which share a common tube bundle configuration, as in the case of the 27, 44, and 51 Series feedring generators. In these situations, the overall tube bundle flow fields will be similar and the individual plant ratios will differ only as a result of the effects of variations in the basic thermal/hydraulic parameters.

7.2 ATHOS Analysis Model

The calculation of relative stability ratios involves comparing the stability ratio calculated for one or more tubes to the ratio calculated for the ruptured Row 9 Column 51 tube in North Anna. It makes use of ATHOS computed flow profiles. Since the presence of AVBs in the U-bend region of a tube bundle could influence the overall flow field and/or the local flow parameters for a particular tube of interest, some discussion of the treatment of AVBs is necessary before presenting a description of the ATHOS model.

The ATHOS code does not include the capability to model the presence of the AVBs in the U-bend region. However, Westinghouse has modified the code to

include the capability to model the AVBs via flow cell boundary resistance
factors. Practical lower limits of cell size in the ATHOS code, however,
prevent a fine grid representation of the AVB V-bar shape which, in turn,
limits the accuracy of the AVB representation. ATHOS calculations have been
performed with and without AVBs in the model. Calculations of stability
ratios relative to North Anna R9C51 show that the relative stability ratios
for tubes near the center of the steam generator are essentially the same for
models with or without AVBs. The ATHOS AVB modeling sensitivity studies with
uniform insertion show some tendency for the AVB resistance effects to lower
tube gap velocities near the central regions and to increase velocities near
the peripheral tubes. However, the magnitude of this effect is uncertain due
to the limitations in ATHOS for modeling the AVBs. Further, the global flow
resistance of staggered AVB insertion would be less than that from uniform
insertion. Based on the sensitivity studies using ATHOS models with and
without uniformly inserted AVBs, the most reliable relative stability ratios
(for actual steam generators with non-uniform AVB insertion depths) are
expected using ATHOS models excluding AVBs and effects of variable AVB
insertion depths by using flow test results of actual AVB geometries.

The North Anna analysis is based on a Cartesian coordinate system for the
array of flow cells instead of the typical, and more widely used, cylindrical
coordinate system. With a Cartesian coordinate system the tube array and any
AVBs are arranged in a square pitched configuration which is in-line with the
coordinate axes. This alignment provides an improved representation of the
tube region of interest in the bundle.

The ATHOS Cartesian coordinate system model for the North Anna steam generator
consists of 13,050 flow cells having 30 divisions in the x-axis (perpendicular
to the tubelane) direction, 15 divisions in the y-axis (along the tubelane)
direction and 29 divisions in the axial (z-axis) direction. In the ATHOS
analysis, the steam generator is considered to be symmetrical about the x-axis
of the tube bundle. The model therefore, consists of one-half of the hot leg
and one-half of the cold leg sides of the steam generator. Figures 7-2 and
7-3 show the plan and the elevation views of the model. These two figures
show the layout of the flow cells and identify locations for some of the
geometric features.

As shown in Figure 7-2, with the Cartesian coordinate system, the circular wrapper boundary is represented by a step-wise wall as indicated by the heavy lines. All of the simulated flow cells outside the simulated wrapper boundary above the first axial slab were blocked off by specifying extremely high flow resistances on the faces of the appropriate cells. Tubelane flow slots in the tube support plates are also modeled.

Figure 7-4 reproduces the plan view of the model but with the tube layout arrangement superimposed. This figure illustrates the locations of the tubes in the various flow cells. The fineness of the cell mesh is evident; the largest cells contain only 20 tubes while some of the smallest cells include only three tubes. Note, in particular, that additional detail was added near the bundle periphery (IY=12-15) to more closely model the inner radius tubes (rows ≤15). Five axial layers of cells were included in the U-bend near the top tube support (Figure 7-2, IZ 16 to IZ 21) to more closely model the flow conditions in the area of interest.

7.3 ATHOS Results

The results from the ATHOS analysis consist of the thermal-hydraulic flow parameters necessary to describe the 3-D flow field on the secondary side of the steam generator plus the distributions of the primary fluid and mean tube wall temperatures. Since the velocity components computed by ATHOS are defined on the surfaces of a flow cell, the tube gap velocity, which is the appropriately interpolated cell velocity ratioed upward to account for the minimum flow area between the tubes, and density distributions along a particular tube required for tube vibration evaluation are determined by a post-processor from the ATHOS output. The post-processor generates a data file which contains the gap velocity, density, void fraction and tube metal temperature distributions for all the tubes in the model and the file serves as part of the input data required for tube vibration analyses. Because the majority of the flow cells contain more than one tube inside a cell, the tube gap velocity and density surrounding a tube are obtained by interpolation of the ATHOS calculated velocities (defined on the cell surfaces) and density (defined at the center of the cell). The post-processor performs the

necessary interpolations to determine in-plane and out-of-plane velocity distributions at specific intervals along the length of the tubes.

A selection of ATHOS results for Unit 1 operation in Cycle 7B with the downcomer resistance plates installed are presented in Figures 7-5 to 7-11. As discussed in a previous section, these results are also applicable to recent operation in Unit 2. Figure 7-5 shows a vector plot of the flow pattern on the vertical plane of symmetry of the steam generator (the vectors are located at the center of the flow cells shown in Figure 7-3). It is seen that in the U-bend region the mixture turns radially outward, normal to the curvature of the bends toward the region of least flow resistance (i.e., outside the dome formed by the U-bends). Figure 7-6 shows the resultant vectors of the radial and circumferential velocity components on the horizontal plane at Z = 16, above the top tube support plate (see Figure 7-3). The radial outward flow is more evident from this figure since it ignores the axial component. Figure 7-7 shows the contour plot of the vertical velocity component (Vz) on the same horizontal plane (Z=16). The high velocity gradient around the flow slot openings in the top tube support plate is clearly shown in the figure.

Figures 7-8, 7-9 and 7-10 show a sample of the individual tube gap velocity, density and void fraction distributions along three tubes at Row 9. In each figure the parameters along the length of the tube are plotted from the hot leg tubesheet end on the left of the figure to the cold leg end on the right. The gap velocity shown in these figures are the in-plane gap velocity acting in the direction normal to the tube. The gap velocity, density and void fraction are the data needed for the tube structural calculations. Figure 7-11 shows the plot of the average in-plane gap velocity normal to the tube and density profiles in the U-bend span of the tube as a function of the column number along Row 9. The average values were taken as the numerical average of the parameter over the entire 180° span of a U-bend at a given column location. The average velocity is seen to be relatively constant with values ranging from 9.5 to 10.4 ft/sec. The average density is also quite constant with a value about 8.8 lb/ft^3. The wavy shape in the curves is due to the effect of the flow slots along the tubelane in the tube support plate on the distribution through the top tube support plate.

7.4 Relative Stability Ratio Over Operating History

One aspect of the evaluation of the North Anna 2 steam generators is to examine the operating history data and use it to determine the susceptibility to fatigue from fluidelastic vibration resulting from the 9 years of operation. This assessment has been completed through the use of a parameter termed the normalized stability ratio. The normalized stability ratio compares the fluidelastic stability ratio for each period of a plant's operation (fuel cycle) to a reference stability ratio, typically based on a recent operating condition. A plot of this ratio against operating time, therefore, provides a relative indication of the effect of past operation on the plant's fluidelastic stability ratio. This normalized time-dependent ratio is subsequently combined with an absolute stability ratio for the reference operating point derived from detailed three-dimensional thermal/hydraulic and tube vibration calculations. High values for the net stability ratio, in particular, over a significant period of operation, coupled with other prerequisite conditions (e.g., absence of AVB support and denting at the top tube support plate), could indicate an increased susceptibility to fluidelastic vibration instability and fatigue.

The fluidelastic stability ratio is defined as the ratio of the effective fluid velocity acting on a given tube to the critical velocity at which large amplitude fluidelastic vibration initiates:

$$\text{Fluidelastic Stability Ratio, SR} = \frac{U_{effective}}{U_{critical} \text{ at onset of instability}} \tag{1}$$

In this ratio, the effective velocity depends on the distribution of flow velocity and fluid density, and on the mode shape of vibration. The critical velocity is based on experimental data and has been shown to be dependent upon the tube natural frequency, damping, the geometry of the tube, the tube pattern, and the fluid density, along with the appropriate correlation coefficients.

The detailed calculation of this ratio using velocity and density distributions, etc., requires three-dimensional thermal/hydraulic and tube vibration calculations which are time consuming. Alternately, a simplified, one-dimensional version of this ratio has been used to provide a relative assessment technique for determining the effect of past operation on the stability ratio. The normalized stability ratio is defined by the following equation:

$$\left[\right]^{a,c} \quad [2]$$

In this equation "cyc x" refers to each fuel cycle and "REF" to the reference operating condition. While this simplified approach cannot account for three-dimensional tube bundle effects, it does consider the major operational parameters affecting the stability ratio. Four components make up this ratio: a loading term based on the dynamic pressure (ρV^2), a tube incremental mass(m) term, the natural frequency of the tube (f_n), and a damping ratio (δ) term. It should be noted that the ratio is relative, in that each component is expressed as a ratio of the value for a given fuel cycle or power level to that of the reference operating point.

$$[ ]^{a,c}$$

The particular damping correlation which is used for all normalized stability ratio calculations is based on a dented condition at the top tube support plate (a clamped condition, as discussed in Secti. 5.2). The clamped condition is also assumed in calculating the tube natural frequency.

The reference three-dimensional stability ratio calculation for the North Anna 2 steam generators was based on the following operating parameters which are representative of full power operation in Cycle 5B prior to the installation of downcomer resistance plates:

Steam Flow	4.25×10^6 lbm/hr
Steam Pressure	870 psia
Circulation Ratio	[ ]^{a,c} (Westinghouse calculation)

In addition to the reference pre-modification stability ratio, relative stability ratios were generated for three high power levels within each of the six fuel cycles completed, to date. Since tube vibration and possible fatigue are associated with operation at close to 100% power, only the higher power operating periods are considered important to the evaluation. The high power operating experience is summarized in Table 7-2. It lists the number of days in each fuel cycle that the unit operated within three high power intervals (85-90, 90-95 and 95-100%). Also listed are the full load operating parameters for each cycle. Note that in using this data, it has been conservatively assumed that the total operating time within each of the three power intervals is assigned to the highest power/stability ratio condition in the interval.

The resulting normalized stability ratios for Unit 2 are shown in Figure 7-12. In this figure, the normalized stability ratio is plotted against cumulative operating time above 85% power. The reference value (=1.00) is for the full power operating condition on which the pre-modification 3-D stability ratios are based, i.e., on operation in Cycle 5B prior to the installation of the downcomer flow resistance plates. The additional flow resistance associated with the new downcomer resistance plates has resulted in a significant reduction in the total bundle flow and, in particular, in the flow loading on the tubes in the U-bend. This is evidenced by the 12% reduction in stability ratio which occurred between Cycles 5B and 6. The reduced ratios at 90 and 95% power for the previous cycles are the combined result of both decreased loading on the tubes and increased damping. Higher damping is a result of lower voids in the U-bend which occurs when the steam pressure rises

at reduced power levels. The information shown in Figure 7-12 is utilized in the fatigue evaluation presented in Section 9.0.

References:

7-1 L. W. Keeton, A. K. Singhal, et al. "ATHOS3: A computer Program for Thermal-Hydraulic Analysis of Steam Generators", Vol. 1, 2, and 3, EPRI NP-4604-CCM, July 1986.

Table 7-1

North Anna 2 Steam Generator Operating Conditions
and Comparison with the Corresponding Conditions in Unit 1

	Pre-Modification Operation		Recent Operation with Downcomer Resistance Plates Installed		Proposed Operation with Reduced Primary Fluid Temperature	
	Unit 1 (Cycle 7A)	Unit 2 (Cycle 5B)	Unit 1 (Cycle 7B)	Unit 2 (Cycle 6)	Unit 1	Unit 2
Power (MWt)	968.3	968.3	968.3	975.1 (100.7%)	978.6 (101.1%)	970.2 (100.2%)
Steam Pressure Assigned at SG Outlet (psia)	890	870	886	894	828	823
Steam Flow Rate (lbm/hr)	4.24×10^6	4.25×10^6	4.25×10^6	4.25×10^6	4.29×10^6	4.25×10^6
Feedwater Temperature (°F)	440.	440.	440.5	434.8	440.5	436.4
Water Level Above Tubesheet (%)	44	44	44	44 (assumed)	44	44
Primary Average Temperature (°F)	586.8	586.6	585.5	585.2 (calc'd)	580	577.7

a,c

Calculated Parameters

Circulation Ratio

Bundle Flow Rate (lbm/hr)

1D Relative Stability Ratio

Basis of Performance Analysis

Table 7-2
North Anna 2 Operating History Data

Cycle	Distribution of Days in Each Power Interval 95-100%	90-95%	85-90%	Primary Tavg (Deg F)	Steam Flow 10^6 lbm/hr	Steam Pressure (psia)	Calculated Circ Ratio	Comments
1	324	13	12	581	4.07	860		a,c
2	192	11	2	581	4.07	860		
3	337	13	5	581	4.07	860		
4	363	22	13	581	4.07	860		
5A	114	3	0	587.8	4.08	900		Pressure Uprating
5B	266	8	6	586.8	4.25	870		Core Power Uprating
6	449*	0	0	585.2	4.25	894		With Downcomer Resistance Plates Installed
	2045	70	38					

* EFPD's for Cycle 6 through shutdown on 02/20/89
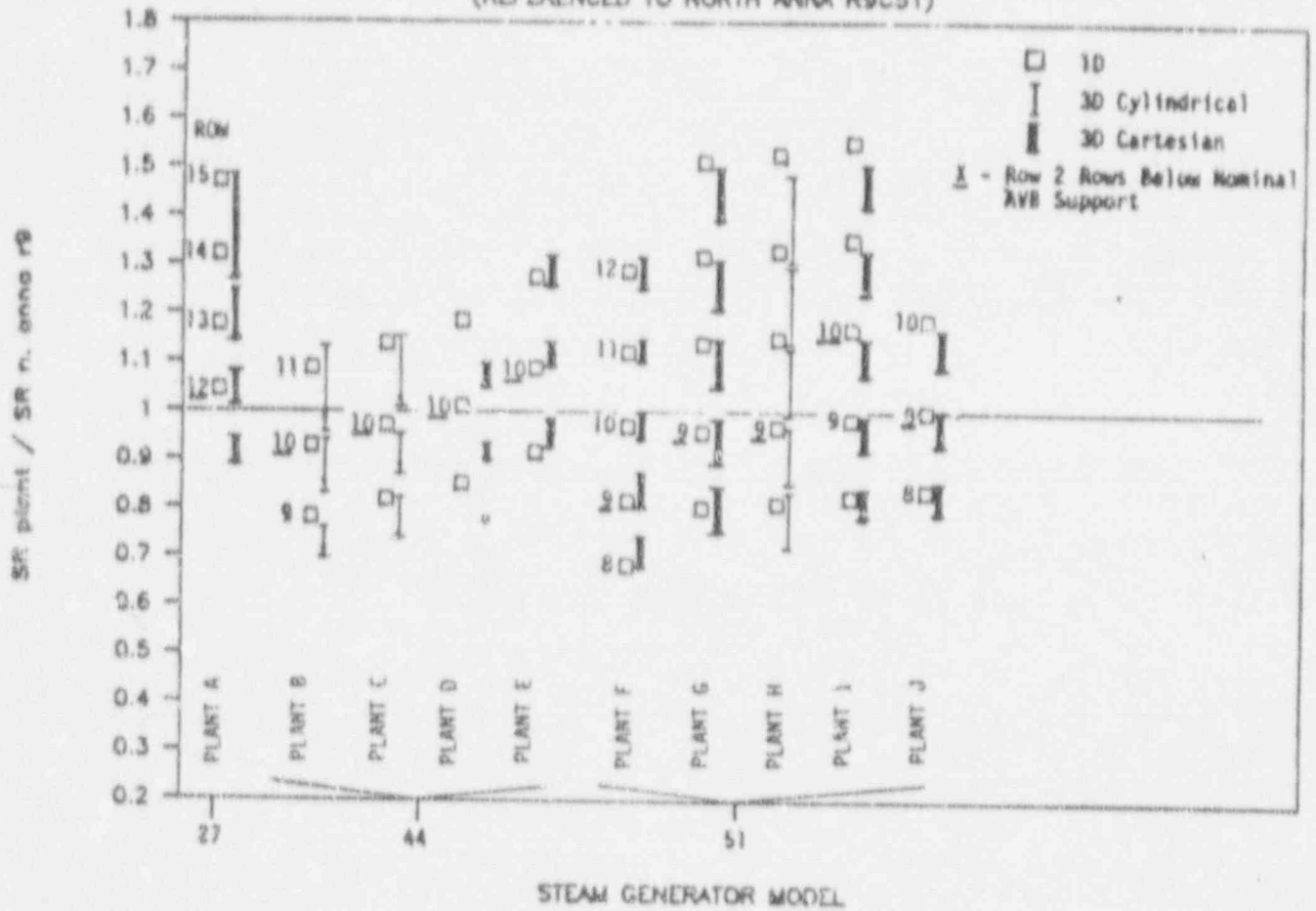
Figure 7-1 Comparison of Relative Stability Ratios
Calculated From 1D and 3D Methods
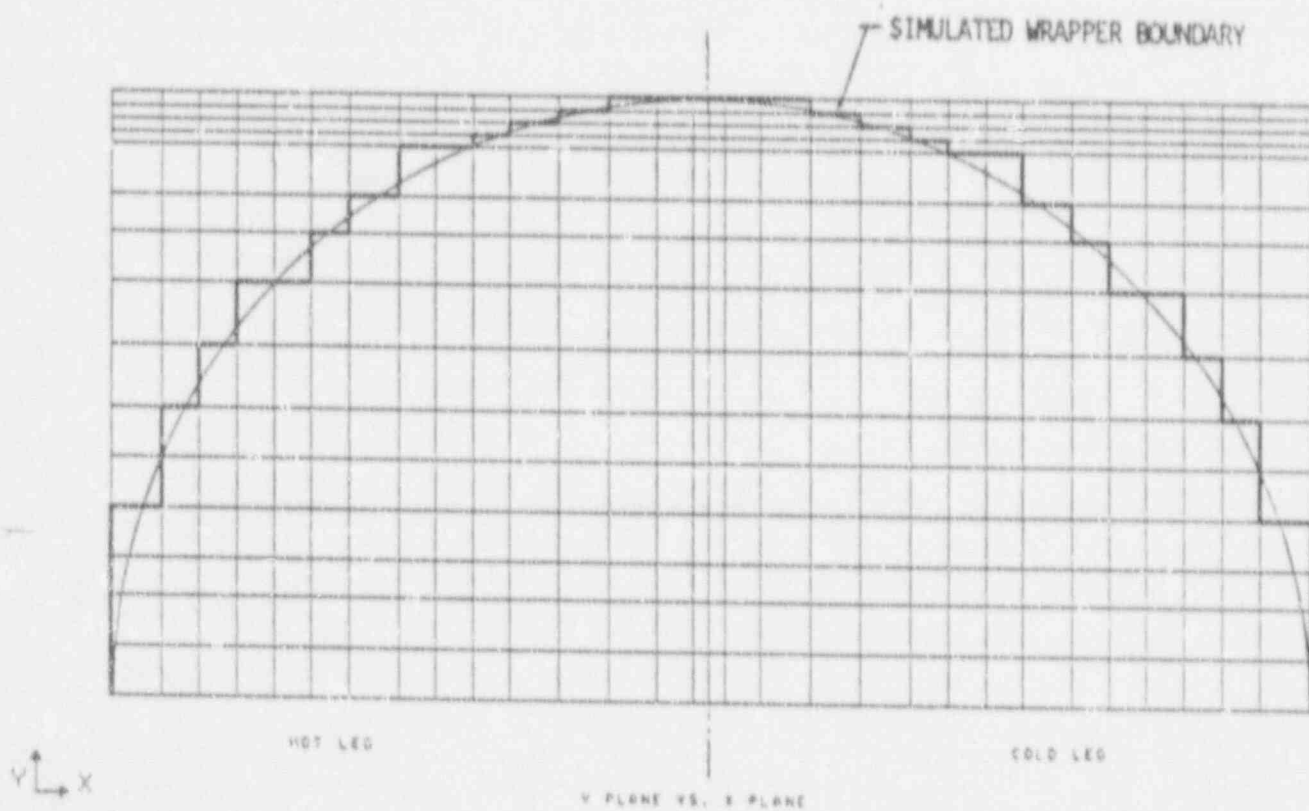
Figure 7-2 Plan View of ATHOS Cartesian Model for North Anna
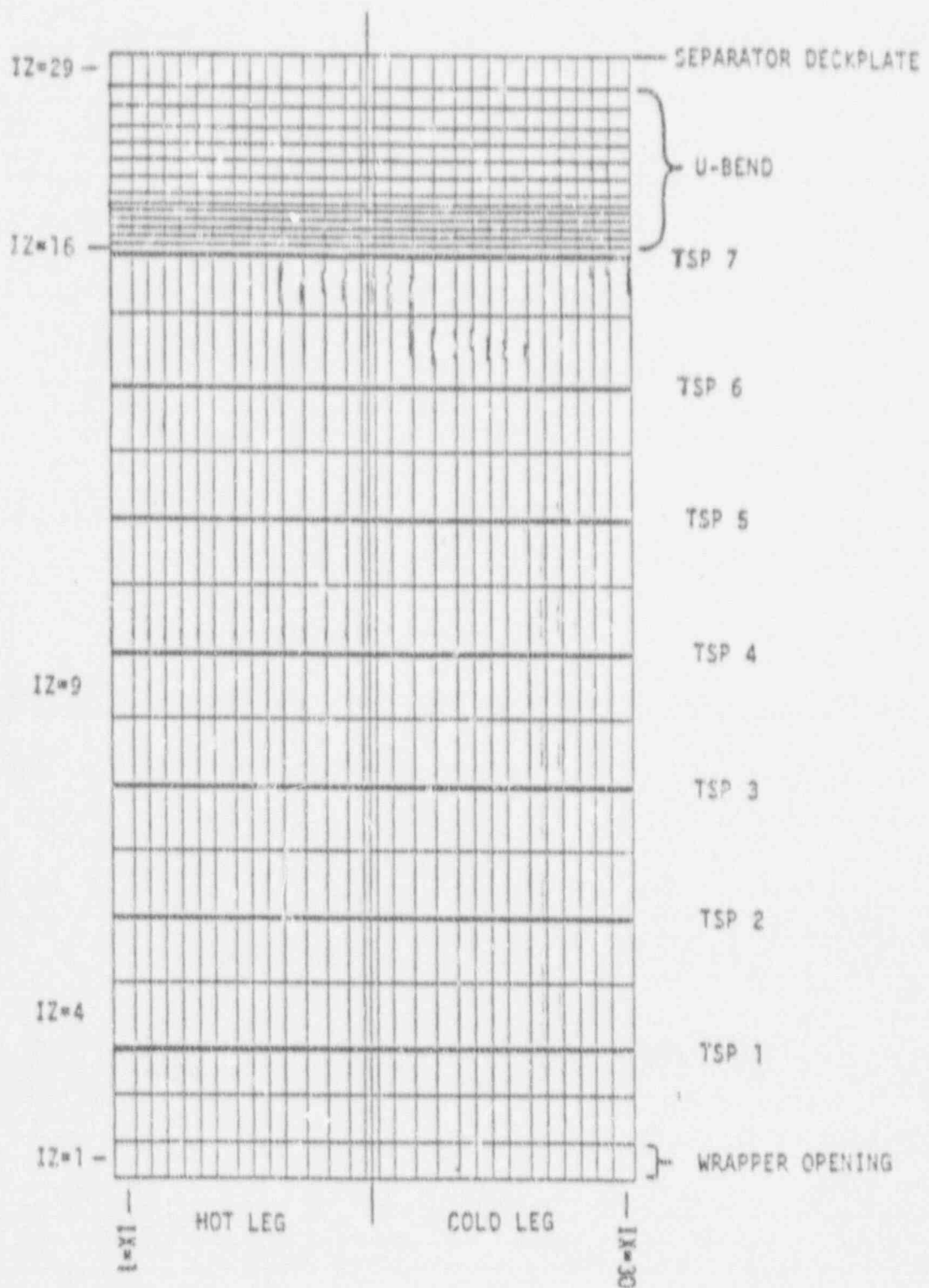
Figure 7-2 Elevation View of ATHOS Cartesian Model for North Anna
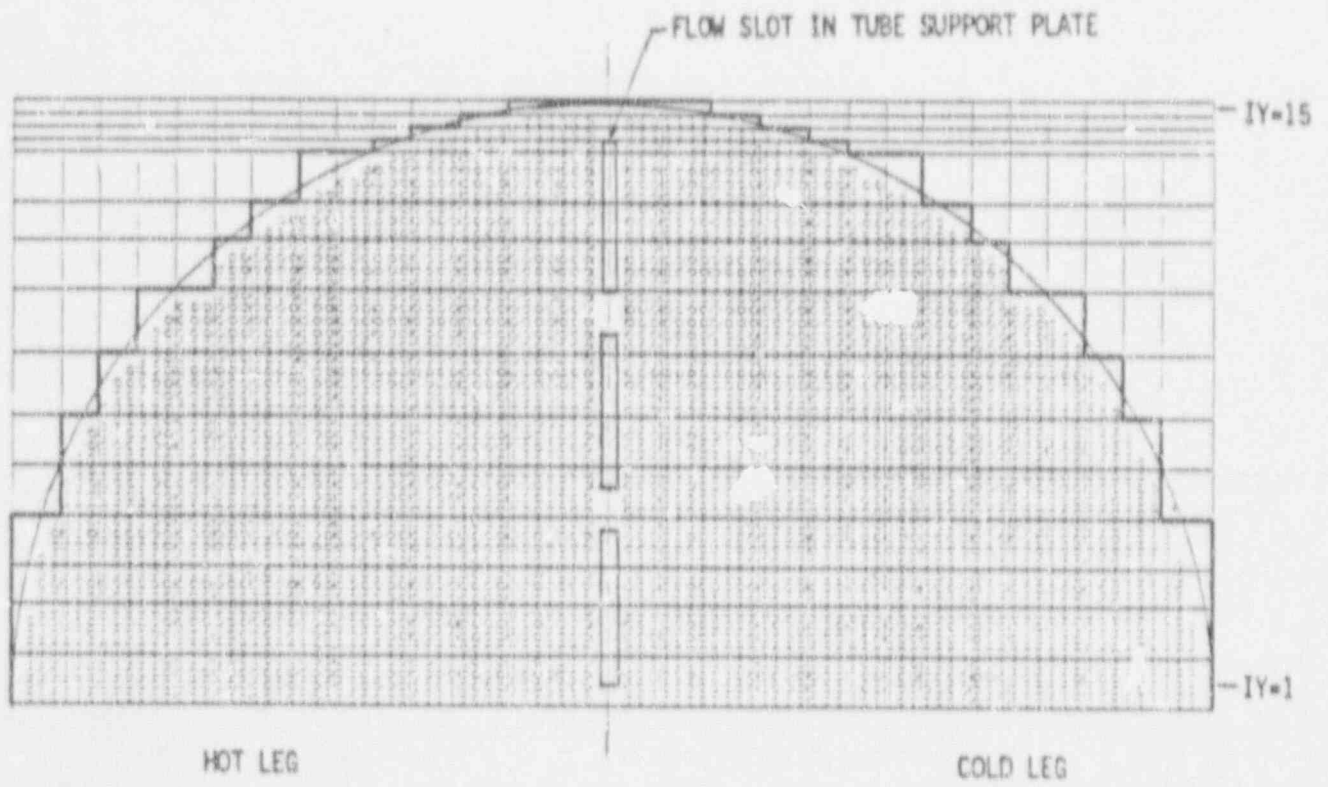
Figure 7-4 Plan View of ATHOS Cartesian Model
Indicating Tube Layout
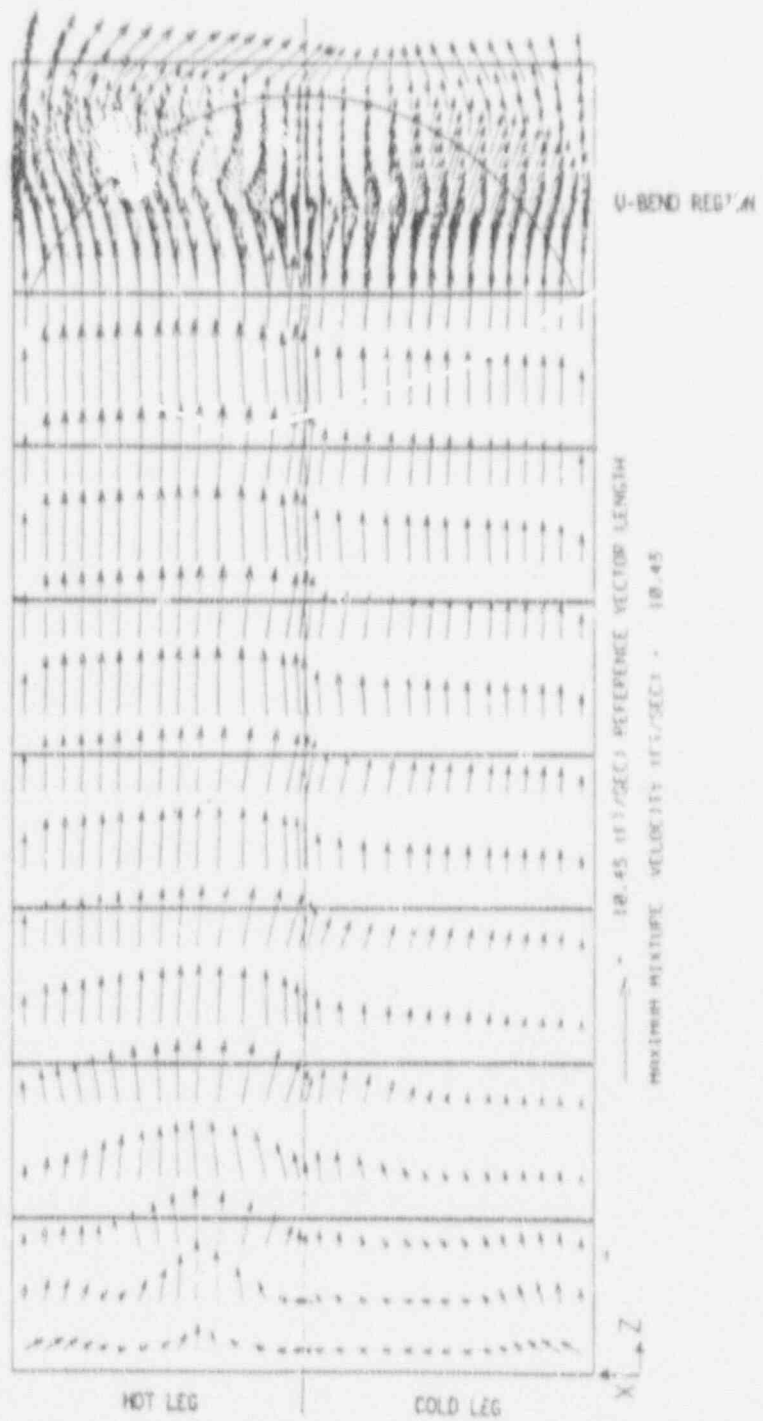
Figure 7-5 Flow Pattern on Vertical Plane of Symmetry
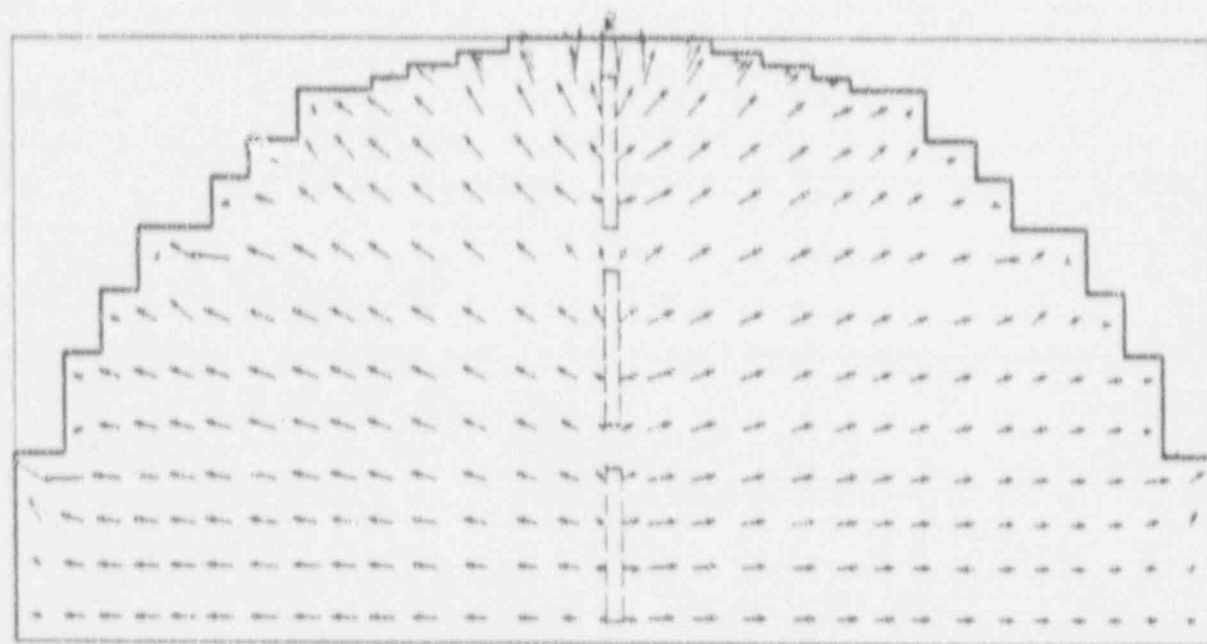
HOT LEG ──► ╼ 4.56 (FT/SEC) REFERENCE VECTOR LENGTH   COLD LEG

MAXIMUM MIXTURE VELOCITY (FT/SEC) = 2.92

Figure 7-6 Lateral Flow Pattern on a Horizontal Plane
in the U-Bend Region
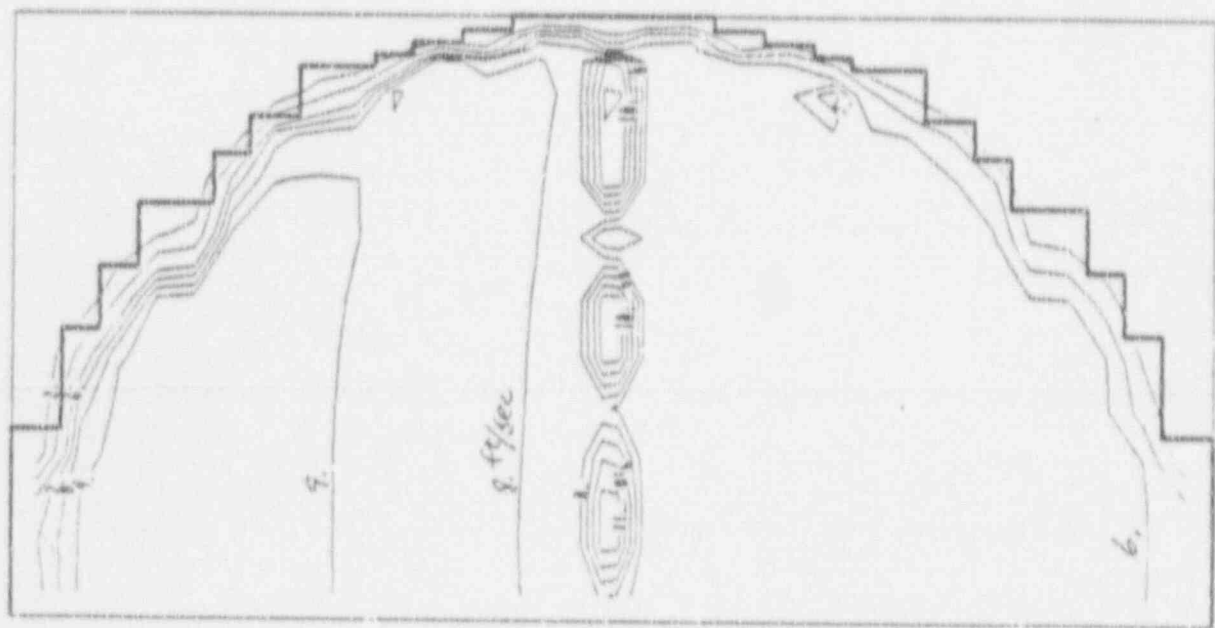
HOT LEG   COLD LEG

J-COMPONENT MIXTURE VELOCITY (FT/SEC)

Figure 7-7   Contours of Vertical Velocity Component on a
              Horizontal Plane in the U-Bend Region
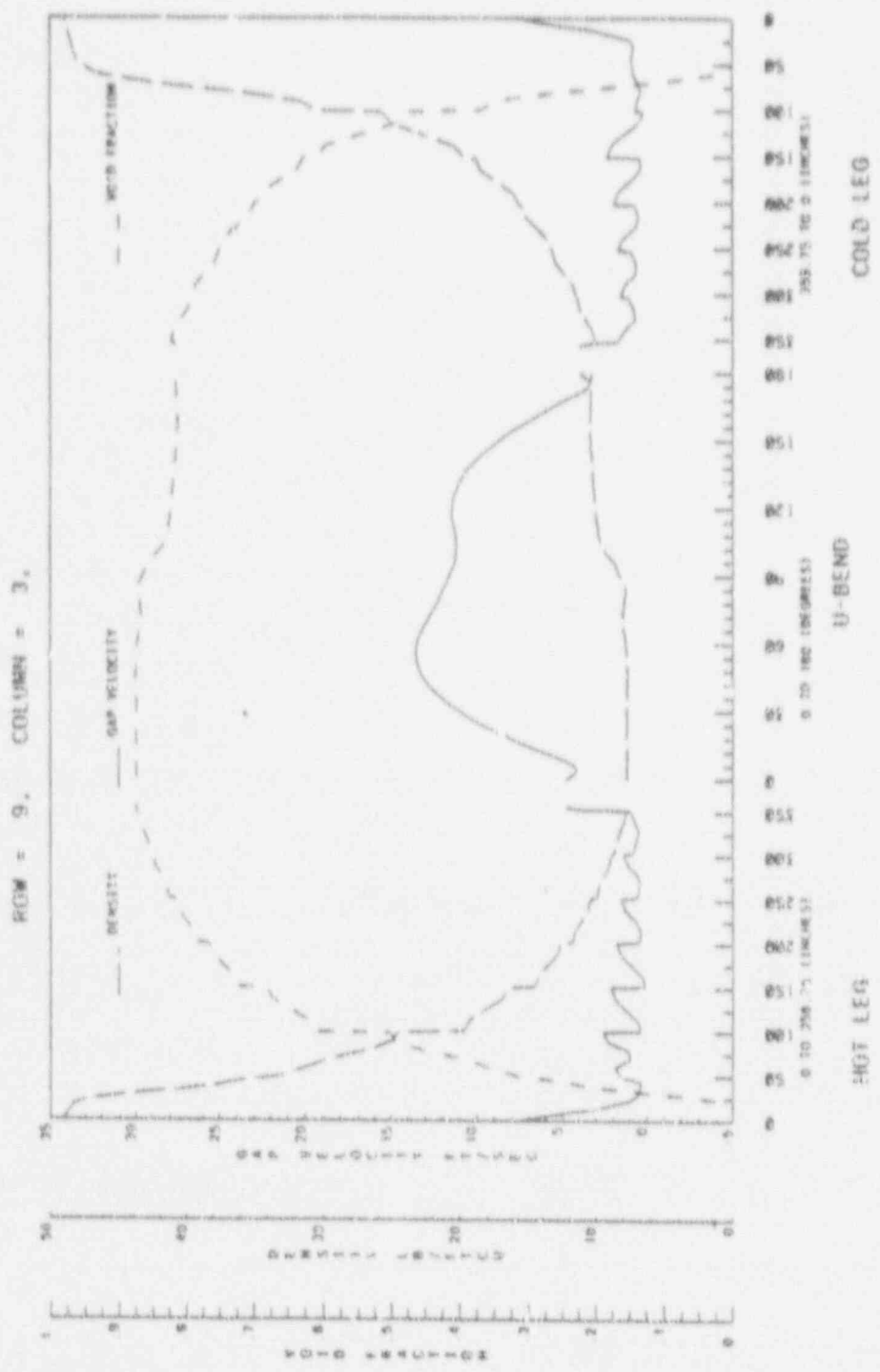
Figure 7-8 Tube Gap Velocity and Density Distributions
for Tube Row 9/Column 3
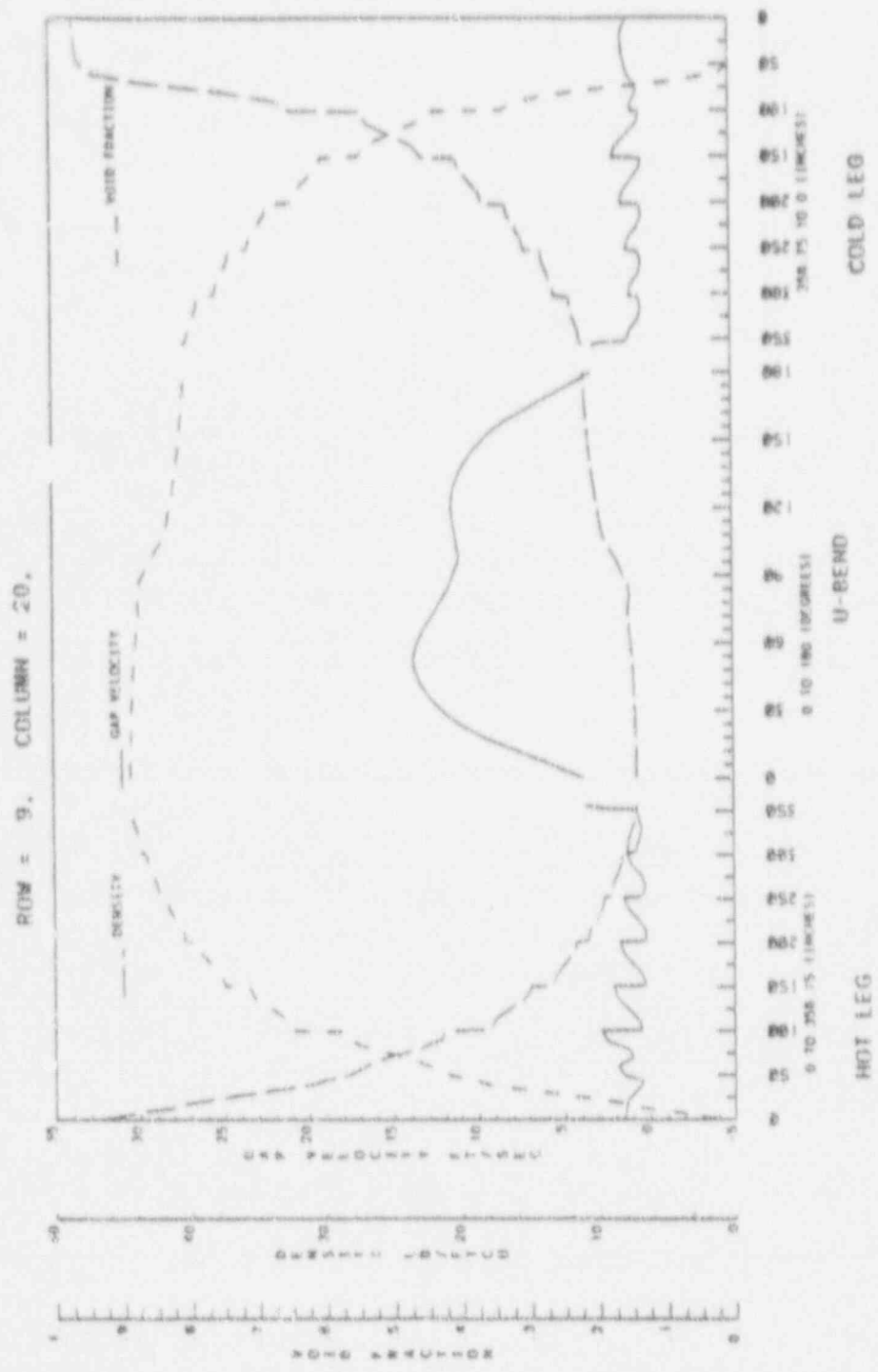
Figure 7-9 Tube Gap Velocity and Density Distributions
for Tube Row 9/Column 20
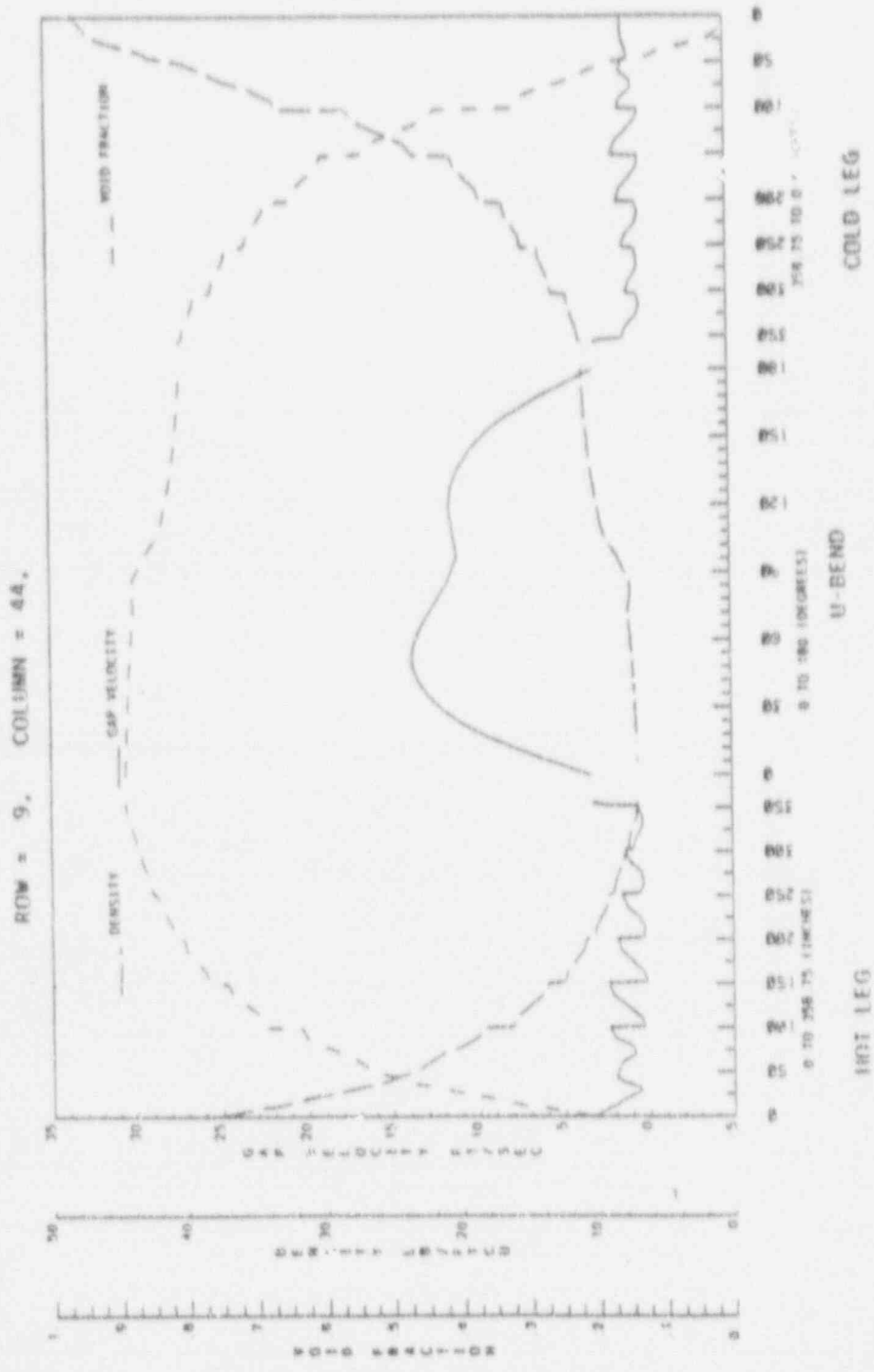
ROW = 9, COLUMN = 44,

Figure 7-10 Tube Gap Velocity and Density Distributions
for Tube Row 9/Column 44
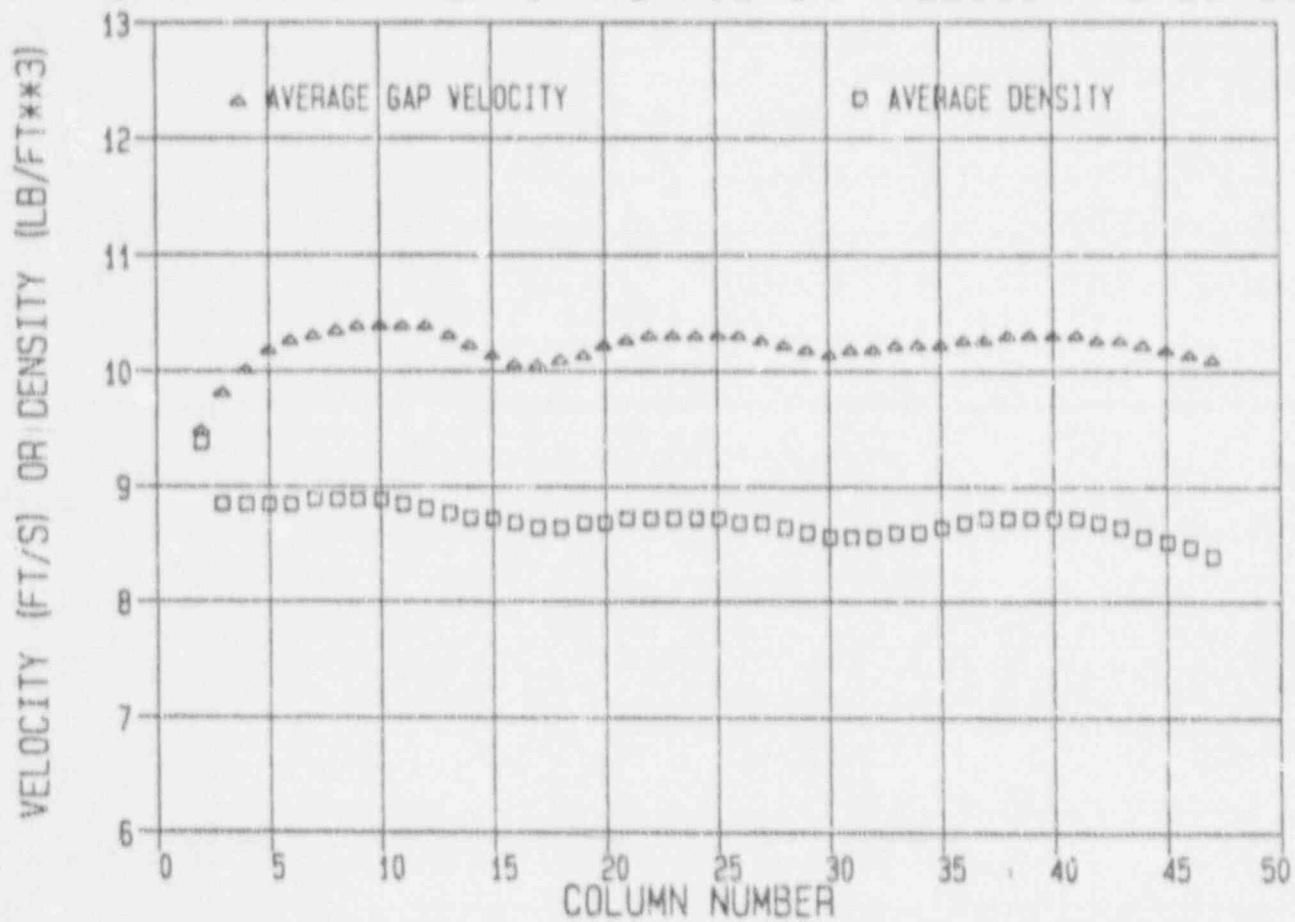
Figure 7-11 Average Velocity and Density in the Plane of the
U-Bends Normal to Row 9

NORTH ANNA 2 NORMALIZED STABILITY RATIO
BASED ON HIGH POWER(>85%) OPERATION
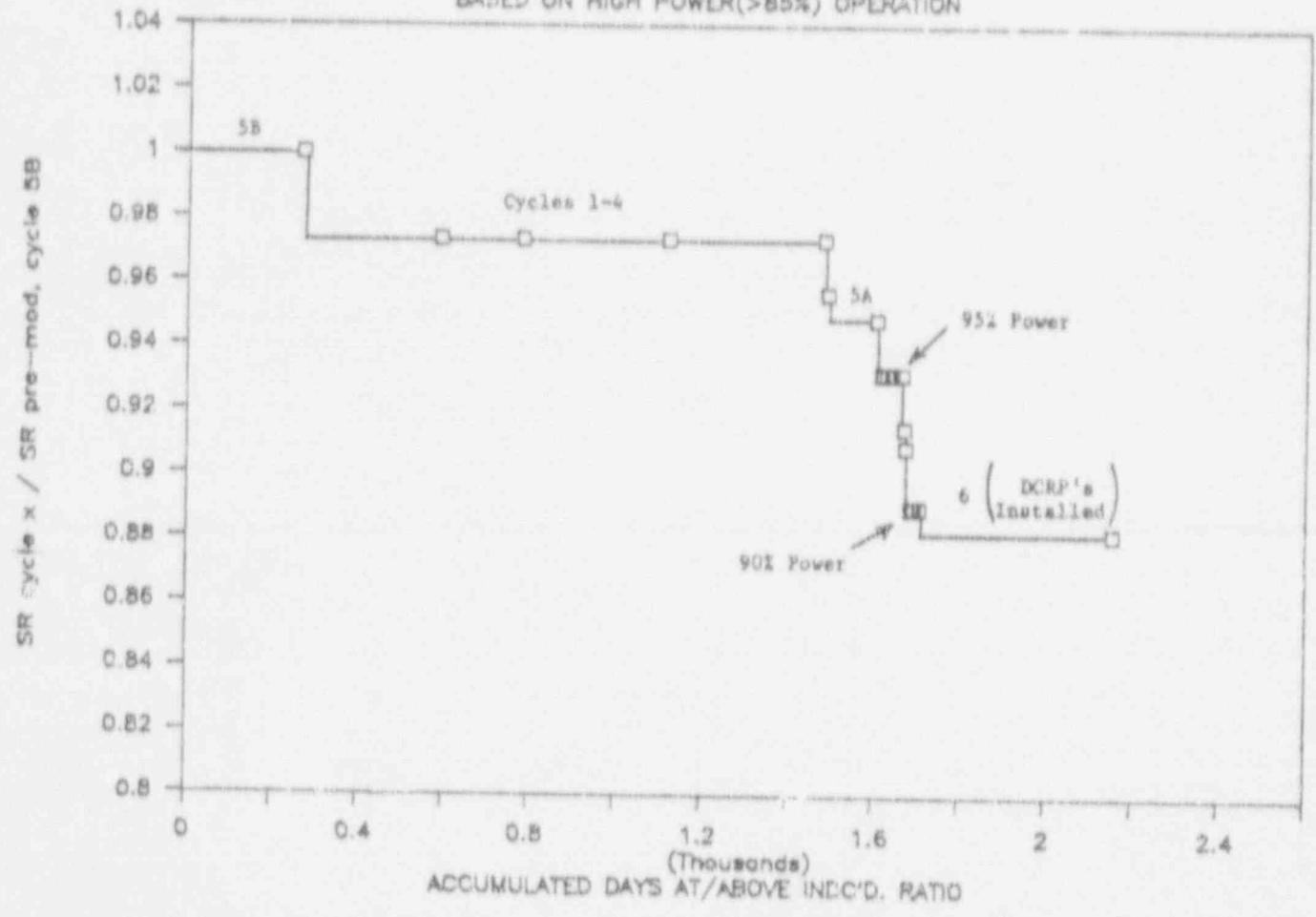
Figure 7-12 North Anna 2 Normalized Stability Ratio
Based on High Power (> 85%) Operation

8.0 PEAKING FACTOR EVALUATION

This section describes the overall peaking factor evaluation to define the
test based peaking factors for use in the tube fatigue evaluation. The
evaluation of the eddy current data to define the AVB configuration for North
Anna 1 Tube R9C51 is described. This configuration is critical to the tube
fatigue assessments as the peaking factors for all other tubes are utilized
relative to the R9C51 peaking factor. Uncertainties associated with applying
the air model test results to the tube fatigue assessments are also included
in this section. Included in the uncertainty evaluation are the following
contributions:

   o   Extrapolation of air test results to two phase steam-water
   o   Cantilever tube simulation of U-bend tubes
   o   Test measurements and repeatability
   o   AVB insertion depth uncertainty

8.1 North Anna 1 R9C51 Configuration

8.1.1 Background

The AVB configuration of the ruptured tube in North Anna 1, R9C51, is the
reference case for the tube fatigue evaluations for other tubes. In
accordance with the NRC Bulletin 88-02, the acceptability of unsupported tubes
is based on tube specific analysis relative to the North Anna R9C51 tube,
including the relative flow peaking factors. Thus, the support conditions of
the R9C51 tube are fundamental to the analyses of other tubes. Because of the
importance of the R9C51 tube, the support conditions of this tube. which were
originally based on "AVB Visible" interpretations of the eddy current test
(ECT) data (Figure 8-1), were reevaluated using the projection technique
developed since the North Anna event. The projection technique is
particularly valuable for establishing AVB positions when deposits on the
tubes tend to mask AVB signals such as found for the North Anna 1 tubes. The
results of this evaluation are summarized below.

8.1.2 Description of the Method

The basic method utilized was the projection technique in which the AVB position is determined based on measured AVB locations in larger row tubes in the same column. In this study, the projection technique was utilized in the "blind" mode, (AVBs called strictly based on the data) as well as the reverse mode (data examined on the basis of predicted AVB positions). The objective of this application was, with the greatest confidence possible, to establish the positions of the AVBs in an 8 column range around the R9C51 tube in North Anna 1, Steam Generator C.

8.1.3 Data Interpretation

The ECT traces for the U-bends in Rows 8-12 (in one case, 13) were examined for Columns 48-55. The original AVB visible calls are shown in Figure 8-1. The data were examined by an eddy current analyst experienced in reading these traces, and by a design engineer knowledgeable in the geometry of the Model 51 U-bend region.

The intent of this review was to determine if the presence or absence of AVBs as shown in Figure 8-1 could be confirmed using the AVB projection technique. Preliminary projected AVB positions were based on geometric data provided for a few of the tubes near R9C51. The features which were sought were evidence of data "spikes" where AVBs were predicted, offset indications (multiple spikes) where offset AVBs were predicted, single indications where single AVB intersections were predicted, etc. The data evaluation method used was a critical examination of the data, which was biased toward the presence of AVBs unless a confident call of "no AVB" could be made, and then checking the consistency of the data among the tubes in a column and against the theoretical data for the predicted AVB positions. [

]a,c.

Figure 8-4 is the "AVB visible" map for columns 48 through 55, based on the
critical review of the data. It should be noted that the original data
interpretations and the review interpretations are consistent.

8.1.4 Projections

The [   ]a,c ECT traces were
utilized for projecting the position of the AVBs according to the standard
format of the projection method.

The results of the projections are presented in Figure 8-5, which shows a
matrix of projections for tube rows 8 through 13 in columns 48 through 55.
For many of the tubes, more than one, and as many as three, projection values

are shown. Multiple projections are expected for a tube if the AVBs on either side of the tube are not at the same elevation, or if the upper and lower AVB support that tube. As many as four different projections are possible if it is assumed that the tube is supported by the upper and lower AVBs, and both upper and lower bars are staggered in elevation as shown in Figure 8-2.

The logic in arranging the projection data is based on the following two rules:

Rule 1. The projections of the same AVB based on different tubes in the same column [   ]^{a,c}.

[

                                                                    ]^{a,c}.

Rule 2. Two adjacent tubes in the same row [
                    ]^{a,c}. Consequently, the difference in the

[

                    ]^{a,c}.

The implementation of this is that if the position (either left or right) of a projected AVB is assumed for a column, then the projections in the adjacent columns are also [

                    ]^{a,c}.

The arrangement of the AVBs as shown in Figure 8-5 satisfies the rules above
and is consistent with the rupture of R9C51. The resulting AVB arrangements,
based on the projection matrix of Figure 8-5 is shown in Figure 8-6.

8.1.5 Conclusions

The general AVB arrangement surrounding the ruptured tube in North Anna 1,
Steam Generator C, which was the basis for the analysis, is confirmed by a
detailed critical review of the ECT data. Differences exist in the AVB
pattern between tube columns 48-49, in which the AVBs appear to be less
inserted than previously indicated. The pattern of Figure 8-6 is the best fit
to the rules which were adopted for determining the position of the AVBs, as
well as consistent with explanation of the tube failure.

The basis of the review was a projection technique which utilizes data from
tubes one or more rows removed from the actual inserted position of the AVB to
determine the position of the AVB. The intent of the review was to establish
the positions of the AVBs by confirming or eliminating features of AVB
alignments such as side to side offsets, etc. of the AVBs adjacent to the
tubes. Overall, the conclusions regarding the positions of the AVBs around
R9C51 in North Anna 1, Steam Generator C are based on consistency among all
the available data.

8.2 Test Measurement Uncertainties

The descriptions of the peaking factor tests and apparatus were provided in
Section 5.4. All practical measures were taken to reduce uncertainties.
Nevertheless, some still remain and should be properly accounted for. The
important parameter measured during testing that has a significant impact on
peaking factor is the air velocity. The air velocity at test section inlet
was measured using a [   ]^{a,c}. Based on considerable
experience with the use of such instruments, it is known that the magnitude of
uncertainty is very small. A [   ]^{a,c} measurement uncertainty is used in
this analysis based on past experience.

8.3 Test Repeatability

During the peaking factor testing of AVB configuration, each test was performed at least two times to confirm repeatability. It has been demonstrated that the tests are quite repeatable with the results often falling within 2 or 3% of one another for the repeat tests. An upper bound value of 5% was used in the current uncertainty analysis.

8.4 Cantilever vs U-Tube

A first order estimate can be made of the validity of modeling a U-bend tube by a cantilever tube in tests to determine the effects of AVB insertion depth on the initiation of fluidelastic vibration. The following assumptions are used:

a,c

For the purposes of this estimate, the geometry of the cantilever measuring
tube in the air test model is compared with the geometry of a prototypical Row
10 tube. [

                ]^{a,c}

The comparison between a U-bend tube and the model tube involve the
consideration of an effective velocity associated with the flow perturbation
caused by the AVBs. [

]^{a,c}. Using these values, the ratio of the effective velocity for the cantilever measuring tube to that for the U-bend tube is about [   ]^{a,c} for the case treated.

A similar evaluation can be made for a Row 10 tube that lies in the projection or shadow of an AVB that is inserted to a depth required to support a Row 9 tube. [

]^{a,c}.

The net result is that the ratio of the effective velocity for the cantilever tube to that for the U-bend tube is about [   ]^{a,c}.

These results indicate that, for the particular assumptions used, the cantilever tube model appears to be a reasonable representation of the U-bend with respect to determining relative peaking factors for different AVB configurations. This evaluation also shows that, on the average, the magnitude of the systematic uncertainty associated with the use of cantilever tube to simulate the U-bend is about [   ]^{a,c}.

6.5 Air vs Steam-Water Mixture

The local peaking factors from the air tests can be applied to the steam generator steam/water conditions either as a direct factor on the mixture velocity and thus a direct factor on a stability ratio, or as a factor on the steam velocity only with associated impacts on density, void fraction and damping. This method leads to a reduction in tube damping which enhances the peaking factor compared to the direct air test value. For estimating an absolute stability ratio, this application of the peaking factor is a best estimate approach. However, for the evaluation of tubes relative to stability ratio criteria, it is more conservative to minimize the peaking factor for the North Anna unit 1 tube R9C51 through direct application of the air test

peaking factor. This conservative approach is therefore used for evaluating tube acceptability.

Under uniform AVB insertion (or aligned AVB insertion), there are no local open channels for flow to escape preferentially. Therefore, air flow is approximately the same as steam/water flow relative to velocity perturbations. Under non-uniform AVB insertion the steam/water flow may differ from air, as the steam and water may separate from each other when an obstruction, such as an AVB, appears downstream. The water would continue along the same channel while steam readily seeks a low resistance passage and thus turns into adjacent open channels. Two phase tests indicate a tendency for steam to preferentially follow the low pressure drop path compared to the water phase.

Based on the above discussion, the F_i are considered to more appropriately apply to the steam phase. Thus, it follows that mixture mass velocity for the tube subject to flow perturbation can be written as follows:

$$\left[\right]^{a,c}$$

where D_g is the vapor density, D_f the water density, F_a the velocity peaking factor determined from air tests, j_g^* the nominal superficial vapor velocity, and j_f^* the superficial water velocity. Steam quality can then be determined as follows:

$$\left[\right]^{a,c}$$

The Lellouche-Zolotar correlation (algebraic slip model), as used in the ATHOS code, is applied to determine void fraction. Subsequently, mixture density, velocity and damping coefficients for the tube which is not supported and subject to flow perturbation is evaluated. Therefore, similar to the air

velocity peaking factor, local scaling factors of mixture density and velocity and damping coefficient can be readily determined. Finally, a local stability peaking factor for fluidelastic vibration can be calculated as follows:

$$\left[\right]^{a,c}$$

where Fs is the stability peaking factor, Fd the density scaling factor, Fv the velocity scaling factor, and Fdp the damping coefficient scaling factor. If we use the air velocity peaking factor without translating to steam/water conditions, then

$$\left[\right]^{a,c}$$

As shown in Table 8-1 stability peaking factors for the steam/water mixture are slightly higher than air velocity peaking factors. The difference between the steam/water and air peaking factors increases as the air peaking factor increases.

For application to tube fatigue evaluations, the ratio of the peaking factor for a specific tube to that for North Anna R9C51 is the quantity of interest. Larger values for this ratio are conservative for the tube fatigue assessment. The North Anna R9C51 peaking factor is one of the highest peaking factors. As discussed in Section 8.7, a peaking factor of nearly [   ]^{a,c} is determined for the R9C51 tube. The differences between [

                                            ]^{a,c}. Typical
values are shown in Table 8-2. These results show that the direct application of the air test data yields the higher relative peaking factor compared to R9C51. To obtain conservatism in the peaking factor evaluation, [
                                            ]^{a,c}.

Comparing the values in the first and last columns of Table 8-1, it may be noted that the stability peaking factor for steam water is [   ]^{a,c} higher than the air velocity peaking factor. On the average, the uncertainty

associated with the conservative use of air velocity peaking factor is
[ ]^{a,c}.

The conclusion that peaking factor for steam water flow would be higher due to
the dependency of damping ratio on void fraction was supported by an alternate
study. In this study, a section of steam generator tubes were simulated using
the ATHOS code under prototypic flow conditions. The objective of this study
was to examine the magnitude of the changes in void fraction and thus
stability ratio as a consequence of non-uniform AVB insertion patterns. The
current version of ATHOS has modeling limitations that prevent accurate
modeling of local geometry effects. In addition, it is believed that an
analysis using two-fluid modeling procedure is mandatory to a calculation of
the peaking factors for a steam generator to account for the preferential
steam flow along the low resistance path. Consequently, the intent of this
analysis is only to help bound the uncertainty on void fraction effects from
extrapolating the air tests to steam-water.

First the analysis was conducted with uniformly inserted AVBs in the ATHOS
model. The ATHOS results were processed by the FLOVIB code to determine
stability ratios for the specific tubes of interest. The calculation was
repeated using a non-uniform AVB insertion pattern in the model. The results
show that the void fraction distribution changes as a result of flow
perturbation. Further, the impact on stability ratio resulting from the
changes in void fraction profiles was about [   ]^{a,c}. This alternate
calculation provides independent corroboration of the prior discussion
regarding the stability peaking factors under steam-water conditions vs in air.

8.6 AVB Insertion Depth Uncertainty

The most significant uncertainty for the low peaking configurations is not in
the test results, but in the determination of actual AVB insertion patterns
adjacent to specific tubes. The methodology used for obtaining the AVB
insertion patterns from eddy current data can ascertain the AVB location only
approximately. The effect on peaking factor resulting from this uncertainty
is addressed using test results of AVB configurations that varied from one
another by up to [   ]^{a,c}.

Based on maps of AVB insertion depth of various plants, several configurations
have been tested for determining fluidelastic instability flow rate by an air
cantilever model. Stability peaking factors were then determined from the
ratio of critical flow rate for a uniform AVB insertion configuration to a
specific configuration. Figure 8-7 summarizes the AVB configurations tested.

Position of AVB insertion depth is determined from Eddy Current Test (ECT)
data. Positioning of AVB from ECT data reading is subject to uncertainty; its
accuracy is probably about [   ]^{a,c}. A change of an AVB
insertion depth in a given configuration leads to a different configuration,
and thus a different peaking factor. A review of the tested AVB type has been
made and results summarized in Table 8-3. As can be seen, a decrease in depth
of an appropriate AVB tends to decrease the peaking factor, for instance, a
[

  ]^{a,c}. Such a trend can be explained; a decrease in a specific AVB depth
will open up more channels for incoming fluid to distribute and thus less flow
perturbation. However, this applies only to those changes without inducing
the reinforcement of flow perturbation from upstream to downstream.

On the average, the uncertainty in peaking factor resulting from small
variations in AVB insertion (of the order of 1/2 tube pitch) is found to be
[   ]^{a,c}.

8.7 Overall Peaking Factor with Uncertainty

As discussed in the previous subsections, there are several aspects to be considered in applying the laboratory test data to steam generator conditions. These considerations were reviewed one at a time in those subsections. This section will integrate the pieces into one set of stability peaking factors.

Looking forward to how these peaking factors are used in the analysis (Section 9), the relative stability ratio calculated for a given tube without the consideration of flow peaking is corrected using the ratio of the peaking factor of the specific tube to that of the North Anna Unit 1, SG-C R9C51 tube (Configuration 1a).

It is to be noted that the test results would be applied as ratios of a specific tube peaking factor to the R9C51 peaking factor. This will reduce the influence of some uncertainties since the systematic uncertainties would affect both the numerator and the denominator in the ratio of peaking factors. The major difference will be in those configurations whose peaking factors are significantly lower than that of R9C51. The approach employed here is intended to provide that conservative peaking factors are employed for such apparently low peaking configurations.

The uniform AVB configuration (2a) is selected as a reference configuration, and the peaking factors of all configurations tested are recomputed on the basis of this reference. As discussed below, some of the test uncertainties are applied to the reference case to account for its significantly low peaking relative to the R9C51 configuration.

The uncertainties in the test results and their extrapolation are those due to test measurements, test repeatability, cantilever tubes in the test vs U-tubes in the steam generator, and air tests vs steam-water mixture. These were discussed in more detail in the previous subsections. The magnitude of these uncertainties are listed in Table 8-4.

Of these uncertainties, those due to measurement and repeatability of tests are random errors and can occur in any test. Therefore, these are treated together. The total random uncertainties are calculated by [

]^{a,c}. The RSS value of these is [ ]^{a,c}. Since these can occur in any test, these are to be applied to all tests. One way of doing this is to apply it to the R9C51 value, that being in the denominator of the final peaking factor ratio. Thus the peaking factor for configuration 1a (R9C51) is reduced by this amount to yield a value of [ ]^{a,c} instead of the [ ]^{a,c} appearing in Table 5-2.

The next three uncertainties in Table 8-4 are systematic uncertainties. It could be argued that these appear in the peaking factors of both the specific tube under consideration and the R9C51 tube and are therefore counter balanced. However, the relative magnitude of these may be different, particularly for configurations with much lower peaking than R9C51. Therefore it was judged that the [

]^{a,c}. Similarly, as noted above, the effect on peaking factor due to the uncertainty in the field AVB configuration is also included in this reference case. Thus, [

]^{a,c}. The peaking factor of the reference configuration 2a (Table 8-5) is raised by this amount to a value of [ ]^{a,c}.

The change in peaking factors of configurations 1a and 2a resulting from the application of uncertainties as described above are shown in Column 3 of Table 8-5. The peaking factors of all configurations are recomputed on the basis of this reference configuration (2a). These values are displayed in Column 4 of Table 8-5.

Some of the uncertainties were applied to the reference configuration (2a) in order to apply them to all low peaking configurations conservatively. Thus, no configuration should have a lower peaking factor than this reference configuration. Therefore, when a peaking factor value less than [ ]^{a,c} is calculated for any configuration, (in Column 4 of Table 8-5), it should be altered to [ ]^{a,c}. Further, for some of the configurations that are

conceptually similar, the more limiting (higher) value is used. For example, a peaking factor of [ ]^{a,c} is used for configurations 5a and 5b based on their similarity to configuration 5c.

The final stability ratio peaking factors calculated on this basis (with configuration 2a as the reference) are shown in Table 8-6.

The overall conclusions from the peaking factor assessment are:

1. As noted in Table 8-4, five elements have been included in the uncertainty evaluation for the peaking factors. The uncertainty estimates were developed from both test and analysis results as described in Sections 8.2 to 8.6. The largest single uncertainty of [ ]^{a,c} is attributable to uncertainties of up to [ ]^{a,c} on determination of AVB insertion depths from field eddy current data. This relatively large uncertainty is applicable only to low peaking conditions where the AVB uncertainties can contribute to small peaking factors. The definition of "no flow peaking" was increased to encompass the small peaking effects from AVB insertion uncertainties. For the AVB patterns leading to significant peaking factors, AVBs were positioned within uncertainties to maximize the peaking factor. For these configurations, variations of AVB insertion within these uncertainties are expected to reduce the peaking factor compared to the final values of Table 8-6 and Figure 8-7.

2. Including uncertainties directed toward conservatively decreasing the peaking factor for the North Anna tube R9C51, the final R9C51 peaking factor is [ ]^{a,c} relative to a no flow peaking condition such as with uniform AVB insertion depths.

8.8 Peaking Factors for Specific Tubes

The AVB positions on each insertion pattern of Figure 8-7 should be carefully noted. [

]^{a,c}

[

        ]^{a,c} Table 8-7 summarizes the results of peaking factors. Figure 8-7 shows the peaking factors with the pictorial representation of the AVB insertion configurations.

In applying the methodology to North Anna 2, [

        ]^{a,c} Based on the R9C51 tube vibration analysis, flow peaking factors on the order of [   ]^{a,c} for Row 8 tubes and above [   ]^{a,c} for Row 9 tubes would be required for tube fatigue to be a concern.

[

        ]^{a,c}

Determination of peaking factors for identified tubes shown in Table 8-7 are described in detail. Table 8-7 is divided into small tables for ease in following the description.

8.8.1 Steam Generator A

The following table gives the peaking factors for Steam Generator A tubes with unique configurations of AVB insertion depths.

Steam Generator	Row No	Column No	Type of AVB Insertion Depth	Peaking Factor
A	8	64	[	] a,c
	9	60		
		35		
		All of the Remaining		

[

] a,c

8.8.2 Steam Generator B

The following are a list of 5 tubes with unique AVB configurations.

Steam Generator	Row No	Column No	Type of AVB Insertion Depth	Peaking Factor
B	8	81	[	] a,c
		60		
		31		
	9	44		
		35		
		All of the Remaining		

For R8C81 and R8C31, [

] a,c

8.8.3 Steam Generator C

Tubes with unique AVB configurations were evaluated. The following table lists their peaking factors and types of AVB configurations.

Steam Generator	Row No	Column No	Type of AVB Insertion Depth	Peaking Factor
C	9	83	[	] a,c
		60		
		55		
		40		
		35		
	10	60		

R9C83 belonged to [

                    ] a,c

Table 8-1

Stability Peaking Factor Due to Local Velocity Perturbation

Scaling Factors for Steam/Water

Air Velocity Peaking Factor,	Void Fraction Scaling,	Density Scaling,	Velocity Scaling,	Damping Scaling,	Stability Peaking Factor,
F_a	F_v	F_d	F_v	F_{dp}	F_s

$$\begin{bmatrix} & & & & \end{bmatrix}^{a,c}$$

NOTE: 1. Stability peaking factor for steam/water mixture is calculated as follows:

$$\begin{bmatrix} & & \end{bmatrix}^{a,c}$$

2. Damping scaling factor is calculated using modal effective void fraction of [   ]^{d,c} for R9C51 tube.

Table 8-2

Comparison of Air and Steam-water Peaking Factor Ratios

Air Peaking Factor	Air Peaking Ratio	Steam Peaking Factor	Steam Peaking Ratio
			a,c

Table 8-3

Effect of Local Variation of AVB Insertion

Type A	Type B	A to B AVB Variation	Peaking Factor A	Peaking Factor B	Ratio (B/A)	
5b	5a					a,c
4a	5c					
5c	5a					
5a	5b					a,c
5c	4a					
5a	5c					

Table 8-4

Uncertainties in Test Data and Extrapolation

Source of Uncertainty	Type	Magnitude, %
		a,c
1.		
2.		
3.		
4.		
5.		

*   This is not an uncertainty associated with the test data.
     It results from the inaccuracy in determining the true AVB
     position in the field using eddy current data.

Table 8-5

Extrapolation of Test Results to Steam Generator Conditions

Configuration	Test Data	Data with Uncertainties	Peaking Factor Referenced to Configuration 2a
			a,c

Table 8-6

Final Peaking Factor

Configuration	Peaking Factor
	a,c

Table 8-7
Stability Peaking Factors for Specific Tubes
North Anna 2

Steam Generator	Row No	Column No	Type of AVB Insertion	Peaking Factor
A	8	64		a,c
	9	60		
		35		
		All of the Remaining		
B	8	81		
		60		
		31		
	9	44		
		35		
		All of the Remaining		
C	9	83		
		60		
		55		
		40		
		35		
	10	60		
		All of the Remaining		
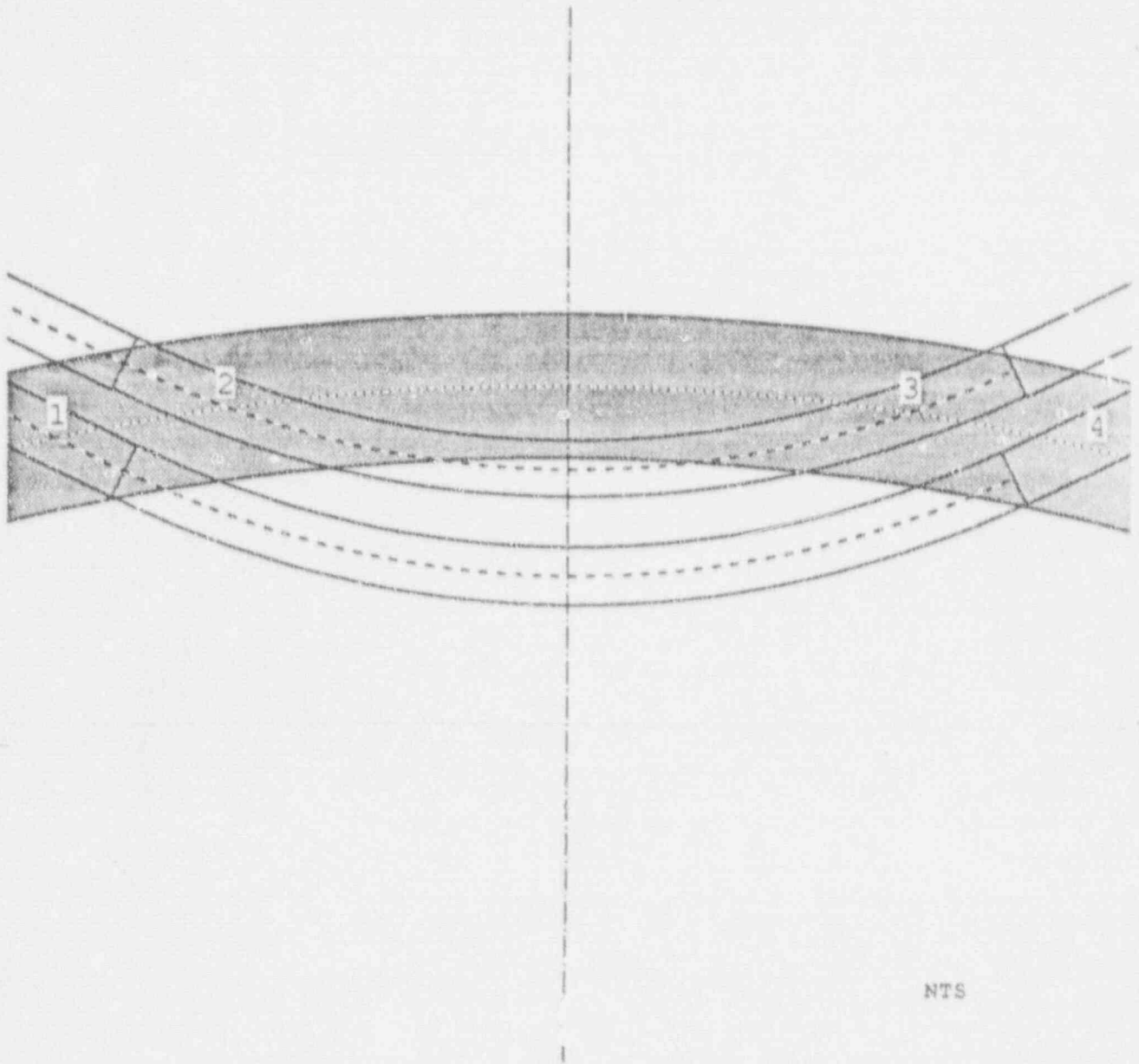
NTS

Figure 8-2

Schematic of Staggered AVBs

a,c
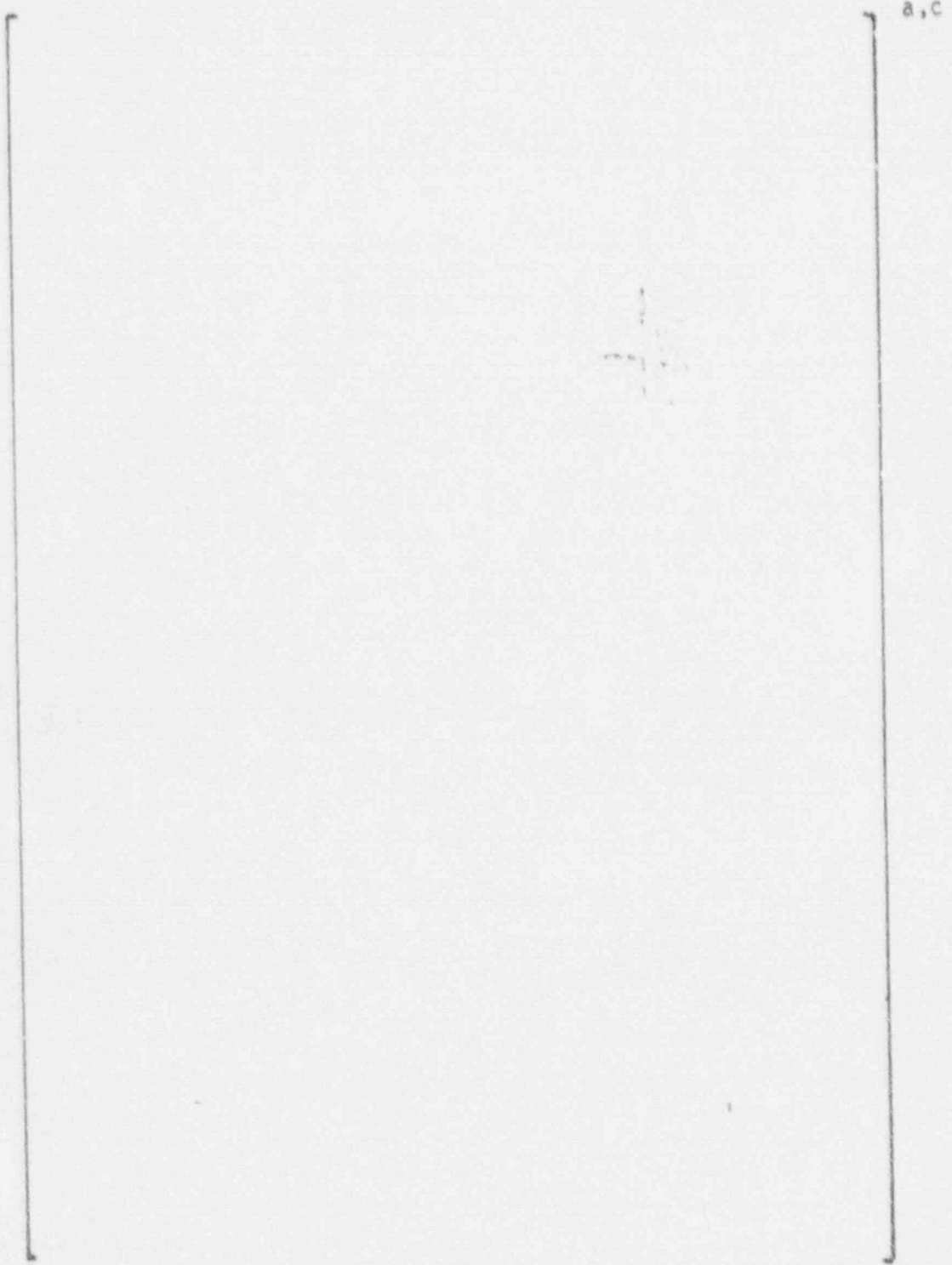
Figure 8-3 AVB "Pair" in ECT Trace
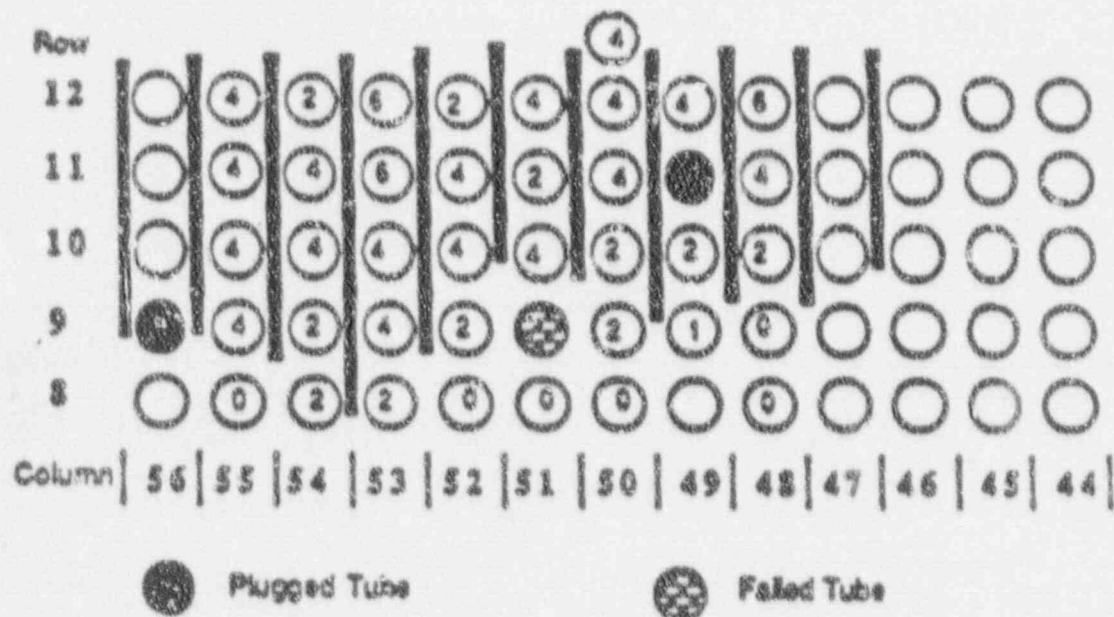
Figure 8-4 North Anna 1, Steam Generator C, AVB Positions
Critical Review "AVB Visible" Calls
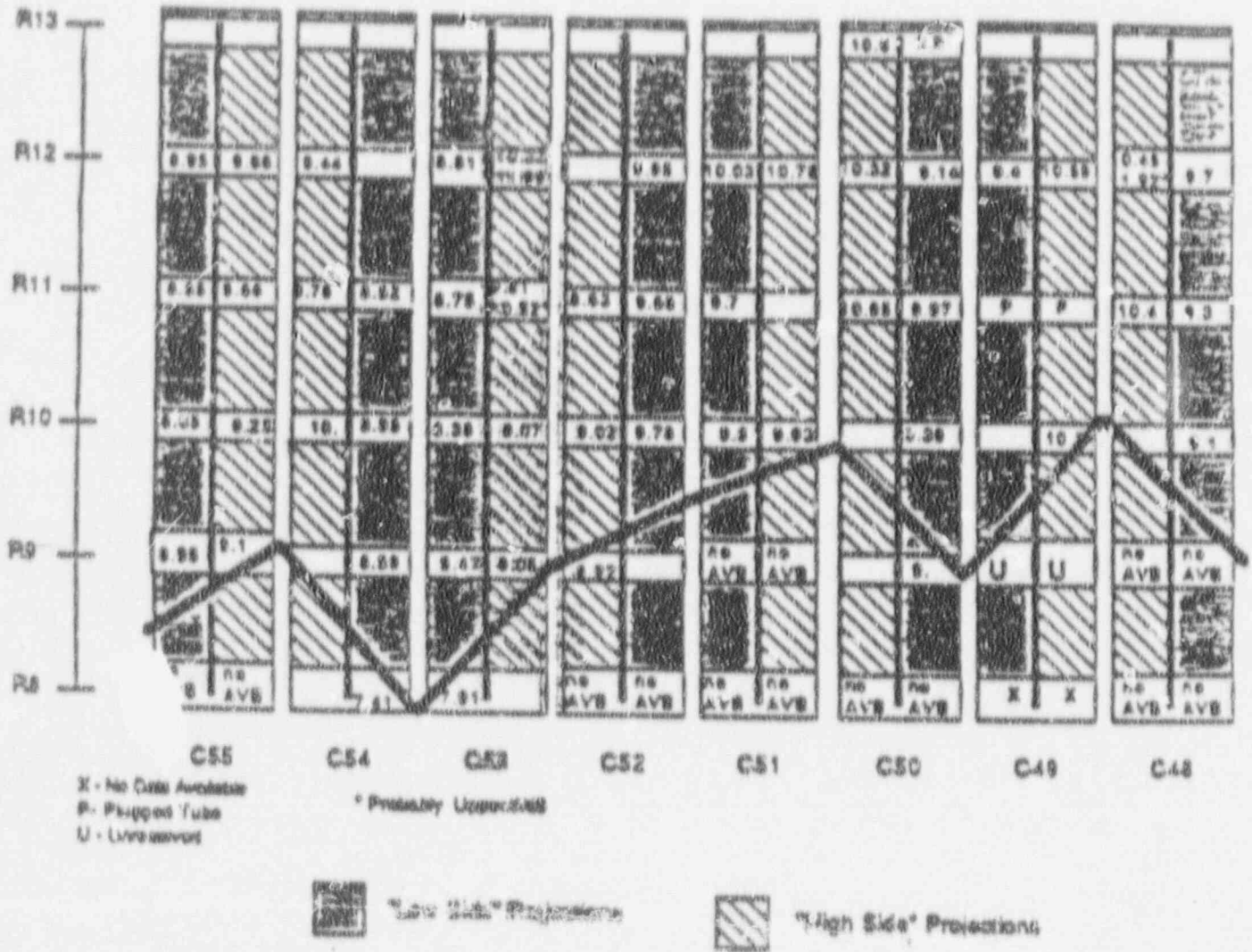
Figure 8-5 North Anna 1, Steam Generator C, R9C51 AVB
[   ]^{m,c} Matrix
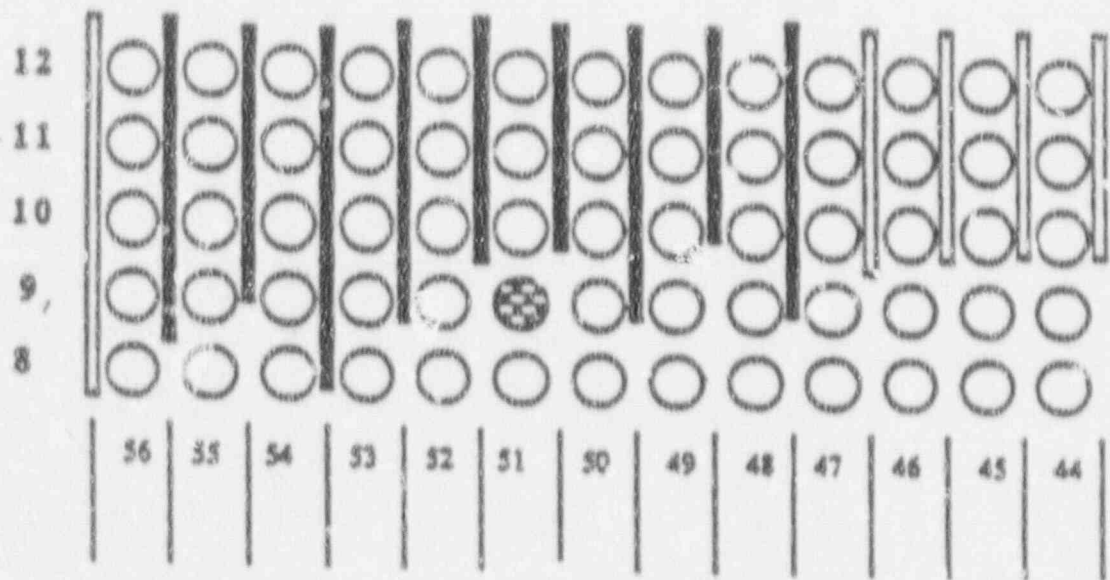
Figure 8-6 North Anna R9C51 Final [   ]^{a,c} Positions
(Configuration 1a)

TYPE OF AVB INSERTION	PEAKING FACTOR	TYPE OF AVB INSERTION	PEAKING FACTOR	TYPE OF AVB INSERTION	PEAKING FACTOR
1a	a,c	2a	a,c	5a	a,c
1b		4a		5b	
1e		4b		5c	
1j		4f		6a	
1w		4r		8d	
1z		4s			

Figure 9-7 Final Peaking Factors for North Anna Unit 2

9.0 STRUCTURAL AND TUBE VIBRATION ASSESSMENTS

9.1 Stability Ratio Distribution Based Upon ATHOS

An assessment of the potential for tubes to experience fluidelastic instability
in the U-bend region has been performed for each of the tubes in rows eight
through twelve. This analysis utilizes FASTVIB, a Westinghouse proprietary
finite element based computer code, and PLOTVIB, a post processor to FASTVIB.
These codes predict the individual responses of an entire row of steam
generator tubing exposed to a location dependent fluid velocity and density
profile. The program calculates tube natural frequencies and mode shapes using
a linear finite element model of the tube. The fluidelastic stability ratio
U_e/U_c (the ratio of the effective velocity to the critical velocity) and
the vibration amplitudes caused by turbulence are calculated for a given
velocity/density/void fraction profile and tube support condition. The
velocity, density and void fraction distributions are determined using the
ATHOS computer code as described in Section 7.2. The WECAN generated mass and
stiffness matrices used to represent the tube are also input to the code.
(WECAN is also a Westinghouse proprietary computer code.) Additional input to
FASTVIB/PLOTVIB consists of tube support conditions, fluidelastic stability
constant and turbulence constants.

This process was performed for the North Anna Unit 2 steam generator tubes
under consideration and also for the premod North Anna Unit 1 Row 9 Column 51
tube (R9C51). Ratios of the North Anna Unit 2 results to those for the premod
R9C51 Unit 1 tube were generated to produce a quantity that could be used to
provide an initial assessment of the North Anna Unit 2 tubes relative to the
ruptured R9C51 Unit 1 tube.

Note that three separate steam generator conditions are to be considered in
this evaluation:

  1) Premod - The conditions that existed in the steam generator before the
      downcomer resistance plate was installed.

2) Postmod without T_{hot} Reduction - Conditions that exist after installation of the downcomer resistance plate (not including any T_{hot} reduction effects).

3) Postmod with T_{hot} Reduction - Conditions that exist after installation of the downcomer resistance plate (including the effects of T_{hot} reduction).

Relative stability ratios (and stress ratios) have been generated for each of the conditions listed above. Section 7 contains details of the calculations used to define the fluid conditions used in the evaluation. However, it can be noted in this section that results for both the Postmod With T_{hot} reduction case and Postmod Without T_{hot} reduction case were obtained through the use of ratios applied to the Premod results.

Figure 9-1, 9-2 and 9-3 contain values of relative stability ratio (including flow peaking) for each of the 3 cases described above. The relative ratios contained in the figures were obtained using the following conditions for the Premod Unit 1 R9C51 tube and also for the Unit 2 tubes under consideration:

1) Tube is fixed at the top tube support plate,

2) Void fraction dependent damping,

3) No AVB supports are active,

4) Location dependent flow peaking factors.

It is to be noted that the stability ratios plotted in Figure 9-1, 9-2 and 9-3 are composites of all steam generators using mirror image tubes. That is, any peaking effect for a given tube located on the plot represents the maximum value of the peaking factor in all steam generators at that location.

A horizontal line is drawn at the relative stability ratio value of 0.90. This identifies the point where a ten percent reduction in stability ratio exists relative to the premod Unit 1 R9C51 tube. (See Section 4.1 for a discussion of the stability ratio reduction criteria.) All the tubes with ratios above this line would be considered to have stability ratios larger than ninety percent of the premod R9C51 value.

These figures indicate that several tubes in Row 9 have relative stability ratios that lay above the 0.90 line. These tubes (SG:A R9C60, SG:B R9C35, SG:C R9C35 and R9C60) are enveloped by a single value and appear in the figure as a single point. (Note that all tubes in Rows 11 and 12 are supported and therefore can be removed from consideration. These tubes were included in the figures for completeness and comparison purposes.)

Table 9-1 contains a summary of values of relative stability ratio, including flow peaking, for the tubes with significant relative flow peaking or relative stability ratio for the cases described above. As can be observed in the table, all tubes that have a relative stability ratio greater than 0.90 for the Premod conditions have relative stability ratios less than 0.90 both the Postmod and Postmod with T_{hot} reduction cases. This indicates that additional analysis is required to determine acceptability of these tubes.

9.2 Stress Ratio Distribution with Peaking Factor

An evaluation was performed to determine the ratio of the North Anna Unit 2 tube stress over the premod North Anna Unit 1 R9C51 tube stress. This ratio is determined using relative stability ratios discussed in the previous section, relative flow peaking factors (Table 8-7 factors divided by [ ]^{a,c}) and bending moment factors. Sections 4.2 and 4.3 contain additional information and describe the calculational procedure used to obtain the results presented in this section. The results presented below are based upon the following conditions:

1) Tube is fixed at the top tube support plate,

2) Damping is void fraction dependent,

3) Tubes have no AVB support,

4) 10% criteria with frequency effects,

5) Tubes are assumed to be dented ($\sigma_{max} = \sigma_y$)

A tube can be considered acceptable if the stress ratio is less than 1.0 when calculated using the procedure described in Sections 4.2 and 4.3 and including the conditions listed above and subject to confirmation of fatigue usage acceptability. Conformance to these requirements implies that the stress acting on a given tube is expected to be insufficient to produce a fatigue event in a manner similar to the rupture that occurred in the R9C51 tube at North Anna Unit 1.

Figures 9-4, 9-5 and 9-6 show the results of the stress ratio calculations for each of the North Anna Unit 2 tubes in Rows 8 through 12 for the three cases described earlier. These ratios are applicable for tubes that are dented (tube deformation) at the top tube support plate. This case bounds the clamped tube condition with no tube deformation, i.e., the case corresponding to the NRC definition of denting with top tube support plate corrosion plus magnetite in the crevice without tube deformation.

As can be observed in Figures 9-4, 9-5 and 9-6, several tubes have stress ratios that lay above the 1.0 acceptance line for the pre-mod case. These tubes (SG:A R9C60, SG:B R9C35, SG:C R9C35 and R9C60) are enveloped by a single value and appear in the figure as a single point. (Note that all tubes in Rows 11 and 12 are supported and therefore can be removed from consideration. These tubes were included in the figures for completeness and comparison purposes.) As with the relative stability ratio figures, the stress ratio figures are also composites of all three steam generators using mirror image tubes. Specifically, any peaking effect for a given tube location indicated on the plot represents the maximum value of the peaking factor in all steam generators at that location.

Table 9-2 contains a summary of values of stress ratio for the tubes with significant relative flow peaking or relative stability ratio for the cases

described previously. As can be observed in the table, all the tubes that have stress ratios greater than 1.00 for the Premod conditions have stress ratios less than or equal to 1.00 for both the Postmod and Postmod with T_{hot} reduction cases. Note that acceptance, based upon 40 years of operation, is determined in part on tubes having stress ratios less than or equal to 1.00. The tubes having stress ratios greater than 1.00 for the Premod condition but having stress ratios less than or equal to 1.00 for the two Postmod cases must be evaluated in detail to determine the actual and projected fatigue usage associated with each tube. Final acceptance will be determined using this method.

An evaluation has also been performed to determine the required relative flow peaking that will produce a stress ratio not greater than 1.0. Figure 9-7 contains the results of this process for all the tubes in Rows 8 through 12. This figure was generated using the conditions described earlier for the Premod case. The Premod case was selected to because it is the most limiting of all the conditions currently under consideration. Note that this figure reads opposite of the previous figures, i.e., the top curve in the figure corresponds to Row 8 and the bottom curve corresponds to Row 12. Maximum Allowable Relative Flow Peaking is the required relative flow peaking (0.68 corresponds to no flow peaking) that, if used on the given tube, will produce a stress ratio not to exceed 1.0.

This curve can be used to help identify the relative flow peaking required before preventative action would be recommended and, when used in conjunction with the actual flow peaking associated with each tube, to determine the margin (if any) present. This has also been performed in Table 9-2. The column with heading "Max Allow Flow Peak" identifies the relative flow peaking factor that would be permitted, on a tube by tube basis, before the stress ratio criteria would be exceeded. As can be observed in the tables and figures, the inner row tubes have larger values of allowable relative flow peaking when compared to the outer rows.

9.3 Cumulative Fatigue Usage

All tubes that are unsupported and have a stress ratio ≤ 1.0 have a maximum stress amplitude that is < 4.0 ksi (from 9.5 ksi) since a 10% reduction in the stability ratio for the North Anna Unit 1 R9C51 tube was the criteria basis. Stability ratios have been calculated for all the North Anna Unit 2 tubes using the three cases described earlier; Premod, Postmod Without T_{hot} Reduction and Postmod With T_{hot} Reduction. The tubes are not expected to rupture as a result of fatigue if: 1) they meet the stress ratio criteria of ≤ 1.0 and 2) their current and future fatigue usage will total less than 1.0.

Determining acceptability of the North Anna Unit 2 tubes is complicated by the fact that several tubes have stress ratios greater than 1.00 for the Premod conditions, but have values less than 1.00 for the Postmod conditions and less than or equal to 1.00 for the Postmod with T_{hot} reduction conditions. Acceptance of these tubes must be determined by calculating the actual fatigue usage factors for each tube on a case by case basis. Tubes with current and projected fatigue usage factors less than 1.00 will be acceptable (with respect to U-bend fatigue) and will not require preventive action or can be returned to service if currently sentinel plugged.

Table 9-3 contains a summary of fatigue usage factors for tubes that have stress ratios near or greater than 1.00 (calculated using the more limiting Premod conditions and assuming the tubes became dented since the first cycle). As can be observed in the table, all tubes currently have fatigue usage factors less than 1.00. Future usage factors have been determined for operation under current operating conditions and for conditions where T_{hot} reduction is implemented. Results are presented for both 40 years of total operation and for 10 more years of operation. These results indicate that, for a total of 40 years of operation, two tubes are at potential risk if T_{hot} reduction is implemented. These two tubes (SG:A R9C60 and SG:B R9C35) currently have usage factors equal to 0.49 but will have projected fatigue usage factors greater than 1.00 after 40 years of total operation. Usage factors calculated after 10 more years of operation with T_{hot} implemented have been determined to be 0.84.

The results of the fatigue evaluation indicate that currently no tubes in the North Anna Unit 2 steam generators require preventative action to preclude a North Anna Unit 1 R9C51 type tube rupture and that any tubes currently plugged with sentinel plugs, to detect such a rupture, can be returned to service. However, two tubes previously identified, SG:A R9C60 and SG:B R9C35, will require preventive action in the future, to preclude such a rupture, after approximately 10 more years of service. Note that in the event of a future uprating or increase in general plugging level the potential for tube fatigue would need to be re-evaluated.

Table 9-1

North Anna #2 Tubes with Significant Flow Peaking or Relative Stability Ratio

RELATIVE STABILITY RATIO * RELATIVE FLOW PEAKING
(Assumes all tubes are dented with deformation)

S.G.	Row	Column	Premod	Relative Stability Ratio * Rel Flow Peak Postmod w/o T_{hot}	Postmod With T_{hot}
A	8	64	0.810	0.720	0.755
	9	11	0.648	0.577	0.607
		35	0.851	0.757	0.796
		40-55	0.687	0.611	0.643
		60+	0.961	0.854	0.899
		79-84	0.654	0.581	0.612
B	8	31	0.608	0.540	0.568
		60	0.817	0.726	0.764
		81	0.583	0.518	0.546
	9	34+	0.680	0.605	0.636
		35+	0.960	0.854	0.899
		40-52	0.687	0.611	0.643
		92	0.637	0.565	0.596
		93	0.462	0.411	0.433
C	9	35	0.930	0.828	0.870
		40-56	0.687	0.611	0.643
		60	0.930	0.828	0.870
		61	0.680	0.605	0.636
		79-85	0.654	0.581	0.612
	10	44	0.797	0.709	0.746
		45	0.798	0.709	0.747
		49	0.798	0.709	0.747
		50	0.798	0.709	0.747
		60	0.798	0.709	0.747

+Tubes which are currently sentinel plugged which are recommended to remain sentinel plugged.

Table 9-2

North Anna #2 Tubes with Significant Flow Peaking or Relative Stability Ratio

STRESS RATIO
(Assumes all tubes are dented with deformation)

S.G.	Row	Column	Rel. Flow Peaking	Max Allow Flow Peak	Stress Ratio Premod	Postmod W/O T_{hot}	Postmod With T_{hot}
A	8	64		a,c	0.68	0.36	0.47
	9	11			0.16	0.09	0.11
		35			0.73	0.38	0.50
		40-55			0.22	0.12	0.18
		60			1.61	0.75	1.00
		79-84			0.17	0.09	0.11
B	8	31			0.14	0.07	0.10
		60			0.72	0.37	0.49
		81			0.11	0.06	0.08
	9	34₊			0.21	0.11	0.15
		35₊			1.61	0.75	1.00
		40-52			0.22	0.12	0.16
		92			0.15	0.08	0.10
		93			0.03	0.01	0.02
C	9	35			1.21	0.63	0.83
		40-56			0.22	0.12	0.16
		60			1.21	0.63	0.83
		61			0.21	0.11	0.15
		79-85			0.17	0.09	0.12
	10	44			0.43	0.22	0.30
		45			0.43	0.22	0.30
		49			0.43	0.23	0.30
		50			0.43	0.23	0.30
		60			0.43	0.23	0.30

Tubes which are currently sentinel plugged which are recommended to remain sentinel plugged.

Table 9-3

Summary of North Anna Unit 2 Fatigue Usage Factors

| Tube	S.G.	Current Usage	Usage Factor 40 Year Total Life		Usage Factor 10 More Years	
			w/o T_{hot}	With T_{hot}	w/o T_{hot}	With T_{hot}
R9C35	A	0.02	0.03	0.08	0.02	0.04
R9C60	A	0.49	0.75	1.68	0.57	0.84
R9C35	B	0.49	0.75	1.68	0.57	0.84
R9C35	C	0.17	0.29	0.69	0.21	0.32
R9C60	C	0.17	0.29	0.69	0.21	0.3?

NA 2 – PREMOD – RSR*REL FLOW PEAKING

a,c

Figure 9-1 Relative Stability Ratio and Relative Flow Peaking - North Anna Unit 2 Premod
(Composite of all Steam Generators with Umbrella Flow Peaking)
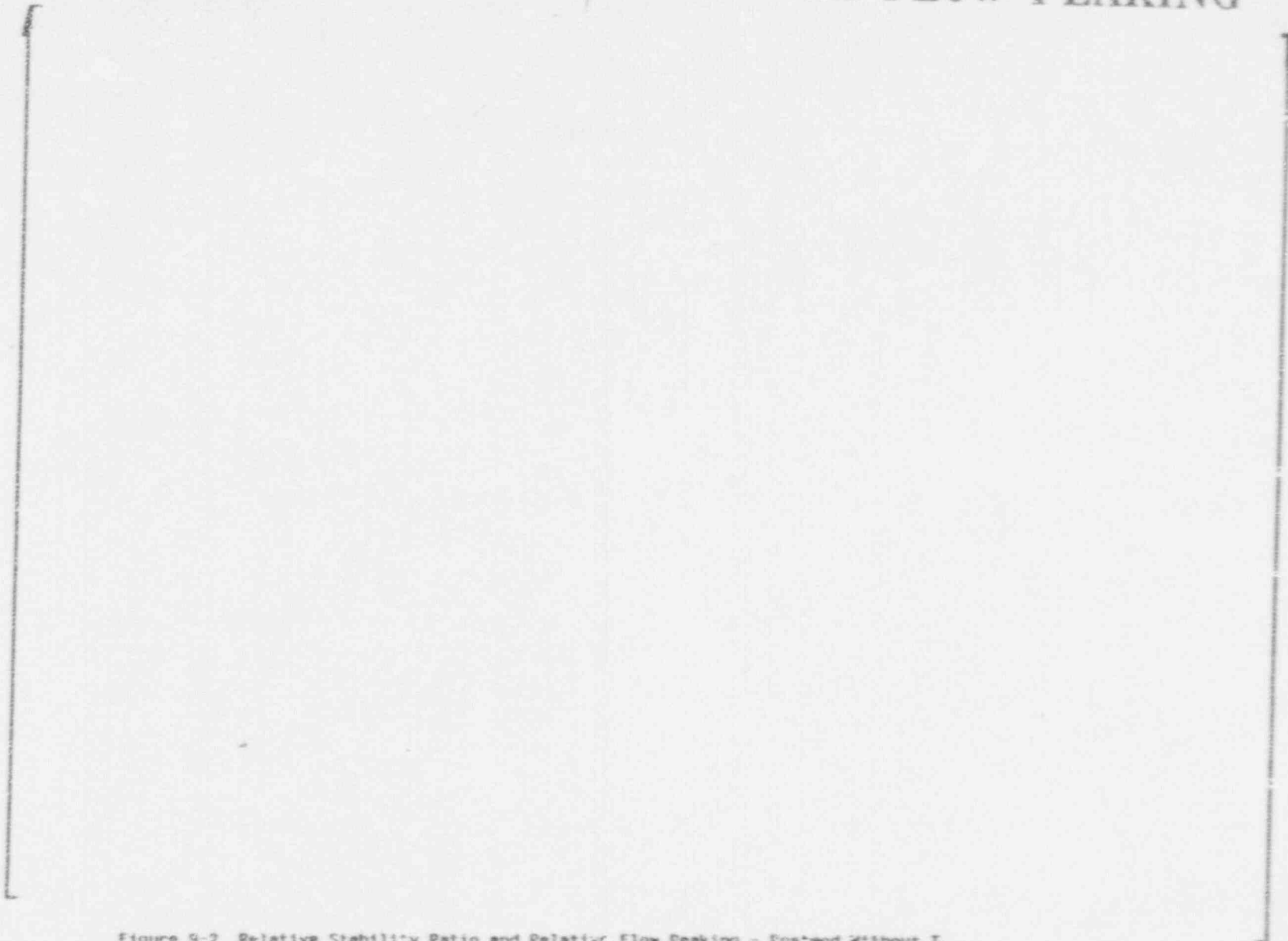
a,c

Figure 9-2 Relative Stability Ratio and Relative Flow Peaking - Postmod Without T_{hot}
Reduction (Composite of all SGs with Umbrella Flow Peaking)

9214M:1E-042789

$$NA\ 2\ -\ THOT\ -\ ^{'}RSR*REL\ FLOW\ PEAKING$$

a,c

Figure 5-3 Relative Stability Ratio and Relative Flow Peaking North Anna Unit 2 - Posted With T_{hot} Reduction

NA 2 — PREMOD — STRESS RATIO WITH DENTING

a,c

Figure 9-4 Stress Ratio vs. Column Number - Premod - North Anna Unit 2
(Composite of all SGs with Umbrella Flow Peaking)

9214M:1E-042789

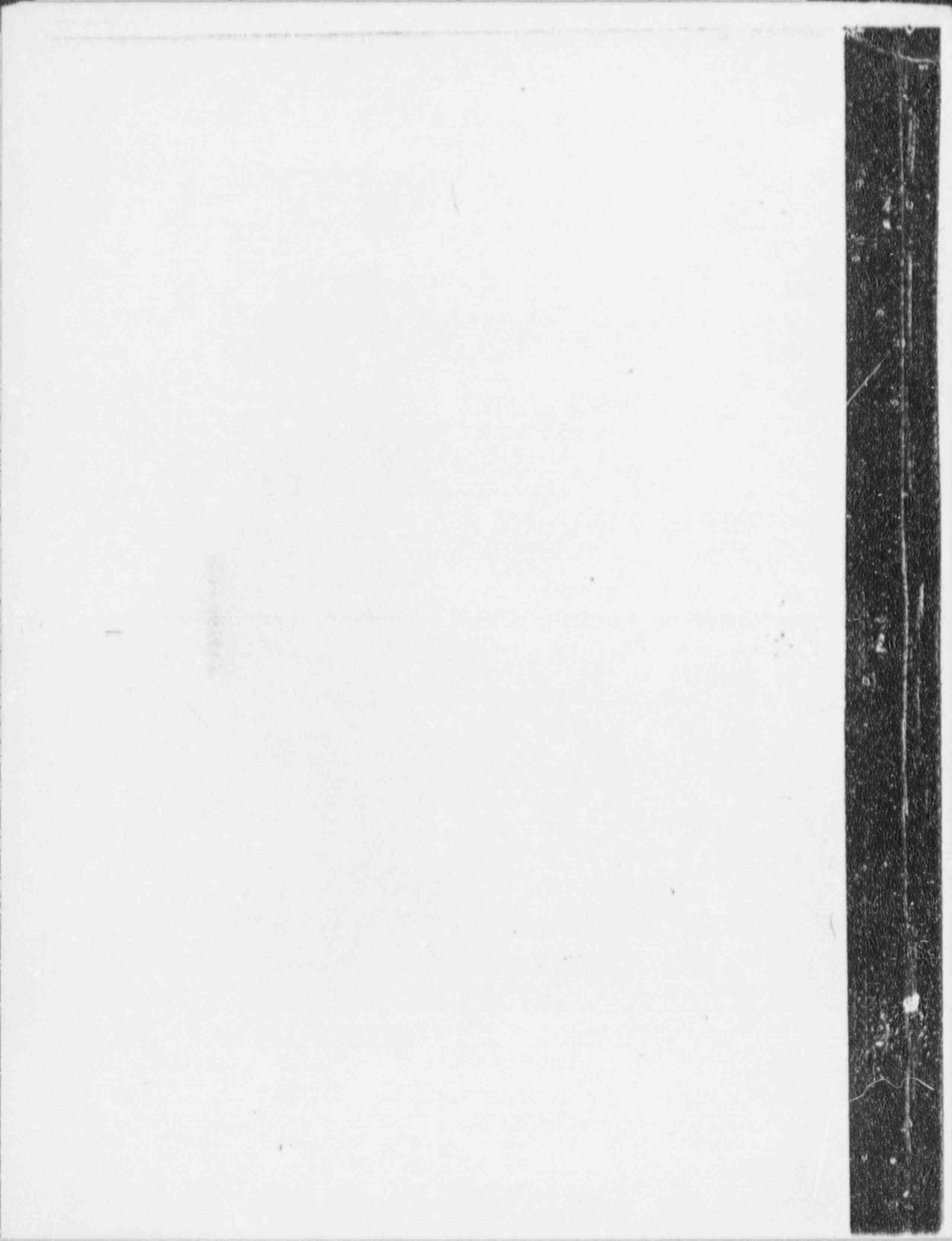NA 2 – POSTMOD – STRESS RATIO WITH DENTING

a,c

Figure 9-5. Stress Ratio vs. Column Number - Postmod Without T_{hot} Reduction North Anna Unit 2 (Composite of all JGs with Umbrella Flow Peaking)

NA 2 – THOT – STRESS RATIO WITH DENTING

a,c

Figure 9-5. Stress Ratio vs. Column Number – Dotted With T_{hot} Reduction – North Anna Unit 2 (Composite of all SGs with "Umbrella Flow Peaking")

PROPRIETARY INFORMATION
ENCLOSED

AUG 1 8 1988

MEMORANDUM FOR: Don Neighbors, Senior Project Manager
                   Project Directorate I-I
                   Division of Reactor Projects-I/II

FROM: C. Y. Cheng, Chief
                   Materials Engineering Branch
                   Division of Engineering and Systems Technology

SUBJECT: EVALUATION OF WESTINGHOUSE METHODOLOGY TO ADDRESS
                   ITEM C.2 OF NRC BULLETIN 88-02

The Materials Engineering Branch, Division of Engineering and Systems
Technology, has completed its review of the generic program developed by
Westinghouse to resolve item C.2 of Bulletin 88-02, "Rapidly Propagating
Fatigue Cracks in Steam Generator Tubes." Item C.2 is applicable to
Westinghouse-designed plants where denting is known or assumed to be present
at the uppermost carbon steel support plate in one or more steam generators.
Item C.2 of the Bulletin requests that a program be implemented to minimize
the probability of a rapidly propagating fatigue crack such as occurred at
North Anna Unit 1.

A proprietary and non-proprietary version of our Safety Evaluation is enclosed.
This evaluation specifically addresses generic aspects of the program described
in WCAP-11799 (Proprietary Version) and WCAP-11800 (Non-Proprietary Version),
"Beaver Valley Unit 1 - Evaluation for Tube Vibration Induced Fatigue," April
1988. However, similar programs are being implemented a number of other
facilities which have implemented similar programs to that for Beaver Valley
Unit 1. These conclusions will be incorporated by reference in plant-specific
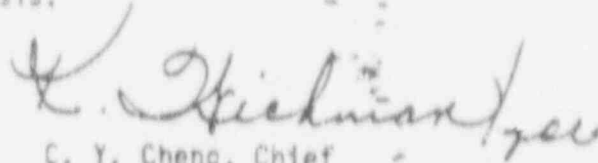SERs, where applicable.

Based on the enclosed evaluation, we have concluded that the Westinghouse
program is an acceptable approach for resolving item C.2 of the Bulletin. The
Westinghouse program, if properly implemented, will provide reasonable
assurance against future failures of the kind which occurred at North Anna
Unit 1.

Contact: E. Murphy
            X 20945

Licensee programs which utilize alternate approaches to that developed by Westinghouse will be evaluated on a case basis.

C. Y. Cheng, Chief
Materials Engineering Branch
Division of Engineering and
Systems Technology

Enclosures: As stated

cc: F. Miraglia
     S. Varga
     D. Crutchfield
     R. Capra
     T. Martin
     L. Shao
     J. Richardson
     C. Berlinger
     K. Wichman
     K. Conrad
     E. Murphy